DOE/PC/93221--T9

Combustion of Pulverized Coal in Vortex Structures

Grant No. DE-FG22-93PC93221

Final Report

Period Covered: October 1, 1993 -December 31, 1995

Prepared by

S. R. Gollahalli and N. Butuk
School of Aerospace and Mechanical Engineering
The University of Oklahoma
Norman, OK 73019

Submitted to

Document Control Center
U. S. Department of Energy
Pittsburgh Energy Technology Center
P. O. Box 10940, Pittsburgh, PA 15236-0940
Project Officer: Walter Fuchs

The Office of Research Administration
1000 Asp Avenue, Room 314
The University of Oklahoma
Norman, OK 73019

Administrative Contact:
Ms. Brenda Barton
March 1996

Combustion of Pulverized Coal in Vortex Structures

Grant No. DE-FG22-93PC93221

Final Report

Period Covered: October 1, 1993 -December 31, 1995

Prepared by

S. R. Gollahalli and N. Butuk
School of Aerospace and Mechanical Engineering
The University of Oklahoma
Norman, OK 73019

Submitted to

Document Control Center
U. S. Department of Energy
Pittsburgh Energy Technology Center
P. O. Box 10940, Pittsburgh, PA 15236-0940
Project Officer: Walter Fuchs

The Office of Research Administration
1000 Asp Avenue, Room 314
The University of Oklahoma
Norman, OK 73019

Administrative Contact:
Ms. Brenda Barton
March 1996

Table of Contents

Executive Summary

This report describes the details of the research conducted at the University of Oklahoma, Norman, Oklahoma, on the project entitled "Combustion of Pulverized Coal in Vortex Structures."

The objectives of the project were: (i) to understand the effects of heating one of the streams on the characteristics of shear layers, (ii) to investigate the changes in the characteristics of large scale vortex structures in the shear layer caused by the introduction of inert solid particles in one of the feed streams; (iii) to understand the effects of pyrolyzing solids on the shear layer behavior; and (iv) to study the effects of combustion of particles and their pyrolysis products on the shear layer structure, heat release rate, and pollutant emission characteristics.

An experimental facility for generating two-dimensional shear layers containing vortex structures has been designed and fabricated. The experimental facility is essentially a low speed wind tunnel designed to (i) provide two gas streams, initially with uniform velocity profiles and isotropic turbulence, mixing at the end of a splitter plate, (ii) introduce vorticity by passively perturbing one of the streams, (iii) allow heating of one of the streams to temperatures high enough to cause pyrolysis of coal particles, and (iv) provide a natural gas flame in one of the streams to result in ignition and burning of coal particles. The test section where the shear layer was formed measured 15 cm width x 8 cm depth x 47 cm length. The facility consisted of two air supply blowers, flow conditioning sections, an optically accessible test section, an exhaust diffuser, and a particulate collector. Instrumentation included a pitot tube and a laser-Doppler velocimeter for velocity field probing, thermocouples for temperature probing, iso-kinetic sampling system for determining the particulate concentration in the flow streams, smoke generator and color schlieren system for flow visualization, and gas sampling probes, sample conditioning system and analytical instruments to determine concentrations of some pollutant species.

Experiments were conducted in six phases: (i) shear layers formed by initially unperturbed gas streams with uniform velocity profiles, (ii) shear layers formed by two streams one of

which had passively introduced additional vorticity (iii) shear layers where one of the streams was heated, (iv) shear layers where one of the streams consisted of a gas flame, (v) shear layers where one of the streams contained inert particles, (vi) shear layers where one of the streams contained pyrolyzing coal particles, and (vii) shear layers where one of the streams contained burning coal particles. The following characteristics were investigated: (a) velocity profile development along the shear layer, (b) temperature profile development in heated and burning cases, (c) shear layer growth rate in terms of visual, vorticity and thermal thicknesses, and (d) composition profiles. The variables were: (a) strength of the shear layer (velocity difference of the streams), and (b) size of the particles (in some experiments).

The following is the summary of results and conclusions: (1) The velocity profiles in homogeneous shear layers of two gas streams which are initially unperturbed agree with the error function description. Perturbing the initial conditions of one of the streams and introducing initial vorticity distort the velocity profiles so that the error function description is reasonable at the initial and final stages of the shear layer growth. Heating of one of the streams or having a flame in one of the streams distort the velocity profiles over the entire growth period of shear layer; (2) While heating one of the streams or having a flame in one of the streams, the temperature profiles also do not fit the error function description; (3) Velocity profiles collapse into a single curve by normalization only in the case of shear layers of streams which are initially unperturbed; (4) The visual growth rate and the growth rate of vorticity thickness of homogeneous shear layer of streams with initial uniform velocity profiles and unperturbed flows agree well with the data available in the literature; (5) When one of the streams is heated or a flame exists in one of the streams (Richardson number (1.11 and 3.34) the growth rate of shear layer decreases; (6) The rate of increase of thermal thickness of shear layer in homogeneous shear layer is approximately twice that of vorticity thickness. The growth rate of thermal thickness agrees well with the rate of increase of density thickness quoted in the literature, and of visual thickness noted in the schlieren pictures of the present study; (7) In the shear layer with initially unperturbed streams, turbulence intensity increases when one of the streams is heated; (8) In the shear layer with perturbed streams the effect of heating on turbulence intensity depends on the velocity difference between the streams. Turbulence intensity increases when the velocity difference is large (strong shear), and decreases when the velocity difference is small (weak shear). The visual and thermal thicknesses also decrease when the flame exists in one of the streams; the same behavior is noted at both velocity differences tested, because of the continuous heat release which lowers the local velocity difference and strength of the shear layer; (9) When inert particles are present in one of the streams (Stokes number $\approx$ 3) the velocity profiles do not follow error function

shape. With pyrolysis and burning particles, similar changes occur; (10) The shear layer growth rates (based on visible, thermal, and vorticity thickness) decrease with the presence of particles in one of the streams; The effects of pyrolysis or burning of particles on the growth rate of the homogeneous shear layers (which are heated to pyrolyze particles) are weak; (11) Pyrolyzing particles increase the CO, decrease CO_2, and increase NO formations in the shear layer; (12) Burning particles decrease the concentrations of CO and CO_2 and do not change the concentration levels of NO and NO_x, because of the large amount of volatile products released from coal and insufficient residence time available for their oxidation.

Two papers have been presented in conferences based on this work and three more papers are planned for publication. One doctoral student, one master's student, and three undergraduate students were supported by the funds of this project and trained in the fossil energy field.

ACKNOWLEDGMENTS

The authors thank the help of several students in the combustion laboratory, Subramanian Thenappan, Kok Wah, Tan Ming, Eric Wright, Mike Babb, Darius Pardiwalla, Azfar Kamal and the technical staff of the School of Aerospace and Mechanical Engineering. The funding for this project was provided by the U.S. Department of Energy through the grant DE-FG22-93PC93221.

List of Tables

List of Photographs

List of Figures

NOMENCLATURE

D	Width of channel
f	Similarity variable. Its rate of change with respect to transverse direction represents the streamwise velocity U.
g	Acceleration due to gravity
r	Velocity ratio U2/U1
T	Temperature
U	Streamwise Velocity
x	Coordinate in the streamwise direction
y	Coordinate in the transverse direction
β	Volumetric thermal expansion coefficient (1/T)
δ	Thickness of the shear Layer
η	Similarity variable corresponding to y
λ	Dimensionless velocity parameter (U1-U2)/(U1+U2)
σ	Spreading Rate Parameter
subscripts	
1	Upper channel of wind tunnel
2	Lower channel of wind tunnel

A. INTRODUCTION

Since the physical processes of mixing are relatively slower than the chemical kinetics, the heat release rates of diffusion flames are limited by the characteristic rates of fluid mechanics processes. As the fluid mechanics also govern the availability of oxygen for the completion of reactions, the generation and destruction of pollutant species also depend upon it. Hence, a significant advancement in combustor technology can be achieved by understanding the interaction of fluid mechanics with the thermochemical processes occuring in flames. This study aims at furthering knowledge base about those interactive processes in heterogeneous flame systems, in particular pulverized coal flames.

The role of coherent large-scale structures in turbulent shear layers and reacting jets has been studied extensively over the past few decades [Brown and Roshko (1974)]. In our laboratory, a number of studies have been carried out on the influence of these coherent structures on flame stability of burners [Gollahalli et al. (1988), Savas and Gollahalli (1986), Shekarchi et al. (1988). It is clear that the development and behavior of those structures affect several critical processes, such as fuel pyrolysis and devolatilization, oxidation of pyrolysis fragments, and other thermochemical processes that occur in the near nozzle region. Furthermore, these structures also determine the rate of entrainment of surrounding air, and hence affect the rate of heat release in far-nozzle regions. These observations were further corroborated by the recent studies in which it was noticed that the modification of coherent structures by using elliptic geometry for the jets markedly changed the flame performance [Prabhu and Gollahalli (1989, 1990)]. Since all the previous studies had been performed in homogeneous gas phase systems, it was not yet clear how the coherent structures and their modulations would affect the heterogeneous systems such as pulverized coal flames.

The work of Brown and Roshko (1974), perhaps, is the milestone of our current understanding of the nature of turbulent mixing layers. They have established that the turbulent mixing layers comprise an organized flow configuration with building blocks that are vortical concentrations. Savas and Gollahalli (1986) presented an overview of the nature of the flow fields in a propane jet flame in air. It was noticed that combustion occurred away from both jet boundary and cores of coherent structures in that case. The amalgamation characteristics of coherent structures also changed substantially in the presence of flame. The fundamental frequency of coherent structures, the single most essential feature exciting them, increased. This frequency of the eddies was approximately 640 Hz and 840 Hz for the cold jet and the flame respectively. Thus, the modulation frequencies determined by cold flow studies that are available in the literature seem to be inaccurate in burning systems even of homogeneous

flows. Shekarchi et al. (1988) showed that under certain conditions the coherent structures might influence the characteristics to such an extent as to create a two zone structure of the so-called split flame.

From the information available in the literature at the beginning of this project, it was clear that the effects of coherent structures on the flame characteristics were substantial in homogeneous mixing systems and their flames. Also, it was evident that the information obtained in cold flows were of limited applicability to the flame situations. Furthermore, such information in heterogeneous mixing systems, particle laden flows for instance, was conspicuously lacking. This study, hence was directed to obtain such information. An experimental study was designed to understand the fundamental processes that occur in the shear layer regions of gas jet flames seeded with pulverized materials. The flow geometry was kept simple and amenable for good flow visualization and clear interpretation of results.

B. OBJECTIVES

The overall objectives of the project were: (i) to understand the effects of heating one of the streams on the characteristics of shear layers, (ii) to investigate the changes in the characteristics of large scale vortex structures in the shear layer caused by the introduction of inert solid particles in one of the feed streams; (iii) to understand the effects of pyrolyzing solids on the shear layer behavior; and (iv) to study the effects of combustion of particles and their pyrolysis products on the shear layer structure, heat release rate, and pollutant emission characteristics.

C. ORGANIZATIONAL DETAILS

Professor S. R. Gollahalli was the principal investigator of this project. Mr. Nelson Butuk, a graduate student in the School of Aerospace and Mechanical Engineering, pursuing his Ph. D. degree program was employed as a research assistant to assist the principal investigator Professor Gollahalli. Several undergraduate students (Kok Wah, Tan Ming, Eric Wright) and other graduate students in the Combustion Laboratory (Mike Babb, Azfar Kamal, Subramanian Thenappan and Darius Pardiwalla) were involved in the project and received training in Energy and Combustion areas. The mechanical engineering technician of the School, Mr. Bill Hill, and the machinist, Mr. Steve Dean helped the research team in various phases of the project.

D. TECHNICAL APPROACH

An experimental approach was taken to carry out the project. A two-dimensional shear layer tunnel was constructed for this study. Two separate streams of air supplied from independent sources mixed at the edge of a splitter plate in the test section which was accessible for both optical studies and probing. In the first phase, baseline data were obtained with the unheated streams at different velocity ratios and compared with the information existing in the literature to establish the suitability of the apparatus and procedures. The experiments with one of the streams heated to different temperatures followed in the second phase. Bituminous coal particles were introduced into the heated stream in the third phase. Fourth phase consisted of experiments in which one of the streams consisted of a gas flame to support the combustion of coal particles. Mean velocity, turbulence intensity, and temperature were measured in most of the experiments. Gas sampling and composition measurements were performed in some of the experiments. Flow visualization by direct and schlieren photography were carried out in all the runs with heated and burning conditions.

E. LITERATURE SURVEY

Homogeneous Stream Shear Layers

In the past, turbulent flows were considered to be composed of random motion of different length scales. Statistics were the only means for exploring the nature of these type of flows. Simple quantities like turbulence intensity and its spectrum were the parameters of interest [Cantwell (1981)]. Several experiments conducted in the late 1960's and early 1970's changed this. Kline et al. (1967), showed that the turbulence in a wall boundary layer is not only random but has some organized motions. Brown and Roshko (1974) presented shadow photographs of organized motion in a free shear layer.

The characteristic organized motions in a wall boundary layer are called "bursts", and those in shear layer are called "coherent" or "vortex" structures. Bursts consist of two processes; ejection of low momentum fluid from the wall region to the main stream and sweep of high momentum fluid into the wall region. Much fluid mixing and heat transfer occurs within these bursts. The coherent structures which are characteristic of shear flows, are large scale vortex structures observed when two fluids traveling at different velocities meet and interact, as well as when a fluid flows around an obstruction. Because of their high local velocities and intense stirring action, they also play a key role in fluid mixing and heat transfer. These structures influence the spreading rate or growth rate of the mixing layer.

The influence of large scale organized structures on the mixing and combustion characteristics in single phase gas flow systems has been well established. In comparing reacting and nonreacting shear flows, Ganji and Sawyer (1980) found that the reacting eddies have a lower growth rate, are more closely distributed in space, and have a slightly smaller rate of coalescence than nonreacting eddies. They also found that the spreading rate of the mixing layer was about 30% smaller in the reacting case. Gollahalli et al. (1986) and Savas and Gollahalli (1986) investigated gas jet flames. They found that for cold jets the Kelvin-Helmholtz instabilities (these are the instabilities which initiate the vortex roll-up structures) became visible on the jet boundary near the nozzle. In the presence of a flame these structures were suppressed; their initiation and development were delayed. They also found that the coalescence of vortices became less frequent and they were moved downstream resulting in slower growth rate of the shear layer. They noted that combustion did not occur inside the cores of the vortices since the mixture in the core was well beyond the flammable limits and

could not support combustion. Other investigators [(Yule (1978), Peters and Williams (1982), Shekarchi et al. (1988), and Hermanson et al. (1986)] have concluded that combustion in flames seemed to conserve coherent structures in the flow by delaying transition to turbulence.

Other investigators, for example see the review by (Coles, 1985), have studied perturbed shear layers in which the coherent structures are controlled by either passive or active means. Turbulence management is realized in this way. Passive control is achieved by changing the initial conditions and introducing azimuthal instabilities. It can also be done by issuing jets from noncircular nozzles. Active control is achieved by exciting the flow with an acoustic driver or a set of acoustic speakers. By controlling the structures, Gutmark et al. (1989) were able to increase the energy release in combustion, extend the flammability limits, and eliminate or reduce combustion instabilities in coaxial air and fuel jets. In their study, the optimal performance was achieved when reaction of the fuel/air mixture was initiated and sustained in the near-nozzle region of the shear layer. They used an active means to excite the initial shear layer at the higher harmonics of the preferred mode frequency, thus accelerating the transition to turbulence. They concluded that by triggering and amplifying the initial instabilities of the jet which were at higher frequencies relative to the preferred mode frequency, the natural evolution of large-scale coherent vortices roll-up would be hindered, and distributed combustion pattern would be promoted due to more intense small-scale mixing.

Hussain and Hussain (1987) have also shown that coherent structures are capable of enhancing or reducing the mixing of coflowing reacting streams, and hence can lead to methods of controlling combustion efficiency through the control of initiation, evolution, and interaction of coherent structures. Chemical reactions between the streams may also effect the structure of the mixing layer, either through compressibility effects such as baroclinic vorticity production and expansion as energy is released, or by changing the frequency content of the mixing layers with the introduction of characteristic frequencies of the chemical processes. The combustion time scales themselves, in turn, may be modified by the natural acoustic frequencies of the mixing layer or by those imposed through excitation.

Linear stability analysis may be used for predicting the performance of perturbed shear layers. An understanding of the physics of shear layers is important in the dispersion and hence mixing of scalar quantities such as heat or matter, for example, small particles. Kamalu et al. (1988) showed that in a mixing layer, the fluid tended to be entrained into the center of mixing layer from both sides, and the particles on average were flung away from the mixing layer center. Forcing the flow at the first subharmonic of the preferred vortex rollup frequency produced larger vortical structures and enhanced particles dispersion. Yang et al. (1990),

using stability analysis, found that the presence of particles enhanced the stability of the two-phase flow and decreased the amplification rate of the perturbation in the flow. The most amplified growth rates occurred near the same angular frequencies as that of the particle free flow.

Particulate Laden Shear Layers

The above discussion has dealt mostly with coherent structures in single gas-phase flows. In two phase flows, such as those that exist in combustion of coal particle streams, the interaction of coherent structures with the particles becomes complex. There is an immense potential to improve the combustion characteristics of pulverized coal flames if we have an understanding of the shear layer dynamics and interactions of the vortex structures with mixing parameters in two-phase flow systems. This knowledge, however, is conspicuously lacking at present.

In particle-turbulent flow interaction two issues are of concern; one is particle dispersion caused by fluid turbulence and the other is modification of fluid turbulence caused by particles. Viscous forces are dominant when particle surface velocities differ from velocities of the surrounding fluid. When particles have a higher density than the fluid, they have much more inertia than fluid elements moving at similar velocities; because of this they are, in general, unable to follow every scale of fluctuation in the flow. Faster moving particles can increase local fluid velocities by dragging the fluid along with them and vice versa. Particles may dampen or amplify fluid fluctuations of eddies through this interaction.

The extent of particle dispersion is largely a function of the Stokes number. The Stokes number (St) is a time scale ratio relating the magnitude of a particle response time scale (τ_p) and a characteristic fluid time scale (τ_f)

$$St = \tau_p / \tau_f \quad \text{.....(1)}$$

For a free shear layer, the characteristic fluid time scale (τ_f) reflects the motion of the large-scale coherent structures. This can be represented as the ratio of the width of the mixing layer (δ, large eddy length scale) to the velocity difference between the two free streams (Crowe, 1988). The particle response time is related to the time required for a given particle to attain its terminal velocity in a given flow. The Stokes number is somewhat analogous to turbulent Prandtl number defined as the ratio of the eddy diffusivity of momentum to the eddy diffusivity of the passive scalar under examination. Using Reynolds analogy the turbulent Prandtl number has been successfully used to explain transport of passive molecular contaminants. Attempts to

use the same approach for particle dispersion works only if the particles are small enough to follow fluid fluctuations. In this approach, transport is assumed to be driven purely by gradient diffusion (Fick's Law). This approach only works for near-isotropic flows fields.

Based on the Stokes number concepts, we can divide the possibilities of particle response to turbulent flow into three regimes. First, if $St >> 1$, a particle will not respond to fluctuations in the flow. If $St << 1$, a particle would respond completely to the flow, following all fluctuations. If $St \cong 1$, particles respond partially to fluctuations in the flow. Many practical applications of particle laden flows fall within this category.

Coherent structures have been shown to be primarily responsible for particle dispersion (Crowe, 1985), and the particle dispersion cannot be regarded as a gradient diffusion process. In these structures, the particles are trapped in the circulating velocity fields and subsequently centrifuged beyond the structures. For small values of the Stokes number, the particles approximately follow the large-scale structure and the particle dispersion rate approximates the spreading rate of the mixing layer. For large Stokes numbers, the particles pass through the vortices with nearly straight trajectories and are dispersed little by the turbulent field. For Stokes number of the order of unity, the particles are entrapped in the vortices and some centrifuged beyond the vortices. In general, for the particles not to affect the flow field, they must be smaller than the small scale turbulence (Kolmogorov microscale) and are introduced into the flow field at a low Mass Loading Ratio ($MLR=M_p/M_g$, where M_p is mass of particles per unit volume and M_g is mass of gas per unit volume).

In calculating Stokes numbers there is no consensus on the relevant time scale to use in calculating the fluid response time (Hishida et al., 1992). Many authors have used both the micro and the integral time scales. This suggests that data found in literature should be compared with caution. Apart from inertia (Stokes number) effects and fluid turbulence eddies effects treated by Fick's law discussed above, one other mechanism is said to be responsible for particle dispersion. It is the crossing trajectories effect (Crowe, 1988). This refers to the effect of external forces, which act upon finite size, particles and cause them to cross fluid point trajectories.

Gore and Crowe (1989) and Hetsroni (1989) have summarized experimental results on turbulence modification by particles. They concluded that small particles suppress the fluid turbulence and large particles increase the turbulence. The profiles of streamwise, turbulence intensities are also modified by the presence of particles. The magnitude of the effects is related closely to particle loading. Also, the temporal growth rate of the shear layer, decreases linearly

with increasing particle loading. Much of the data described in literature, however, show poor agreement with one another and some are characterized by a large scatter. Eaton (1994) has described some of the reasons for the experimental scatter observed. He mentions some of the reasons as a very difficult control of experimental conditions and difficulties in the measuring of gas phase velocities at high mass loading ratios (MLR). Many other factors also affect turbulence measurements including the type of flow (whether wall bounded or free) Reynolds number, particle diameter, particle density, and presence of active or passive disturbances.

From the above discussions of the effects of organized structures and particles on fluid flow, it is clear that they are interdependent and highly nonlinear. These relationships are currently poorly understood. However, the interactions via vortex structures offers great potential for optimizing fluid mixing and heat exchange in combustion and other processes such as control of pollutant emissions.

In coal combustion, for example, the action of vortex structures segregate particles (except when the structures change more rapidly than the particles can move around in the fluid). For example particles with small Stokes numbers are in general centrifuged out of vortices, becoming concentrated in relatively stagnant, irrotational regions of the flow. This causes relatively high local particle concentration spots, which influence combustion characteristics. By controlling the vortex structures through forcing (by active or passive means), particles can be concentrated or dispersed. This regulation of coal particle distribution in a combustor, is a key factor in reducing pollutant formation during combustion. This is also important in maximizing efficiency.

Another factor not mentioned above and has received very little attention is that of coupling effects. Particles-fluids interaction in two-phase flow can be considered as a one- way or two-way coupled. The amount of particle loading and particle size determine whether particle laden flows comprise 'one-way' coupled or 'two-way' coupled interactions. If the amount of particles and particle size are small enough that the particles do not appreciably modify the gas flow field, and the trajectories of the particles are determined by the motion of the carrier gas, a 'one-way' coupling is said to occur. On the other hand, if the amount of particles and/or particle size in the flow is large enough to modify the gas flow field and require that the volume fraction occupied by the particles be accounted for, then the 'two-way' coupling between particles is assumed. One-way coupling occurs in low dispersed-phase concentrations. However, with increased concentration such as those that exist in combustors, the disperse-phase can affect the fluid motion and two-way coupling becomes important. Tang et al. (1990) have incorporated two-way coupling in the numerical calculation of a developing

plane shear layer. Because of this, experiments reported here were carried out at a low particle to air mass loading ratio .

F. EXPERIMENTAL DETAILS

F.1 Shear Layer Tunnel

Some preliminary studies were conducted to determine the feasibility of modifying the combustion facility that existed in the lab for the experiments of this project. Since that combustion chamber was originally constructed for axisymmetric flames, it was found that a substantial amount work would have been needed to make it suitable for generating the two-dimensional shear layers required for this project. Hence, in order to save time and to retain the existing facility for other future axisymmetric flame studies, it was decided to design and construct a new facility for this project.

Figure F.1 shows the schematic diagram of the experimental facility which is essentially a low speed wind tunnel designed to create a two-dimensional mixing layer between two flow streams. The complete facility consisted of four modular flow conditioning sections each of length 15.3 cm, a contraction section, a test section, and an exhaust section. Figure F.2 shows the details of the contraction and test sections. Three walls of the channel were made of 6.35 mm thick Pyrex glass plates. The top plate was made of 6.35 mm thick aluminum sheet with a 12.5 mm slot cut in the middle for introducing probes. The splitter plate was machined out of a 6.35 mm thick aluminum plate and polished over 150 mm length with a bevel angle of 4 degrees to make the end as sharp as possible.

Each flow conditioning module section was fabricated of six aluminum plates of 6.35 mm thickness joined together by aluminum angle pieces. The upstream part of the splitter plate extending into these modules divided the section into two channels - upper and lower. To ensure air-tight connections, each section was assembled with the aid of silicon glue and gaskets. The holes of the plate facing the inside of the channel were counter sunk so that the screws joining the plates to the angle pieces were flush with the plates. The inside cross-sectional area of each channel measured 20 cm x 14 cm. Two of these channels were filled with sharp-edged and thin-walled aluminum tubes (6.25 mm o.d. and 0.5 mm thick) to function as a honeycomb to straighten the flow.

The contour of the contraction section was designed following the analysis of Libby and Reisser (1951). In this method, potential flow theory was used to derive a profile for walls of a channel to accomplish a monotonically increasing velocity in the flow direction. The calculated profile for a contraction ratio of 5 was cut out of 6.35 mm thick steel plate for the

two side walls of each channel. The profiles decreased from a depth of 20 cm to 4 cm over a length of 60.6 cm.

Air flow was supplied by two centrifugal blowers. The large blower supplied air to the upper channel of the shear layer facility. The large blower was a standard centrifugal blower with a 0.35 m diameter impeller driven by a 5.6 kW electric motor and capable of delivering air at a flow rate of 0.253- 2.02 m^3/s. The smaller blower supplied air to the lower channel and was driven by a 2 kW motor.

Heating System to Increase the Temperature of One of the Streams

For the purpose of studying the effect of heating on the shear layer structure, one of the streams was heated. This was accomplished by two methods: (i) A Mecker burner supplied with compressed natural gas from a storage bottle was located in the duct immediately downstream of the blower and was well upstream of the flow straightening devices and thus the shape of the initial velocity profiles of the two streams was not affected by heating. A flame stabilizer was included to prevent the flame from being blown-out at high velocities. This system allowed the heating of the top stream to about 360 K. The flow rate of natural gas was monitored with a calibrated rotameter; (ii) For studying the effects of pyrolyzing particles in the shear layer, the gas stream had to be heated to a condition exceeding the pyrolysis temperature of the particles. The pyrolysis temperature of the coal (bituminous) employed in this study was 570 K (Prasad, 1987). Since, the temperature dropped in the shear layer due to mixing with the other stream, to ensure that the temperature remained above the coal pyrolysis temperature the particle stream was to be heated to approximately 1100 K. Also, to study the effects of burning particles in the shear layer, ignition and sustainable combustion of coal particles in the shear layer had to be achieved. For this, the shear layer had to be maintained above the ignition temperature of coal which in the present case was about 673-1073 K (Bartok and Sarofim, 1991). To allow for the radiation cooling and convective heat transfer to the test section walls, it was decided to maintain an over ventilated diffusion flame of natural gas in the test section. For accomplishing both these goals, a burner system fueled with compressed natural gas was used. This burner was designed such that it could be mounted at different distances upstream of the splitter plate and could be easily exchanged from the top stream to the bottom stream.

Figure F.3 shows a sketch of the burner. It consisted of several 6.35 mm diameter stainless steel tubes attached to a 25 mm diameter manifold which was connected to a CNG cylinder through a pressure regulator and a rotameter. On each tube, holes of 1 mm diameter were

drilled to allow the natural gas flow in the air stream direction. This burner tube bank could be mounted in either top or bottom flow stream, downstream of the contraction section in the shear layer tunnel, thus allowing heating and combustion in either of the flow streams. In most of the experiments of this study, the burner was mounted 100 mm upstream of the splitter plate end in the lower channel. With regulation of the location of the burner relative to the splitter plate, the location of ignition of particles injected could be changed. Also, by suitably regulating the natural gas flow, the temperature in the test section could be adjusted to the desired value. The temperature profile in the section at the end of the splitter plate showed that the temperature was uniform within ± 2% except near the walls of the test section due to the thermal boundary layer.

Particulate Feeding System

Figures F.4 and F.5 show the details of the particulate feeding system designed to supply solid particles to one of the shear layers. The system shown in Fig. F.4 consisted of a two-dimensional trough and a motor-driven grooved shaft rotating at the bottom of the trough. Particles were dropped by the shaft into the venturi of the contraction section upstream of the splitter plate and the rate was controlled by the rotational speed. This system was suitable for carrying particles only into the top stream, and at large feed rates of particles. For carrying the particles at low feed rates into both bottom and top streams the system shown in Fig. F.5 was designed and fabricated. This system was used to supply magnesium oxide particles (tracers for laser-Doppler velocimetry) and coal particles into the shear layer. It consisted of two feeders and three injectors (the third injector for the upper channel MgO injection is not seen in this perspective view). The feeders were operated on fluidization principle. The feeders were made of standard 50.8 mm PVC pipes and fittings to provide smooth surfaces and to minimize adhesion of particles to the walls. Each feeder was 650 mm long with flanges mounted at 150 mm from the bottom. An 80-mesh stainless steel screen was placed at the flange fitting. A 60 mm thick bed of fine sand particles was placed on top of this screen. At 20 mm above the sand bed an asymmetric Y fitting and inlet tube were attached. The particles (coal or MgO) supplied through this inlet, fluidized, and delivered with a feeding rate that was held constant within ± 10%. A 6.35 mm diameter tygon tubing attached to the top of the feeder transported the particles to the injectors. The particulate laden stream was split into two branches which were supplied to the top and bottom streams of the shear layer tunnel. The injectors installed upstream in the contraction sections were made of 6.35 mm diameter steel pipes drilled with 1 mm holes along their entire length. The injectors were inserted into matching holes on the sides

of the channels and fastened with rubber seals. The tygon tubes were attached to both ends of the injectors to ensure that the particles were distributed uniformly across the flow streams. Compressed nitrogen/air was used to fluidize the particles and carry them to the injectors. Moisture traps were used to keep the fludizing medium dry. Calibrated rotameters were employed to monitor the fluidizing gas flow rate which was less than 0.1 % flow rate of the streams forming the shear layer. A solenoid valve was installed in the gas stream upstream of the particle feeders to facilitate the particle injection only when desired. This saved wastage of MgO particles and also decreased frequency of cleaning the test section glass walls during optical probing and schlieren visualization.

Exhaust Filtering Systems

As the first step, a large cyclone chamber was constructed and installed downstream of the test section to reduce the resistance to the flow and thus reduce the positive static pressure in the venturi section. The idea behind this design was the particulate laden exhaust stream entered the cyclone chamber tangentially imparting a high degree of swirl, which caused flinging of the particulates to the walls of the cyclone chamber and only the gases were discharged into the atmosphere. With that no additional filtering medium was to be interposed and hence the flow resistance was to be decreased. However, the pressure drop resulting from the cyclone chamber was high enough by itself. Thus the venturi section still developed positive pressure and hence this design was scrapped.

As the next step, an induced-draft electric blower was introduced in to the exhaust system with an intention of providing suction to compensate for the positive pressure due to the filtering system. However, the selection of blowers handling particulate-laden gases turned out to be expensive and controlling the blower output to match the test section flows was found to be impractical. As the third step, an attempt was made to combine the first two steps, which again was not successful because of the flow disturbances they imposed upstream, particularly in the test section.

Finally, we decided to install a long diffuser with a large area ratio and an impaction type particulate collector system which not only created a negative static pressure at the venturi section where particulates were introduced, but also enabled us to trap the particles without flow resistance to conduct the experiments in an environmentally safe manner. This deign is described below.

A diffuser system mentioned earlier was constructed of sheet metal. Since the overall length of the system exceeded the laboratory room length, complete rearrangement of the test

apparatus had to be undertaken. Figure F.6 shows the final version of the installation containing the exhaust particle collector system.

Pulverization and Preparation of Coal Particles

Pulverized coal of known size, preferably containing monosized particles was needed for this study. However, coal particles were not spherical and were not commercially available with monosize range. The possibilities of using monosized particles of other materials were explored. The cost of such particulate material, when commercially available, was prohibitively high. Since particles could not be retrieved and recycled in the present set up the budgetary limitations precluded this approach. Hence, it was decided to grind and sieve coal locally to obtain particles of a narrow size range. Several US standard sieves and an existing pulverizing mill and shaker system were employed. The Illinois-No. 6 bituminous coal was used for this study. Since coals had different moisture content, they had to be conditioned by preheating them for 4 hours at 340 K before each test. For this purpose an electrical oven was installed.

F.2 Instrumentation

The instrumentation consisted of the following: (i) Flow visualization (smoke flow tracing and schlieren flash photography), (ii) Mean velocity profile (Pitot-static tube and LDV), (iii) Root mean square velocity of turbulent fluctuation (LDV), and (iv) Temperature profile (thermocouple).

Mean Velocity and Turbulence Measurement

The flow field in the vicinity of the flame base was probed with a pitot-static probe and a laser Doppler velocimeter (LDV). The pitot-static tube (OD = 1.5 mm) was connected to an electronic barocell with a sensitivity of 0.001 torr. The output of the barocell was fed to a microcomputer-based data acquisition system for recording and processing. Pitot-static tube was mounted on a stepper-motor driven traversing mechanism and its location was controlled and varied by the microcomputer. Pitot-tube measurements were used to obtain time-mean data only. A commercial software was employed for probe position controlling and data acquisition of pressure signals.

The laser Doppler analyzer (Figure F.7) operated with a transmitter lens of focal length 500 mm, a receiver lens of focal length 500 mm, and a 10 mW helium-neon laser. The transmitting and receiving optics were mounted on two identical precision x-y traversing mechanisms located on opposite sides of the combustion chamber. These devices had a traverse resolution of 80 μm. The instrument was operated in the forward scatter mode with a beam separation of 23.8 mm and a beam intersection waist width of 176 μm. Both nozzle and air-flow streams were seeded with magnesium oxide particles whose average size was about 5 μm. A microcomputer-based data acquisition system with a 16-MHz clock was used to acquire and process the output data of the LDV. The mean velocity in the axial direction, U, and the root mean square value of the fluctuating component, u', were determined from the LDV measurements. During experiments with cold jets only nitrogen was used as the jet fluid and its flow rate was adjusted to yield the same exit Reynolds number as that of the fuel jet of the corresponding flame. In all runs 200-2000 validated samples with a sampling time less than 15 seconds were acquired. The preliminary experiments showed that above 200 samples per run the measured values of the mean and r.m.s. components of the velocity were not sensitive to the sampling rate. Some experiments were repeated 3 to 5 times to establish repeatability. The estimated values of the uncertainties in the measurements with thermocouple and LDV were ±3% and ±10% respectively.

Temperature Measurement

For temperature measurement, a type K thermocouple with ungrounded junction (0. 25 mm diameter) was used. A hand-held digital readout meter and computer data board were employed to collect the data on the initial test settings and temperature profiles respectively. Figure F.8 shows the computer controlled system employed to traverse pitot tubes and thermocouple probes.

Smoke Flow Visualization

For observing the boundaries and interface of the two streams in the developing shear layer smoke flow visualization was carried out. For this an oil-based smoke generator was employed. The smoke from the generator was introduced into the inlet of the blower of the low velocity stream. The shear layer was photographed by illuminating the test section with sheet light from two 500 W halogen lamps. A 400 ASA color film was used to photograph the scattered light from the smoke particles in the shear layer from a direction of 90 degrees to the direction of the flow.

Flash Schlieren System

The experiments with the continuous light source and using 35 mm camera with as low as 1/8000 second exposure on a 3600 ASA film showed, the time scale was not short enough to resolve the individual vortex structure. Hence, a xenon arc flash light source was obtained. This light source produced white light flashes at duration as short as 1.5 μs. A schlieren system was assembled using 75 mm diameter achromatic lenses of 250 mm focal length. A horizontal knife edge was employed and the schlieren picture was directly imaged on to the film plane of the camera without an intervening screen. This system yielded pictures of the flow field showing the development of the shear layer.

Color Schlieren System

Following the recently developed rainbow schlieren technique developed at NASA (Greenberg, 1995) the horizontal knife edge described above was replaced by a computer-generated color filter in the focal plane. In this technique, the deflections of the light beam due to variations in refractive index is translated into hue of the color on the image. Some photographs were obtained by using this system and panchromatic color films. Figure F.9 shows the schlieren flow visualization arrangement.

Direct Photography

In the experiments with a natural gas flame in one of the two streams direct color photography was also used for flow visualization. A 35 mm SLR camera with an exposure time as small as 1/4000 second was used to obtain the photograph on a 400 ASA color film.

Iso-Kinetic Sampling System

The concentration of particulates (coal or MgO) were determined by drawing samples of the particle-laden flow with a large probe (internal diameter 5 mm), filtering the sample of a known volume of flow, and weighing the filtered particles. In turbulent flows, if the velocity of flow entering the probe is not the same as the free stream mean velocity, because of the deflection of the streamlines, sampling bias will be introduced. Hence, iso-kinetic sampling where the two velocities were kept equal was employed in this project. Figure F.10 shows the experimental facility constructed for this purpose. The apparatus consisted of a stainless sample probe, a detachable filter holder in the line, a calibrated rotameter, and a vacuum pump. The procedure

included adjusting the flow rate through the filter to make the velocity at the entrance to the probe equal to the free stream mean velocity in the gas flow with the filter and timing the flow for a known volume of gas passing through the filter. The filter paper was conditioned and weighed before and after the particle collection. By noting the flow rate, time of collection, and the particulate mass collected, the particle loading (mass concentration) in the gas was determined.

F.3 Data Acquisition System

A major fraction of the project time was spent in developing PC-based data acquisition system. Although initially the system was configured to handle two sensors, a system capable of handling up to 8 sensors in differential mode was eventually selected. These two sensors were used to measure temperature and streamwise mean velocity in the test section. The pressure sensor had a large range of 10 V and a resolution of 1 mV, with dynamic range of 10,000:1. This dynamic range required a minimum of 14 bits (2^{14} =16,384 which is greater than 10,000 and 2^{13} =8192 which was less than 10,000). The thermocouple sensor dynamic range was lower than for the pressure sensor because an accuracy of only 1°C was required. However, the ADC requires high gain in order for it to deal with the millivolt level signals of the thermocouple. The amount of computer memory for a n experiment of 1 hour duration assuming a mean velocity sample rate of 1 per second would be 72 kbytes.

With the above requirements in mind, a computer data acquisition system (GATEWAY, Model P-60 Pentium microprocessor, 60 MHz, 540 MB drive) available in the Combustion laboratory, was used for this project. Figure F. 11 shows a simplified block diagram of the data acquisition system implemented. The heart of this system was the high speed analog and digital I/O plug-in-card by the trade name "WorkMate" manufactured by Strawberry Tree Company of Sunnivale CA. A stepper-motor and power supplies were purchased to automate the traversing of the probes. For temperature measurements, a signal conditioning panel with cold-junction compensation was built in for automatic processing of thermocouple signals. The software provided by the manufacturer of the board was sufficient for our purposes. In summary, the WorkMate card was totally software-controlled for data logging, process monitoring, and control. The stepper-motor required four digital outputs from the card. One pulse was used to feed all the four digital outputs manipulating the signals to obtain the required phase-differences. A second and third pulse

were used to control the direction of movement of the stepper motor. A fourth pulse was used to control sampling and logging of data.

Computer Driven Traversing Tables

The laser velocity meter had to be traversed along a vertical plane at several streamwise directions. For this purpose, a three-dimensional traverse was designed and constructed. The traverses in two directions x and y (streamwise and horizontal direction perpendicular to it) were manually controlled. The traverse in the vertical z direction was computer-driven.

The entire wind tunnel was mounted on top of three screw jacks arranged in a triangle and driven by one-stepper motor. Flexible standard 152.4 mm diameter aluminum pipes connected between the blowers and wind tunnel inlet allowed the independent movement of the tunnel in the vertical direction. The soft ware-using "Strawberry Systems Workbench" program was adopted for controlling the traverses of the probes. Photographs (Ph) F.1 to F.6 show some views of the experimental facility.

F.4 Experimental Procedure, Conditions, and Data Analysis

Four series of experiments were conducted: (i) isothermal homogeneous shear layers formed by room temperature gas layers, (ii) nonisothermal homogeneous shear layers with one stream heated, (iii) isothermal heterogeneous shear layers with coal particles, and (iv) heterogeneous shear layers with burning coal particles.

All experiments in the first and second series were performed with homogeneous single-phase gas streams. Tables F.1 and F.2 show a summary of the runs performed and the conditions for each run. The shear layer was distinguished by two modes; the unperturbed mode and the perturbed mode. The shear layer became perturbed when the burner was inserted close to the end of the splitter plate in the bottom stream as described above. The burner acted as a passive control device introducing additional vorticity.

Table F.1 shows the experimental conditions for the unperturbed mode of the shear layer. The runs are numbered from 1-10 and the names that appear for each run are used to identify the runs in the graphical plots to be presented below. In runs 2-5, the top stream was heated by

about 60K in order to study the effect of small heat release with no chemical reaction. The heating was done upstream of the honey comb using a Mecker burner, operating on compressed natural gas. The remaining runs were for unheated isothermal conditions at different velocity ratios. The transverse mean velocity profiles for all the runs in the unperturbed mode were obtained using a pitot-static tube. The LDV was used to obtain the r.m.s. values of velocity.

Table F.2 shows the experimental conditions for the perturbed mode of the shear layer. They are numbered and named in a way similar to the unperturbed mode described above. Runs 1 and 2 were performed at two velocity ratios; "cold1" and "cold2" runs were experiments for unheated homogenous gas shear layers only. The next set of experiments 3 and 4 was performed when the bottom stream in the test section was heated to above the pyrolysis temperature of the coal particles (570K). The runs "hot1" and "hot2" were conducted with two velocity ratios same as those in the cold stream experiments for homogeneous gas streams. The last set of experiments 5 and 6 was conducted at conditions same as those of the runs 3 and 4, except that the bottom stream in the test section consisted of a flame to achieve ignition of the coal particles.

The pyrolysis temperature of the coal employed in this study was 570 K (Prasad, 1987). Hence, to study the effects of pyrolyzing particles on the shear layer characteristics, the stream into which the particles were injected had to be heated above that temperature. Since, the temperature dropped in the shear layer due to mixing with the other stream, to ensure the temperature remains above the coal pyrolysis temperature the particle stream was to be heated to approximately 1100 K. Also, to achieve ignition and sustain combustion of coal particles in the shear layer, the shear layer had to be maintained above the ignition temperature of coal which in the present case was about 673-1073 K (Bartok and Sarofim, 1991). To allow for the temperature drop due to radiation cooling and convective heat transfer to the test section walls, an over-ventilated diffusion flame of natural gas was maintained in the test section. For accomplishing both these goals, a burner system fueled with compressed natural gas described in the previous section was used.

In the second series, to establish baseline data of homogeneous shear layers for comparison with the experiments having pyrolyzing particles, experiments were conducted by heating one of the streams. The natural gas flow rate was adjusted such that the bottom stream at the splitter plate end was always maintained close to 1100 K. Experiments were conducted at two velocity ratios of the streams (top stream velocity / bottom stream velocity equal to 12.5/7.1 and 7/4.5 (m/s)/(m/s)).

The purpose of heating coal to pyrolysis and combustion temperatures was to simulate the conditions existing during actual coal pyrolysis and combustion. The important condition simulated was that of large heat release. The results of experiments with coal particles undergoing pyrolysis and combustion will be presented in later sections. In all experiments with homogeneous shear layer (shown in Tables F.1 and F.2), except in the last set of combustion runs, velocity and temperature profiles were taken at 8 x-locations in the streamwise direction starting at the end of the splitter plate (see Fig. 4 for the coordinate system). The locations were at 0 mm, 30 mm, 50 mm, 70 mm, 90 mm, 125 mm, 165 mm, and 200 mm from the edge of splitter plate. For the last set of combustion runs, it was discovered that the laser beam was not powerful enough to penetrate the luminous flame present during combustion. For these runs, therefore, measurements were taken at 0 mm, where the flame was not luminous and at 200 mm, to which point the gas flame did not extend.

Tables F.3 shows the details of coal particles used and ranges of variables covered for particle-laden shear layer experiments. The concentration of coal particles in the top stream was held at 0.01kg/kg. In the third series of experiments, coal particles came in contact with the heated stream just at the splitter plate edge and underwent pyrolysis while the shear layer was being formed and was developing. Hence, the modulation of the velocity profile may be attributed to the processes of devolatilization which include endothermic reactions and mass addition to the shear layer. One set of experiments was also conducted with a higher concentration coal (0.02 kg/kg).

The series of particle combustion experiments was similar to the series of pyrolysis experiments except that the temperature of the bottom stream was raised to a temperature so that coal particles in the top stream were ignited and burned in the shear layer. Higher temperatures of the top stream were accomplished by increasing the natural gas input to the burner and also moving the burner location closer to the splitter plate edge. In many experiments a gas flame supporting the continued combustion of coal in the test section was also maintained. The gas stream temperature in the test section was approximately 1100 K. These experiments were also conduced at two velocity ratios and at two concentrations of coal particles in the stream. The values were maintained same as those in pyrolysis experiments.

Shear Layer Spreading Parameter

In this section, the theory of analyzing mixing layers using the spreading rate parameter σ is discussed. A brief mention is also made of the linear stability theory used to analyze the stability of a mixing layer.

An important parameter for comparison of mixing layers is the spreading rate parameter popularly denoted by σ. There are two accepted ways of determining this parameter; one way is to determine the parameter from the transverse velocity profiles using the maximum rate of change of velocity within the profiles at each streamwise location; the other way is to fit the entire mean velocity profiles to a solution function of the boundary layer equations.

In the first method, use is made of the maximum-slope of the transverse velocity profile. A thickness of the mixing layer is defined (Brown and Roshko, 1974) as:

$$\delta_w = (U_1-U_2)/ (dU/dy)_{max} \quad \text{.....(1)}$$

Its x - derivative, is then used as a measure of the spreading rate.

$$\delta'_w = d (\delta_w) / dx. \quad \text{.....(2)}$$

To use the second method, the boundary layer equation is first solved. The well known analytical solution of a plane shear layer assuming similarity, (Schlichting, 1968) reduces the boundary - layer equation to a third order ordinary differential equation.

$$f''' (\eta) + 2 \sigma^2 f' (\eta) f'' (\eta) = \text{Constant} \quad \text{.....(3)}$$

with boundary condition

$$f'(\infty) = 1+\lambda \quad \text{and } f'(-\infty) = 1-\lambda \quad \text{.....(4)}$$

where $f' = 2U /(U1+U2)$; $\lambda = (U_1-U_2)/ (U_1+U_2)$; and $\eta = \sigma y / x$

The coordinate system of the shear layer is shown in Fig. F.12. Using perturbation techniques, Gortler in 1942, (Schlichting, 1968) first solved the above equation retaining only the first order term of a series expansion; see Nayfeh (1981) for the technique. His solution yielded:

$$U= 0.5 (U_1+U_2) (1+ \lambda \text{ erf } (\eta+d)) \quad \text{.....(5)}$$

By fitting the experimental data to the error function, the spreading rate parameter σ (in η) in equation 5 is determined. The other constant d is also determined during the fitting. It takes care of the missing third boundary condition of the differential equation 4 above. The

advantage of this method, over the first method in determining the spreading rate parameter, is that all parts of the profile are involved in the fitting. Its disadvantage is that it does not work, for non-self similar profiles.

Brown & Roshko (1974) give a relationship between the two spreading rate parameters as:

$$\sigma \cdot \delta'_w = \pi^{\frac{1}{2}} \qquad \ldots\ldots(7)$$

In this study both methods were used to characterize the mixing layer.

In order to determine the effects of buoyancy forces, the Richardson number was calculated as:

$$Ri = (\beta\ g\ D\ \Delta T)\ /\ (\Delta U)^2 \qquad \ldots\ldots(8)$$

This equation gives the ratio of buoyancy forces to the strength of the shear layer.

G. RESULTS AND DISCUSSION

G.1. Homogeneous Shear Layers

In this section the measured and processed data of all the runs shown in Tables F.1 and F.2 are discussed; the discussion is grouped under two modes of the shear layer: the perturbed shear layer and the unperturbed shear layer. First, the unperturbed shear layer is discussed followed by the perturbed shear layer. The shear layer was perturbed when the burner was introduced in the lower stream closer to the splitter plate end. The burner appeared to function like a passive control device as evidenced by the results discussed below. This specially designed burner was necessary in order to maintain pyrolysis and combustion temperatures in the test section as explained previously.

G.1.1. Unperturbed Shear Layer Experiments

The experimental runs for the unperturbed shear layer results are shown in Table F.1. To determine the spreading rate parameter δ'_W whose values are shown in Tables F.1 and F.2. Lagrangian interpolation and the three point formula for approximating derivatives were used. To determine the spreading rate parameter σ, based on error function fit, the Levenberg-Marquardt non-linear least squares technique was used (Press et al., 1992). All of the experiments of Table F.1, were conducted for homogeneous single-phase fluid streams. The operation of the test facility was confirmed by comparison of results of these runs with published data as described below.

Mean Velocity Profiles

Figure G.1 shows the average streamwise velocity (U-U2)/(U1-U2) plotted as a function of the transverse (y) spatial coordinate for the 8 streamwise (x) spatial coordinate positions for homogeneous shear layers formed by the unheated streams (runs 9 and 10). Figure G.2 shows the corresponding information in the shear layer when the top stream was heated to 385 K at approximately the same velocity ratio (run 4). Both sets of profiles exhibit the typical error function variation at all x-locations as confirmed in the bottom rows of the figure where the data are fitted to the error function. This indicates similarity among the profiles and further

provides an evidence of a fully developed velocity profile. Mehta and Westphal (1986), however, states that a linear growth rate achieved at any point in the mixing layer, is not a good indicator of the attainment of asymptotic fully developed profile. According to them a better indicator for this is the behavior of the Reynolds stresses. Figure G.3 (a and b) shows a comparison of velocity profiles when both streams were cold (run 1) and when the top stream was heated (run 2). The conditions of these runs are shown in Table. F.1.

Temperature Profiles

Figure G.4 (a and b) shows the temperature profiles when only the top stream was heated (run 2). On figures G.3 and G.4, x refers to the distance from the edge of the splitter plate in the unheated case, and Hx refers to the corresponding distance when one of the streams was heated. The initial bulk velocities of the top and bottom streams in the unheated case were 19.6 m/s and 6.3 m/s with a velocity ratio of 0.32. The corresponding values in the heated case were 25.3 m/s, 8.3 m/s, and 0.35. The Reynolds number based on the channel depth for the two streams were 50,000 and 16,000 in the cold case, and 54,600 and 20,554 in the hot case. The triangles represent the velocity when the air streams were at room temperature (301 +/- 3 K) and the circles represent the velocity when the top stream was heated to 360 +/- 5K. Because of the unavoidable heat transfer through the splitter plate, the bottom stream at the beginning of the test section was also heated by approximately 15 K.

The initial temperature profile in the top stream was not flat as expected because of the heat transfer from the gas to the upper and side-walls. However, the sharp change in temperature between the upper and lower streams near the splitter plate (y=0) is clearly noticeable. As expected, the velocity profiles at x=0 are flat except near the solid walls both in the cold and hot cases. The velocity in the hot case is higher by about 5 m/s and 3 m/s in the upper and lower streams. As the shear layer begins to grow, the mean velocity on the mid-vertical plane keeps increasing and the profile develops a smoother and gradual variation in the y direction. The top part of the profile in the heated case exhibits a sharper peak, presumably due to cooling of the stream near the top aluminum wall, which increases the local density and lowers the velocity. It appears that the shape of the profiles does not change significantly beyond x = 20 cm. At that location the shear layer becomes wide enough to be influenced by the top and bottom walls of the test section. The shape and development of these profiles are similar to those presented by Ganji and Sawyer (1980) in a reacting gas shear layer.

Similarity of Flow Structure

For this analysis, it was first necessary to determine x_o, the location of the virtual origin where the shear layer thickness is zero. This was done by calculating the vorticity thickness at each x location and plotting it versus x. The location of the point x_o was determined from the location of x for which the vorticity thickness was zero after fitting data with the best linear regression. All of the x_o values were negative. Shear layers developing from turbulent boundary layers all have negative virtual origins and those developing from laminar boundary layers have both negative and positive virtual origins depending on the particular experiment (Bradshaw, 1966). One intuitively expects that a shear layer developing from laminar boundary layers to have a negative virtual origin and that one developing from turbulent boundary layers should have a positive virtual origin because of the faster spreading of the latter. However, data in literature does not support this. Having determined x_o, the velocity profiles U/U2 versus y normalized by the distance from the virtual origin x_o, were plotted (Fig. G.5). This figure shows the data for the unheated stream case (run 1). It is noticed that the velocity profiles collapse into a single curve, particularly on the plane of the splitter plate (y = 0). The data diverge near the top and bottom walls due to the boundary layer effects. It is clear that some similarity is achieved in the transverse velocity profiles in the shear layer at least where the end-wall effects are negligible. Figure G.6 shows a similar plot for the heated case of run 2. The behavior seems to be invariant even when one of the streams is heated to 360 K; however it is noticed from Fig. G.6 that similarity is achieved further downstream in the heated case than in the cold case.

Fluctuating Component of Streamwise Mean Velocity

Figure G.7 shows the plot of the root mean square value of the fluctuating quantity of the streamwise component of the velocity across the shear layer in both cold (run 1) and hot (run 2) cases. The r.m.s. value seems to be higher in the bottom stream side than in the top stream side. Since the initial velocity of the bottom stream is lower than that of the top stream it appears that the top stream with a higher momentum flux penetrates more toward to the side of the lower stream. This result is in conformity with Brown and Roshko's work (1974). When the velocities of the streams are close to each other, it is seen that the turbulence intensity (the ratio of the r.m.s value to the mean velocity) in the shear layer core (y=0) seems to be approximately 1.3% in the cold case and 1.7% in the heated case. This result is in contrast to water channel measurements of Hishida et al. (1988) who noticed that the fluctuation velocity decreased with heating of the top stream. They attributed it to lowering of momentum transport

because of the upward buoyancy of the top stream which tends to push the top stream fluid away from the bottom stream and hence increase shear stresses at the interface of the two streams. The notable differences between the present experiment and that of Hishida et al. (1988) are the nature of the fluid and the role of buoyancy. Since water was the fluid in their experiments, the increase in temperature lowers the fluid viscosity without a marked change in density of the fluid. In the present experiments, heating increases viscosity of air and lowers density, and consequently increases the shear stress at the interface of the two streams, which results in higher momentum transfer between the two streams. Also, in the present experiments, the bottom stream was heated and the buoyancy pushes the bottom stream upwards which increases turbulence. Both these factors appear to dominate which manifest in the higher turbulence level in the heated shear layer.

Shear Layer Growth

Figures G.8 and G.9 show the variation of vorticity thickness δ_w with the streamwise coordinate x at different velocity ratios for both unheated (runs 1, 6, and 7) and hot (runs 3, 4, and 5) conditions. It is noticed that the vorticity thickness grows approximately linearly with x until about 0.2 m from the splitter plate. It is noted that the vorticity thickness is different from the visual thickness of the shear layer observed previously from smoke traces and schlieren photographs (Butuk and Gollahalli, 1995). In Brown and Roshko study (1974) the vorticity thickness was approximately half of the visual thickness at a given location. In this study also, the flow visualization pictures confirm that finding. The reason for the leveling of the shear layer thickness may be attributed to the fact that the vortex size grows large enough to be influenced by the wall at that location. Further, it is noticed that the distance at which the variation of δ_w departs from linearity decreases with the increase in velocity ratio. This indicates that a low velocity ratio favors a slower growth of shear layer and hence a longer distance is needed before the vortex size is large enough to be influenced by the walls. From Fig. G.9 it is clear that the increase in velocity ratio (i.e., the decrease in velocity difference between the two streams) results in a lower shear layer thickness. This result is in conformity with several studies including the classical work of Brown and Roshko (1974). The smaller difference in the velocity between the two streams results in a lower shear stress at the interface and hence lower momentum transport between the two streams, and consequently results in lower growth rate of shear layer. The interesting result of this study is that the same feature is retained even when one of the streams is heated. It is also noticed that when the velocities were adjusted to

the initial setting, only the temperature increase from 295 K to 360 K produces very little change in the vorticity thickness. The observation that the vorticity thickness is not significantly changed by heating although the turbulence levels in the shear layer was changed is somewhat puzzling. Heating not only causes an increase in viscosity which influences the turbulence levels as explained previously, but also changes the density ratio of the fluids in the two streams. This change in density ratio is expected to decrease spreading angle although by a small extent according to Brown and Roshko (1974) who changed the density of the two streams by using different fluids (helium and nitrogen) and not by heating. This lower spreading is caused by the weaker penetration of the low density (and lower momentum flux) stream into the shear layer without a significant change in viscosity. In the present study, the effects attributable to heating through the routes of viscosity and density change seem to counteract each other as evidenced by the negligible effect on vorticity thickness.

Shear Layer Spreading Rate parameter

An important parameter for comparison of mixing layers is the spreading rate parameter defined in equation 3. Figure G.10 shows the variation of the spreading rate parameter with the dimensionless velocity parameter used by Brown and Roshko (1974). This figure includes the data of the present study for cold and heated cases (dark squares and open triangles) and the data of several investigators shown in the Fig. 10 of Brown and Roshko's paper (open circles). It is interesting to note that the present results fall well within the scatter of the data obtained by other investigators.

Flow Visualization

Photograph G.1 shows the smoke flow patterns of the typical shear layers of unheated streams. The smoke was present in the bottom stream. The interface between the stream indicates the typical vortex structure boundaries. However, that even at the shortest exposure time possible (1/4000 s) it was not possible to resolve the vortex structures fully. Hence, it was decided to employ schlieren flow visualization with a very short exposure time (1.5 μs). However, the only economical way of generating the density change in the flow field required for that purpose was by heating one of the streams. That introduced another variable, temperature difference between the streams, which effect is discussed in section G.2.

G.1.2. Perturbed Shear layer Experiments

This section consists of a discussion of the results of experiments whose conditions are shown in Table F.2.

Mean Velocity Profiles.

In Figs. G.11 and G.12 the normalized streamwise mean velocity (U-U2)/(U1-U2) is plotted as a function of the transverse (y) spatial coordinate for the 8 streamwise (x) spatial coordinate positions measured. The nomenclature to the left of the individual plots represents the name of the runs as indicated in Table F. 2. Figure G.11 compares the plots for the unheated stream experiments for the two velocity ratios, and Fig. G .12 shows similar plots for the heated case. It is noted that the unheated shear layer profiles developed exhibiting the typical shapes of mixing layer velocity profiles documented in the literature. The heated shear layer velocity profiles also exhibited a similar trend, except that the velocities in the lower heated stream were higher. At stations x = 165 mm and 200 mm the heated cases indicated a more developed velocity profiles than the unheated cases. The buoyancy effects were significant, particularly for the high velocity ratio cases as indicated by the values of Richardson numbers shown in Table 2. Hishida et al.(1988) pointed out that buoyancy effects would become significant at Richardson numbers of order unity.

Figures G.11 and G.12 also show the error function fit of unheated and heated velocity data. Not all of the velocity profiles exhibited the error function shape. Considering the error function fit for the first velocity ratio, in particular for Cold1 run shown in figure G.11, it is noticed that the error function at station x=30 mm, 50 mm, and 70 mm fit the data fairly well. At the x-stations 90 mm and 125 mm, it departs from the data, and then again it fits the data reasonably well at stations x=165 mm and x=200 mm. Since there is no heating for this run this observation must be due to the perturbations introduced in the shear layer by the burner. Ho and Huere (1982) observed the same change in the velocity profiles in perturbed shear layers. They noticed that in the perturbed mixing layer, the velocity profile data first follow the error function profile, later show deviations from the erf profile, and again follow it further downstream. They explained that the deviation from the erf profile as due to the vertical movement of the vortices. After vortex merging, the velocity profile becomes an erf profile once again. At the lower velocity ratio (stronger shear), the error function fit seems to be better,

which indicates that the induced vorticity effects become weaker with the increase in shear layer strength.

The above observation suggests that the burner can be used as a control device to manipulate the vortex structures of the mixing layer. Wygnanski (1979) used a passive control device almost similar to the burner in the present study. He used a grid of steel rods 3.2 mm in diameter and reported that the disturbances imposed on the flow did not affect the two dimensional character of the large eddies, but they did affect their rate of growth and amalgamation as well as their detailed turbulent structure. From schlieren photographs (discussed later) it was found that the qualitative structure of the coherent structures was indeed not affected by the burner. Further work needs to be done, to find out exactly what type of control devices are appropriate to enhance mixing and combustion in shear layers. In this regard "Linear Stability Analysis" can be an important mathematical tool in the search for optimal control devices for mixing layers. In a mixing layer the velocity fluctuations are produced by large coherent structures. In other words given a mixing layer that is controlled (either passively or actively) by a known disturbance, its development can be predicted. The Reynolds stresses at the various amplification modes can also be predicted.

It is noted that the error function fit of the velocity data for "Hot 1run" was poorer than for the "Hot 2" case. The shear layer in "Hot 2" case was stronger and the influence of buoyancy was weaker than in "Hot 1" experiments. The growth rate of Hot 2 run shear layer discussed later was linear without any peak exhibited by the "Hot 1" data. This behavior can be explained by the effect of velocity ratio on the growth of disturbances or perturbations. Monkewicz and Huere (1985) found that the maximum amplification rate of the perturbations was a linear function of the velocity ratio (U1- U2)/(U1+U2). The amplification rate of the disturbances can be related to the shear layer growth rate. This means that the amplification of the perturbation in Hot 2 run was high enough to prevent reverse momentum transfer. Similarly, the Cold 2 run velocity profiles fitted the error function very well except at the x = 70 mm location. This is also confirmed by the linear growth of the shear layer. The conformity of the heated shear layer data with the error function suggested that there was little acceleration of the fluid with heating.

Figure G.13 shows a comparison between velocity profiles at 0 mm and 200 mm x-streamwise locations in combustion, heated and unheated runs. As explained above, combustion data for the other x-locations were not obtained. Except for the wall boundary effects, the initial velocity profiles at x=0 mm were flat as expected for both the unheated and the heated cases. The combustion case profiles indicated a peak in the lower stream. This peak

was due to the increased temperatures in the reaction zone. The increased velocities in the heated cases were due to volumetric expansion. For both the heated and the reacting shear layer, the downstream pressure gradient effects might be important as explained below.

Unlike the results of the unperturbed shear layer, the velocity profiles of the perturbed shear layers, both in cold and hot cases were not self-similar. This is partly explained as due to the presence of disturbances in the initial region. Although not determined, the role of pressure gradient cannot be downplayed. It was assumed that the streamwise pressure gradient was zero in our study, however, with heat release this is unlikely to be true. For example, in the velocity profiles shown in Fig. G.12, the effects of heat release was to reduce the velocity difference across the shear layer, thereby reducing the shear across the layer. The velocity profile at 200 mm, was more developed than for the cold case. Since the free stream velocities are not constant in the presence of a pressure gradient, the boundary conditions of the velocities are functions of x. This means that the stream velocities U1 and U2 and their ratio r = U1/U2 vary with x. This is partly the reason why the plots of the shear layer thickness with x-locations were not linear. At each x location the effect of velocity ratio has to be considered.

Temperature Profiles

Figures G.14 and G.15 show the normalized temperature profiles in the shear layer for the heated and (combustion) cases of the bottom stream. The nomenclature to the left refers to similar cases as the velocity profiles, except that the names of the runs start with the letter T. The "Thot" cases refer to heated runs and "Tcmb" cases refer to combustion runs. The fairly constant temperature of the top stream was evident in all cases. The cooling effect of the bottom wall as well as the absence of the reaction zone near the wall was also evident in all of the profiles. The buoyancy effects were substantial as indicated by the magnitudes of Richardson numbers exceeding unity as shown in Table F. 2. It is a well known characteristic of turbulent shear flows that the spread of scalar quantities, i.e. heat or matter, is faster than the spread of momentum (Fielder (1974). The turbulent Prandtl number is less than 1.0. However, this Prandtl number is not the same at every location of the flow. This means that the transport of scalar quantities can vary from location to location. The difference in shape of temperature and momentum profiles for the heated cases may be explained as due largely to the transport mechanism determined by large scale vortex motion. The temperature profiles in the combustion runs exhibited a high temperature zone in the bottom stream, which was due to the presence of the reaction zone.

Figure G.16 shows an attempt to fit the error function to the temperature profiles of the heated and combustion runs. As seen the data do not fit the error function. For the heated flow with no combustion the temperature profiles could not be represented by an error function; with combustion, however, the continuous heat release in the shear layer makes the profiles similar to the error function shape.

Shear Layer Thickness

A two dimensional mixing layer can be viewed as an infinite vortex sheet. Infinite vortex sheets are unstable to even infinitesimal perturbations. The initial region of a mixing layer exhibits such behavior. In fact, it has been found theoretically (Michalke, 1965) as well as experimentally (Hussain and Hussain, 1983) that the instability of a mixing layer is controlled by the length scale of the momentum thickness at the origin of the mixing layer. The location of the roll-up of the mixing layer into organized vortical structures and the subsequent pairing interaction location are directly proportional to the initial momentum thickness. The coalescence of the discrete vortices downstream into larger structures are the primary source of mixing layer growth. Thus, an understanding of the physics governing this process is essential to the manipulation of the shear layer spreading rate (Ho and Huang, 1982).

Figure G.17 shows the shear layer thickness determined by velocity data as a function of x streamwise location for both the perturbed and the unperturbed cases. The unperturbed results indicated the expected linear growth rate of the shear layer as discussed above. The perturbed results are not linear especially for the profiles in Cold 1 and Hot 1 runs. These profiles exhibited a peak where the shear layer grew to reach a maximum width and then decreased. They exhibited regions of stepwise growth due to localized merging process. Initially in the developing mixing layer, transfer of momentum occurs between high momentum fluid to low momentum fluid and the shear layer grows, but further downstream a reversal in momentum transport direction occurs. Energy begins to be transferred from large scale structures back to the mean flow. This is what causes the shear layer to collapse after attaining a peak. This collapse of the shear layer was observed for cases "Cold 1" and "Hot 1". The reverse transfer in momentum maybe due to presence of pressure gradient as explained above or maybe due to the nature of initial disturbances. If disturbances are present, it has been found (McInville et al., 1985) that the phase angle between the forcing wave and the initial response wave greatly affects the shear layer structure. Depending on this angle, merging of vortex structures to form

larger vortices can be inhibited and even totally eliminated resulting in the collapse of the shear layer growth.

Figure G.18 indicates the thermal layer thickness plotted as a function of x streamwise location. The thermal layer thickness for the heated cases were higher than the velocity shear layer thickness, thus indicating that the Prandtl number was less than 1.0. It was also observed that combustion decreased the thermal layer thickness as observed in the plots of "Tcmb1" and "Tcmb2" cases shown in Fig. G.18.

Fluctuating Component of Streamwise Mean Velocity

Figures G.19 and G.20 show the plots of the normalized root mean square value of the fluctuating quantity of the streamwise component of the velocity across the shear layer in both cold and heated cases for two velocity ratios.

Figure G.19 shows the data for Cold 1 and Hot 1 runs. after accounting for boundary layer distortion, it was noted that the turbulence level in Cold 1 run rises from the free stream value to a peak in the center of the layer and then returns to the free stream value. This is a typical behavior of a free shear layer. Occasionally there was another peak in the bottom stream. Ho and Huang (1982) observed several peaks in their perturbed shear layers. Similar trends were also observed for the Cold 2 run profiles (Fig. G.20). For the heated runs, there was a clear decrease in turbulence level to almost constant value across the layer.

In Fig. G.21 a comparison is made of the turbulent intensities at x = 200 mm, where combustion data were available. Here also the intensities rise to a peak around the center of test section. It is seen that turbulence intensities for heated and combustion cases were similar for the high velocity ratio (weak shear) runs and also were lower than the turbulence intensities in unheated shear layers. However, at the low velocity ratio (strong shear) the trend is reversed. The increase in molecular viscosity due to heating and combustion dominates under weak shear conditions. With strong shear the penetration of high temperature (and high viscosity) fluid into the other stream results in an overall increase of turbulence in the heated and combustion cases.

Flow Visualization Results

Photograph G.2 shows color schlieren pictures of the shear layer when the bottom stream was heated (run Hot 1 in Table F.2). Because of the diameter of the schlieren lenses were limited to 75 mm in the experimental facility, the picture shown is a composite of the three shots taken at different times by moving the schlieren system along the streamwise direction of the shear layer. Form this picture it is seen that the instabilities begin to form in the first 70 mm. The large scale structures appear in the second picture and grow to the size of about 30 mm. The estimate of the visible shear layer thickness obtained by the slope of the tangent line to the boundaries shows the spreading rate δ' at this condition as 0.12. This value is in agreement with the visible rate of growth of the shear layer at the same density ratio (in the present case the density is primarily the function of temperature since the pressure is essentially atmospheric) shown in Fig. 5 of Brown and Roshko paper (1974). These values are in agreement with δ_T' obtained using temperature profiles (shown in Fig. G.18). In fact, this value also agrees with the δ_ρ' obtained from density profiles by Brown and Roshko. As density and temperature have one-to-one correspondence in this case the agreement appears reasonable.

Photograph G.3 shows the color schlieren picture of the shear layer when the bottom stream consisted of a flame (run comb.1 in Table F.2). It is interesting to note the value of the growth rate of visual thickness determined as described above is 0.1. However, at the same density ratio corresponding to the temperature ratio, the results of Brown and Roshko (1974) show a value of 0.05. This variance may be attributed to the differences in the experimental methods of achieving density difference between the present study and that of Brown and Roshko. Brown and Roshko used helium and nitrogen streams to create the density ratio, whereas in the present case a flame was employed. The continued heat release from the flame while the shear layer is growing accounts for the higher growth rate in the present case.

It is interesting to note that the centerline of the shear layer is deflected upwards into the top stream. The displacement of the centerline (y=0 location) computed from the temperature and velocity profiles shown in Figs. G.46 and G.47 corroborate these observations.

G.2 Shear Layers with Inert Particles in One of the Streams

All experiments with particles injection were performed with the burner placed upstream of the test section, and hence the shear layers were perturbed. Figures G.22 and G. 23 show a comparison of the mean velocity profile development between homogeneous shear layer and the shear layer in which inert particles were present in the top stream. In both cases the temperature of the streams was maintained at the room conditions (295± 3 K). Although coal particles were fed into the top stream, because the stream was maintained at room temperature, essentially the particles behaved as inert particles.

It is noticed that in homogeneous perturbed conditions the data fit error functions only in the initial and final stages of development as discussed earlier. However, in particulate laden shear layers at the low velocity ratio, the agreement between the data and the error function profile seems to be worse, particularly for $x \geq 90$ mm. However, at the low velocity ratio the agreement seems to be better. This suggests that particles stabilize the shear layer with strong shear. Figure G. 24 shows the variation of shear layer thickness δ determined following the Brown and Roshko procedure (1974) with x coordinate in the homogeneous unperturbed shear layer. Figure G.25 shows similar plot for the perturbed shear layer. It is seen that the growth behavior of shear layer is not altered by the presence of particles. The overall growth rate of shear layer, δ', however, decreases from 0.05 to 0.03 when particles were present.

Figures G.26 and G.27 show the turbulent intensity profiles across the shear layer at various distances from the splitter plate. It is seen in that during the initial development of shear layer ($x < 125$ mm) the turbulence intensity levels are not significantly different between the cases of homogeneous shear layers and the shear layer with a particulate laden stream. Probably the small size of the particles and with Stokes numbers less than unity indicate that the turbulence is not altered by the particles. However, at farther locations from the splitter plate, the agglomeration by being in the cores of the vortices lead to large clusters which make the particle flung out of the vortices and enhance the turbulence intensity. Figure G.28 compares the turbulent intensities at $x = 200$ mm at various conditions and at two velocity ratios. It is clear at the first velocity ratio (high ratio U_2/U_1 and weak shear) the effect of particles in unheated shear layers is stronger compared to that at the second velocity ratio (low U_2/U_1 stronger shear). The stronger shear leads to larger vortices and hence the particle influence becomes stronger because of the vorticity in them retains the particles are retained in their cores and hence the particle contribution to the enhancement of turbulence decreases.

G.3 Shear Layers with Pyrolyzing Particles in One of the Streams

Velocity and Turbulence Intensity Measurements

The effects of pyrolyzing particles on the characteristics of shear layers are examined in this series of experiments. Here, the bottom stream was heated to approximately 1100 K with natural gas flame in both cases. Because of the presence of burner these experiments can be classified as "perturbed case" runs. Coal particles (mean diameter = 38±3 μm)were introduced into the top stream. When the two streams mix at the edge of the splitter plate and the shear layer begins to form, the particles begin to undergo pyrolysis and release volatile compounds. However, the temperature in the shear layer is not high enough for the released compounds to undergo ignition and combustion. Hence, the only effect of pyrolysis may be considered to be the mass addition into the shear layer and some cooling due to endothermic processes.

Figures G.29 and G.30 compare the development of streamwise mean velocity profiles in the heated shear layers with and without coal particles. It is noticed that at high velocity ratio the error function fit does not hold as expected for the perturbed shear layers. The agreement is improved at the low velocity ratio. With particles, however, further changes in the velocity profiles are not significant.

Figures G.31 and G.32 show the effects of pyrolyzing particles on the turbulent intensity profiles in the heated streams. The top set of profiles corresponds to the case of homogeneous gas shear layer with one stream heated to 1100 K and the bottom set of profiles shows the effect of pyrolyzing particles on the heated shear layer. Comparing the Fig. G.22 and G.24 we notice the effect of heating is to reduce turbulence intensities markedly. However, the effect of pyrolyzing particles on turbulence intensity seems to be insignificant in further changing it. The effects of pyrolysis in the form of mass addition is to add additional mass in the core of the vortices where the concentration of smaller particles is expected to high. The additional mass tends to increase the rate of mixing and turbulence intensity, whereas the local cooling decreases the gas viscosity and thus reduces mixing and turbulence intensity. These mutually counteracting effects perhaps are responsible for the insignificant change in turbulence intensity in the shear layer. Further, the low Stokes number of the particulate flow is perhaps the driving factor for the particles to follow the gas stream which supports the above observation.

Shear Layer Growth

The effect of particles on the growth of the vorticity thickness δ along x-direction is shown in Fig. G.33. As noticed in the cold particle case, here also the x-distance for the shear layer thickness to reach the maximum value increases with the introduction of particles in the same way as in the case of particle-laden cold shear layers. However, the effects of pyrolysis in further altering the characteristics of shear layer growth seems to be negligible.

Temperature Measurements

Temperature profiles were obtained in the shear layers at various locations. These temperatures were measured with chromel alumel thermocouples. Because of the optically thick flame and high temperature of the test section walls which were in contact with hot gases, the radiation heat losses from the thermocouple were small. The maximum correction in temperature due to radiant heat losses was estimated to be less than 5% of the value measured. Also, for comparison the measured temperatures were normalized by the initial temperature difference, and hence, the readings are reported without any additional corrections.

The temperature profiles in the shear layer where the bottom stream was heated and the particles were introduced into the top stream are shown in Fig. G.34 for two velocity ratios. The temperature profile in the top stream is much flatter than the velocity profiles because the thermal boundary layer was much thinner in this case. An error function fit to the temperature data seems reasonable except at x=90 mm (Fig. G.35). The thermal shear layer thickness was calculated following the procedure similar to that employed by Brown and Roshko for velocity data. While comparing the temperature profiles, it is seen that the peaking of temperature even at x=200 mm is sharper with particles indicating the slower mixing rate and growth of thermal shear layer as observed in cold flow experiments with particles. The calculated values of thermal shear layer thickness for the case of pyrolyzing particles are shown in Fig. G.36. It is seen that the rate of increase of thermal thickness of the shear layer is decreased with particles and the extent of decrease is however dependent upon velocity ratio. The effect of higher difference in velocities (case 2) is to mitigate the effect of particles as expected.

Composition Measurements

In order to further understand the effects of pyrolysis on the shear layer characteristics, the concentration profiles of several chemical species (CO, CO_2, NO, NO_x, and O_2) were measured at x = 160 mm. Figures G. 37 and G. 38 show the results at two velocity ratios. The following behavior is noted: (i) The formation of product chemical species is confined to mostly towards the bottom stream side of the shear layer; this may be attributed to the presence of the post flame gases in the bottom stream, (ii) At the low velocity ratio, the introduction of particles increases CO, decreases CO_2, increase NO, and does not seem to have a significant influence on NO_x and O_2 concentrations; Since CO is the first oxidation species of pyrolysis products, it is reasonable to see only its concentration is affected significantly by the particle pyrolysis; The reduction of CO_2 concentration may be explained by the reduction in oxidative reactions due to endothermic cooling of combustion gases of the natural gas flame, and the consumption of oxygen by the C to CO conversion. The temperatures are low and hence the NO formed through prompt NO scheme are possible and the thermal NO formed through Zeldovich kinetics would be negligible. Furthermore, NO concentration increases are seen closer to y = 0, which suggests that the peak rates of these reactions occur in the cores of large-scale structures. The location of the peak concentration of NO_x also occurs closer to y = 0 than the peak concentration of NO_x without any particles in the shear layer. However, the magnitude of the peak NOx does not seem to be markedly affected by the presence of particles, which indicates that NO_2 component in the pure natural gas flame is higher than that in the presence of particles. The lower amount of NO_2 with particles is supported by the additional CO which competes for O atoms. Indeed, oxygen concentration is lower in the shear layer region (in the neighborhood of y = 0) with particles, which corroborates that particle influence is confined to the core region of the large vortical structures; (iii) At the higher velocity ratio, the qualitative trends of composition profiles remain same as those at the lower velocity ratio; however, the reduction in O_2 concentration is not marked on the scale shown in the figure, primarily because of the higher velocity of the upper stream and the additional oxygen penetration into the shear layer.

The above discussion of the concentration profiles clearly shows that the particles were pyrolyzing and hence were providing additional chemical species in the shear layer.

Flow Visualization Results

Photograph G.4 shows the schlieren picture of a shear layer when the bottom stream was heated and particles were added to the top stream (run hot 1 in Table F.2). The visual growth rate determined by drawing tangents to the boundaries of the shear layer δ' is 0.06, approximately half of the homogeneous shear layer at the same conditions. This result is also in agreement with the variation of shear layer vorticity thickness between the homogeneous and heterogeneous shear layers.

G.4 Shear Layers with Burning Particles in One of the Streams

Velocity and Turbulence Intensity Measurements

This series of experiments was conducted to understand the effects of burning particles which release both energy and mass into the shear layer, similar to the situation in the near-burner region of pulverized coal combustors. To accomplish this a highly over ventilated diffusion flame of natural gas was stabilized fin the lower stream with the burner bank described earlier. This was the same burner as that employed in pyrolyzing particle experiments, except that the natural gas flow rate was increased to such a value that the flame extended into the test section over 70% of its length. The temperature at the splitter plate was approximately 1100 K; however, the flame in this case was longer and could support the ignition and continued combustion of coal particles in the test section.

During combustion experiments the velocity profile measurements in the test sections had to be limited to only x=0 mm and x=200 mm stations, because of the excessive luminosity due to burning coal particles. The high luminosity masked the laser signal, and hence, the signal to noise ratio was unacceptable at all other locations. Figures G.39 and G.40 compare the profiles of the streamwise mean velocity component in normalized as before. It was noticed that having a flame in the bottom stream increased the velocity of that stream. This lowered the velocity difference between the top and bottom streams. As the effect of lowering the velocity difference was found to be decreasing the mixing rate and the growth rate of the homogeneous shear layer, the presence of flame retards the mixing rate between the two streams. Indeed, the peak in the velocity profile in the bottom stream which is persistent until x=200 mm provides a substantiation of this observation. While comparing the velocity profiles in the homogeneous shear layer with only gas flame shown in Fig. G.39 with the corresponding profiles in the experiments with particles shown in Fig. G.40, the effects of particles appear small. The particles seem to increase mixing as evidenced by the smoother velocity profile at x =200 mm when particles were burning. At higher temperatures, because of higher viscosity, the Stokes number is reduced markedly, and hence the effects of particles seem to be not felt significantly on the shear layer growth characteristics.

In Fig. G.21, the turbulence intensity was noticed to increase dramatically at x=200 mm plane when the flame was present when the velocity difference between the streams was

higher. The increase in turbulence intensity can be attributed to a three-fold increase in temperature and 80% increase in viscosity of the gas. Figure G.28 compares the turbulence intensities in the case of particulate laden streams at cold, pyrolyzing, and burning temperatures. While comparing Fig. G. 21 and G. 28 it is noticed that the effect of particulates on turbulence intensity of the flame stream is negligible; the turbulence intensity values remain approximately at 60% in both cases. This again confirms the fact that the higher temperatures reduce the effective Stokes number and thus the particles follow the gas more faithfully and their effect on the turbulence characteristics of shear layers is insignificant.

Shear Layer Growth

The vorticity thickness of shear layer with burning particles could not be computed because the velocity profiles were obtained only at two stations, viz., x =0 mm and x=200 mm. However, the velocity profiles at x=200 mm shown in Fig. G. 25 suggest that the shear layer was growing more slowly. Even at x=200 mm the double peaks corresponding to the bottom and top streams still persist in the burning case, whereas in the cold and pyrolyzing temperature cases, the profile becomes smooth resembling error function variations. This slower growth, in spite of the higher turbulence intensities noted earlier, is surprising. However, the smaller velocity difference between the two streams which reduces the growth rate of shear layer accounts for that behavior.

Temperature Profile Measurements

Figure G.41 shows the effects of burning particles on the development of temperature profiles at two velocity ratios. It is seen that the temperature profile development is not altered significantly by the particles similar to the particle effects in the velocity profiles. Again, in this case also, the error function description of the profiles was not good, particularly at x = 50 to 160 mm (Fig. G.42). From the temperature profiles, hence as in the pyrolysis case, the thermal shear layer thickness was calculated using Brown and Roshko procedure for velocity profiles. The results are shown in Fig. G.43. The growth of thermal shear layer also decreases as does the vorticity thickness by the presence of the flame. However, the effects of particles seem to be weaker in this case compared to the pyrolysis case. Higher temperatures, higher thermal diffusivity than momentum diffusivity, and lower values of Stokes number account for this result.

Composition Measurements

Figures G.44 and G.45 show the concentration profiles of the combustion product species (CO, CO_2, NO, NO_x, and O_2) at x=165 mm station. As in the pyrolysis case, the effects of the introduction of particles into the top air stream forming a shear layer with the bottom flame gases generated by burning natural gas are shown in these figures. In this situation, some particles were seen to ignite and burn as noted by luminous streaks in the test section. Although it appeared that some of the larger particles did not ignite because of the limited residence time available in the test section, the results shown in the figure are good indicators of what would happen when all particles burn, similar to those in practical combustors. In contrast to the previous series of experiments where the average temperature in the test section was low (at the splitter plate 1100K and lower in the rest of the test section, the hotter flame gases (approximately 1100 K over most of the test section) allow pyrolysis of most of the particles and combustion of some of them. At the low velocity ratio (Fig. G.44), the highly enhanced degree of pyrolysis of coal particles, decreased the formation of CO and CO_2 and did not change the concentration levels of NO and NO_x. The increase in the peak O_2 concentration from 5% to 15% explains the mitigated oxidative reactions. The negligible changes in NO/NOx concentrations are probably caused by the additional formation of NOx due to organically-bound nitrogen in coal and reduction of thermal NO formed by the natural gas flame. At the higher velocity ratio (Fig. G.45), the situation seems to reverse as denoted by the lower O_2 and higher CO, NO/NOx concentrations in the presence of particles. Even the CO_2 concentration is higher than that at the lower velocity ratio, but still remains below that in the pure natural gas flame due to the release of a large of quantity of pyrolysis products.

Thus, the particles in the shear layer are seen to provide additional mass and also affect the energy release. In this case, as the measurements were taken at x =165 mm which was still in the location where the shear layer was still developing, the influence of particles is strongly affected by the availability of oxygen. Hence, at farther downstream distances, where more oxygen becomes available, the concentration of all species measured above including NO/NOx increase with the combustion of particles in the shear layer.

Flow Visualization Results

Photograph G.5 shows the schlieren picture of a shear layer when the bottom stream consisted of a flame and particles were added to the top stream (run comb 1 in Table F.2). The visual growth rate determined by drawing tangents to the boundaries of the shear layer δ' is 0.05,

approximately half of its value in homogeneous shear layer at the same conditions. This result is also in agreement with the variation of shear layer thermal thickness between the homogeneous and heterogeneous shear layers.

H. CONCLUSIONS

o The velocity profiles in homogeneous shear layers of two gas streams which are initially unperturbed agree with the error function description. Perturbing the initial conditions of one of the streams and introducing vorticity into it, distort the velocity profiles so that the error function description is reasonable at the initial and final stages of the shear layer growth. Heating of one of the streams or having a flame in one of the streams affect the velocity profiles over the entire growth period of shear layer.

o While heating one of the streams or having a flame in one of the streams, the temperature profiles agree reasonably well with the error function description.

o Velocity profiles collapse into a single curve by normalization, only in the case of shear layers of streams which are initially unperturbed.

o The visual growth rate and growth rate of vorticity thickness of homogeneous shear layer of streams with initial uniform velocity profiles agree well with the data available in the literature.

o When one of the streams is heated or a flame exists in one of the streams the growth rate of shear layer decreases.

o The rate of increase of thermal thickness of shear layer in homogeneous shear layer is approximately twice that of vorticity thickness. The magnitude of thermal thickness agrees well with the value of density thickness quoted by Brown and Roshko (1974), and of visual thickness noted in the present schlieren pictures.

o In the shear layer with initially unperturbed streams, turbulence intensity increases when one of the streams is heated.

o In the shear layer with initially perturbed streams the effect of heating on turbulence intensity depends on the velocity difference between the streams. Turbulence intensity increases when the difference is large (strong shear), and decreases when the difference in velocities is small (weak shear). The visual and thermal thickness decrease when the flame exists in one of the streams at both velocity differences tested because of the continuous heat release which lowers the local velocity difference and strength of the shear layer.

o When inert particles are present in one of the streams (Stokes number ≈ 3)the velocity profiles are not significantly changed. With pyrolysis and burning particles, similar behavior is observed.

o The shear layer growth rates (based on visible, thermal, and vorticity thickness) decrease with the presence of particles in one of the streams.

o The effects of pyrolysis of particles on the growth rate of the homogeneous shear layers (which are heated to cause pyrolysis) are weak.

o Pyrolyzing particles increase CO, decrease CO_2, and increase NO in the shear layer.

o Burning particles decrease the concentrations of CO and CO_2 and do not change the concentration levels of NO and NO_x, because of the large amount of volatile products released from coal and insufficient residence time for their oxidation.

I. REFERENCES

Bartok, W. and Sarofim, A. F., 1991 , "Fossil Fuel Combustion, A Source Book.," John Wiley and sons, New York.

Birch, S. F. , 1966, "Data Evaluation Report for Free Mixing Layers," Report prepared for the Stanford Conference on Complex Turbulent Flows.

Bradshaw, P., 1966, "The effect of Initial Conditions on the Development of a Free Shear Layer," J. Fluid Mech. 26:225-236.

Brown, G. L., and Roshko, A., 1974, "On Density Effects and Large Structure in Turbulent Mixing Layers," J. Fluid Mechanics, 64: pp. 775-816.

Butuk, N. and Gollahalli, S. R., 1995, "Effects of Particles in Two-Dimensional Shear Layers," Oklahoma ASME/AIAA Symposium, Stillwater, Oklahoma, February 20.

Butuk, N. and Gollahalli, S. R.,1996, "Effects of Heating on Two-Dimensional Mixing Layers," Paper presented at Energy Week '96 Conference & Exhibition. API/ASME Houston, TX. January 31.

Cantwell, B. J., 1981, " Organized Motion in Turbulent flow". Ann. Rev. Fluid Mech. 13:457-515.

Chigier, N. A. and Yule, A. J., 1979, "The Physical Structure of Turbulent Flames" AIAA paper 79 - 0219.

Coles, D., 1985, "The Uses of Coherent Structures," AIAA paper 85 - 0506.

Crowe, C. T., 1988, "Particle Mixing in Free Shear Flows," Prog. Energy Combustion Sci. 14:171-194.

Crowe, C. T., Gore, R. A., and Troutt, T. R., 1985, "Particle Dispersion by Coherent Structures; in Free Shear Flows," Particulate Science and Technology 3:149 - 158.

Daily, J. W., Pitz, R. W., Keller, O. J., Ellzey, J. L., and Shepherd, I. G., 1984, "The Structure and Dynamics of Two Stream Plane Mixing Layers," Published in Experimental Measurements and Techniques in Turbulent Reactive Flows, ASME, pp. 175-209.

Eaton, J. K., 1994, "Experiments and Simulations on Turbulent Modification by Dispersed Particles," in Proc. of the Twelfth US National Congress of Applied Mechanics, Applied Mechanics Reviews, Kobayashi A. S.,ed., 47: no 6, part 2, pp S44-S48.

Fiedler, H. E., 1974, "Transport of Heat Across A Plane Turbulent Mixing Layer," Turbulent Diffusion In Environmental Pollution, Frenkiel, F. N., and Munn, R. E., Eds, Academic Press New York.

Ganji, A. R. and Sawyer, R. E., 1980, "An Experimental Study of the Flow Field and Pollutant Formation in a 2-D Premixed Turbulent Flame ," NASA Contractor Report 3230.

Gollahalli, S. R., Savas, O., Huang, R. F., Rodriquez, J. L. A., 1986, "Structure of Attached and Lifted Gas Jet Flames in Hysterisis Region"., 21st Symposium (international) on Combustion /The Combustion Institute, pp. 1463 - 1471.

Gore, R. A and Growe, C. T., 1989, "Effect of Particle Size on Modulating Turbulent Intensity," Int., J. Multiphase flow, 15 (2) 279 - 285.

Greenberg, P. S., and Klimek, R.B., 1995, "Quantitative Rainbow Schlieren Deflectometry," Applied Optics, July 34: No. 19. pp. 3810-3822.

Gutmark, T. P., Parr, D. M., Hanson - Parr., and Schadow, K. C., 1989, "On the Role of Large and Small Scale Structures in Combustion Control," Proc. Western States Sectional/The combustion Institute, Spring meeting, Pullman, Washington.

Hermanson, G. C., Mungal, M. G., Demotakis, P. E., 1986, "Heat Release Effects on Shear-Layer Growth and Entrainment," AIAA Journal, 25:578-580.

Hetsroni, G., 1989, "Particle Turbulence Interaction," Int. J. Multiphase Flow 15 (5) 735-746.

Hishida, K., Ogita, T., Kobayashi, K., Maeda, M., and Yokobori, S., 1988, "Turbulence Transport Phenomena Across Stable Thermal Stratified Layer in a Rectangular Channel Duct," Transport Phenomena in Turbulent Flows, Hirata, M., and Kasagi, N.,eds., Hemisphere Publishing Corporation, New York.

Hishida, K., Ando, A., and Maeda, M., 1992, "Experiments on Particles Dispersion in a Turbulent Mixing Layer," Int. J. Multiphase Flow 18 (2) 181 - 194.

Ho, C. M. and Huerre, P., 1984, "Perturbed Free Shear Layers," Ann. Rev. Fluid Mech., 16:365-424.

Ho Chih-Ming, and Huang, L., 1982, "Subharmonics and Vortex Merging in Mixing Layers," J. Fluid Mech., 119: 443-473.

Hussain, A. K. M. F., Zaman, K. B. M. Q., 1985, "An Experimental Study of Organized Motions in the Turbulent Plane Mixing Layer," J .Fluid Mech., 159: 85 -104.

Hussain, A. K. M. F., and Hussain, H. S.,1987, "Passive and Active Control of Jet Turbulence Management and Relaminarization," Springer Verlag, New York.

Hussain, H. S., and Hussain, A. K. M. F., 1983, Flow Visualization III, Wang W. J., Eds., Springer-Verlag, pp. 510.

Kamalun, N., Wen, F., Troutt, T. R., Crowe, C. T., and Chung, J. N., 1988, "Particle Dispersion by Ordered Motion in Turbulent Mixing Layers," ASME Forum on Cavitation and Multiphase flow, pp. 150-154.

Kline, S. J., Reynolds, W. C., Schraub, F. A. and Runstadler, P. W., 1967, "The Structure of Turbulent Boundary Layers," J. Fluid Mech., 30: 741 - 773 .

Landahl, M. T., Mollo-Christensen, E., 1987, "Turbulence and Random Processes in Fluid Mechanics," Cambridge University Press, Cambridge U.K.

Libby, P. A. and Reisser, H., 1951, " The Design of Two Dimensional Contraction Sections," Quarterly of Applied Mathematics, 10: 95 - 98.

McInville, R. M., Gatski, T. B., and Hassan, H. A., 1985, "Analysis of Large Vortical Structures in Shear Layers," AIAA J. 23 (8) 1165-1171.

Mehta, R. D., Westphal, R. V., 1986, "Near-Field Turbulence Properties of Single and Two Stream Plane Mixing Layers," Experiments in Fluids, 4: 257-266.

Merzkirch, W.,1987, "Flow Visualization," Academic Press, New York.

Michalke, A., 1965, "On Spatially Growing Disturbance in an Inviscid Layer," Journal of Fluid Mech. 23:521.

Monkewitz, P. A., and Huerre, P.,1982, "Influence of the Velocity Ratio on the Spatial Instability of Mixing Layers," Phys. Fluids 25 (7) 1137-1143.

Nayfeh, A. H., 1981, "Introduction to Perturbation Techniques", John Wiley & Sons New York.

Peters, N. and Williams, F. A., 1982, "Lift Off Characteristics of Turbulent Jet Diffusion Flames," AIAA paper 82-O11.

Prabhu, N. and Gollahalli, S. R., 1989, "Comparison of Gas Jet Flames over Circular and Elliptic Nozzles," Paper presented at the Western States Section of the Combustion Institute, Pullman, WA .

Prasad, A., 1988, " Combustion of Pulverized Coal Blends," M.S.Thesis, University of Oklahoma, Norman, OK.

Press, W. H., Teukolsky, S. A., Vetterling, W. T., and Flannery, B. P.,1992, "Numerical Recipes in Fortran", Cambridge University Press, Cambridge U.K.

Robollo, M. R. 1973, "Analytical and Experimental Investigation of a Turbulent Mixing Layer of Different Gases in a Pressure Gradient," Ph. D. Dissertation, Graduate Aeronautical Laboratories, California Institute of Technology, Pasadena, CA.

Rodi, W., 1975, "A Review of Experimental Data of Uniform Density Free Turbulent Boundary Layers," in Studies in Convection, ed., Launder B. E. Academic Press, New York.

Savas, O. and Gollahalli, S. R., 1986, "Flow Structure in Near - Nozzle Region of Gas Jet Flames," AIAA Journal 24 (7) 1137 -1140.

Schlichting, H., 1968, "Boundary Layer Theory," 6th edition pp. 689 - 690 McGraw- Hill, New York.

Shekarchi, S., Savas, O. and Gollahalli, S. R.,1988, "Structure of a Split Gas Flame," Combustion and Flame, 73:221-232.

Tang, L., Crowe, C. T.,Chung, J. N., and Trout, T .R., 1990, "A Numerical Model for Droplets Dispersing in a Developing Plane Shear Layer Including Coupling Effects," Numerical Methods for Multiphase Flows, ASME FED, 91:27-33.

Wygnanski, I., Oster D., Fiedler, H., Dziomba, B., 1979, "On the Perseverance of a Quasi - Two - Dimensional Eddy - Structure in a Turbulent Mixing Layer", J. Fluid Mech., 93: 325 - 335.

Yang, Y., Chung, J. N., Trout, T. R., and Crowe, C. T., 1990, "The Influence of Particles on The Spatial Stability of Two-Phase Mixing Layers," Phys. Fluids A, 2, pp. 1839-1845.

Yates, L. A., 1994, "Images Constructed from Computed Flow Fields," NASA-CR-194397

Yule, A. J., 1978, "Large-Scale Structure in The Mixing Layer of a Round Jet," J. of Fluid Mechanics, 89: 413 - 432

Table F.1 Experimental conditions for unperturbed shear layer.

RUN	1	2	3	4	5	6	7	8	9	10
NAME	CR5& (X)	HX	HR10	HR8 (HRS1)	HR12	CR4	CR6	RS1	RUN	RL1
upper vel.U1,m/s	19.6	25.3	20.3	12.3	24.0	21.2	18.0	12.8	17.6	20.4
lower vel.U2,m/s	6.3	8.9	5.0	4.6	17.3	14.2	14.5	4.6	5.5	4.9
upper temp.T1,K	301	360	360	385	360	297	299	298	299	297
lower temp.T2,K	299	314	305	307	294	298	300	298	299	297
vel ratio r=U2/U1	0.32	0.35	0.25	0.37	0.72	0.67	0.81	0.36	0.31	0.24
$\frac{U1-U2}{U1+U2}$	0.51	0.48	0.6	0.46	0.16	0.2	0.11	0.47	0.52	0.61
spreading rate, δ'_w	0.107	0.088	0.084	0.099	0.049	0.056	0.046	0.088	0.071	0.092
Richardson number		0.0005	0.0006	0.0034	0.0033					

Table F.2 Experimental conditions for perturbed shear layer.

RUN	1	2	3	4	5	6
Name	cold1 cold1p	cold2 cold2p	hot1 hot1p	hot2 hot2p	cmb1 cmb1p	cmb2 cmb2p
upper vel.U1,m/s Renolds #	6.3 16070	12.5 31890	6.3 16070	12.8 32650	6.3 16070	12.5 31890
lower vel.U2,m/s Renolds #	3.0 7650	4.0 10200	4.0 1090	5.5 1500	5.0 1360	6.0 1630
upper temp.T1,K	300	301	294	293	301	300
lower temp.T2,K	300	301	1192	1186	1129	1107
vel ratio r=U2/U1	0.48	0.32	0.63	0.43	0.80	0.48
$\frac{U1-U2}{U1+U2}$	0.35	0.52	0.22	0.40	0.12	0.35
Richardson number			1.11	0.112	3.34	0.134
Stokes Number	1.6	4.2	0.6	1.8	0.3	1.4
spreading rate,δ'_w	0.051	0.076	0.034	0.054		

Table F.3 Characteristics of particulate loading

Particles

Continuous Phase	MgO (2±1 μm)		
Coal:	Bituminous, Illinois No. 3		
Size	38±5 ; 68±5 μm		
Composition	Moisture	5.36 %	
	Volatile matter	39.20 %	
	Fixed Carbon	52.48 %	
	Ash	8.36 %	
	Carbon	73.82 %	
	Hydrogen	4.94 %	
	Nitrogen	1.68 %	
	Oxygen	8.75 %	
	Total sulfur	2.27%	
Calorific Value		31.24 Mj/kg	
Particle Density			
	Coal	1.4 kg/m^3	
	MgO	3.5 kg/m^3	
Particle loading	(top stream)	0.01	kg/kg
Number density		10^9 / m^3	

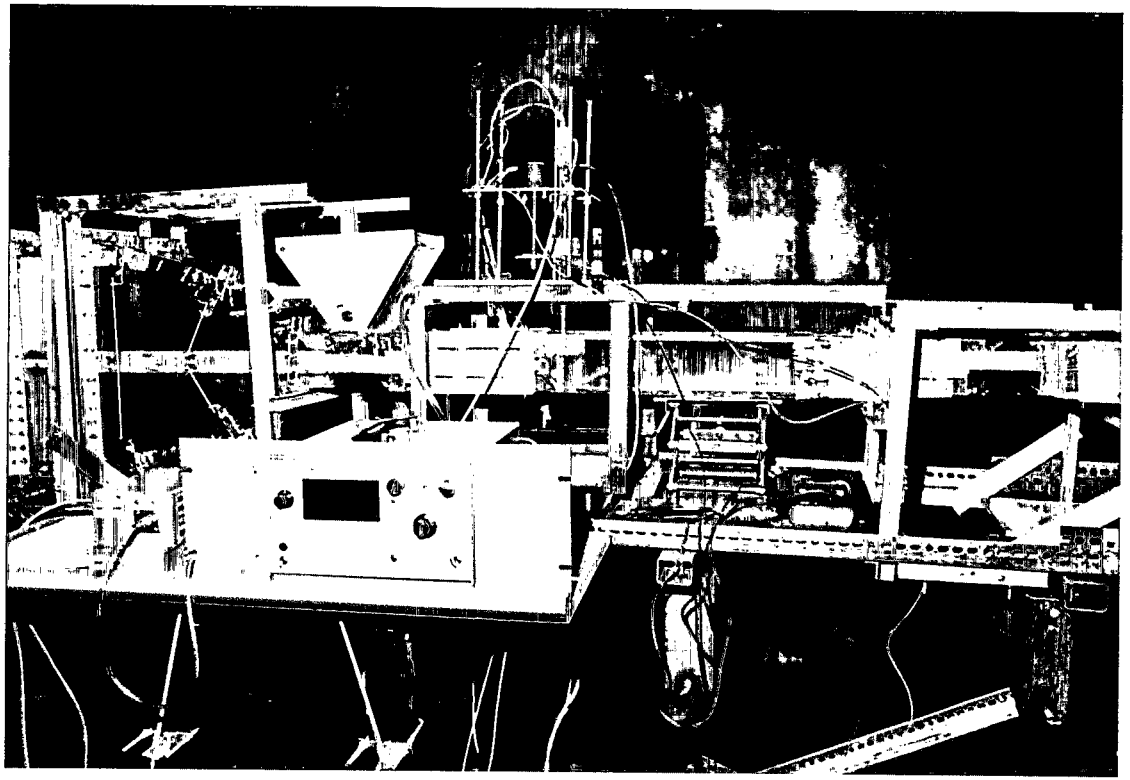

Ph. F.1. A view of the shear layer tunnel showing the large flow rate particle feeder and the test section

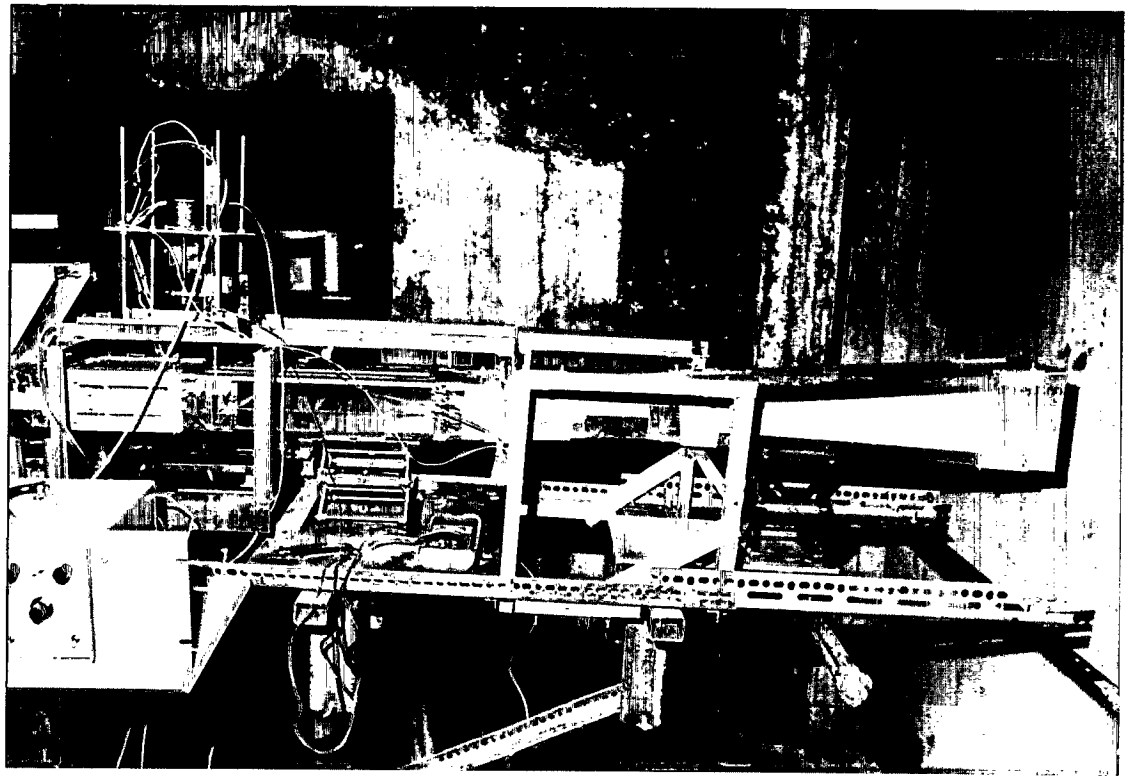

Ph. F.2. A view of the apparatus showing the test section and the downstream diffuser

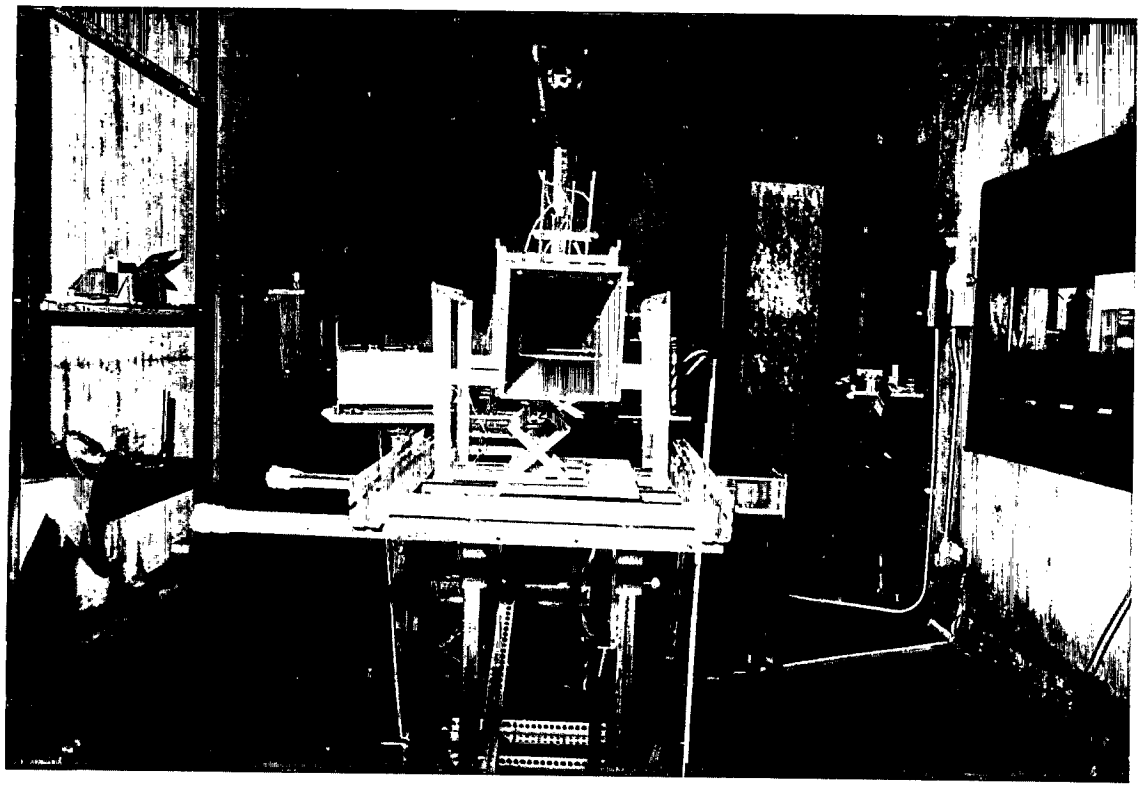

Ph. F.3. A view of the experimental apparatus seen from the exhaust end

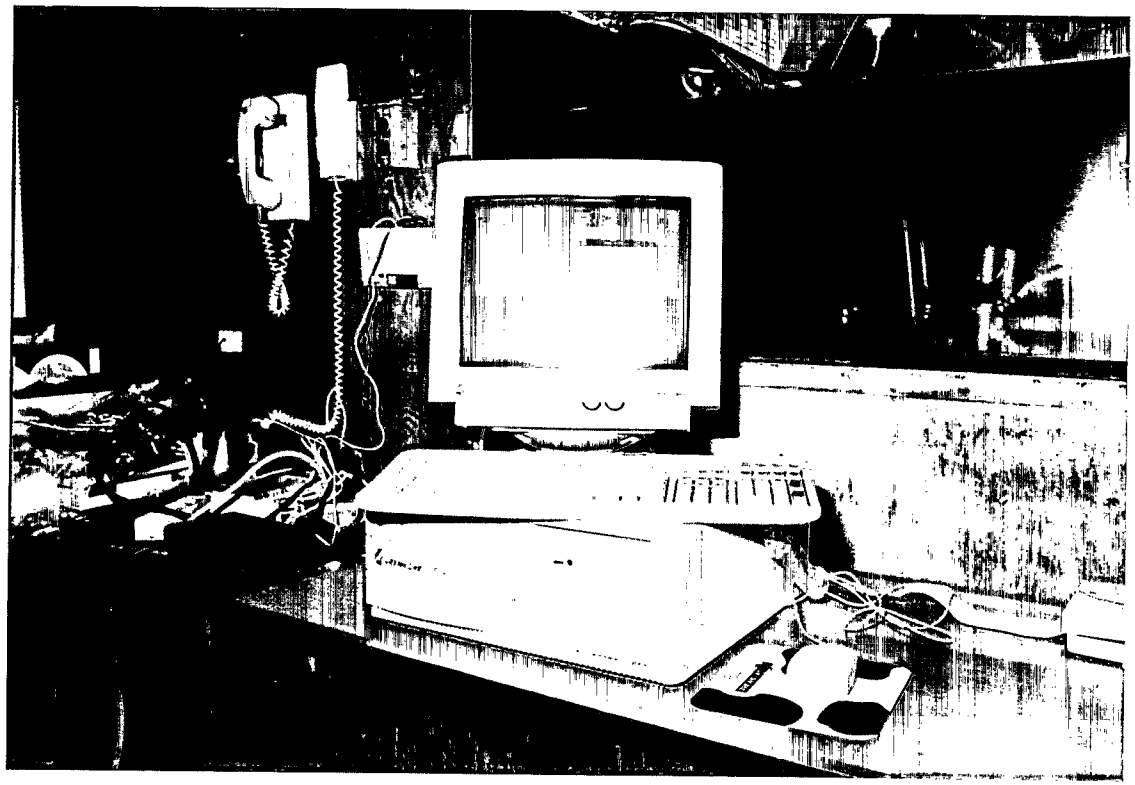

Ph. F.4. A view from the computer in the remote control room and observation window

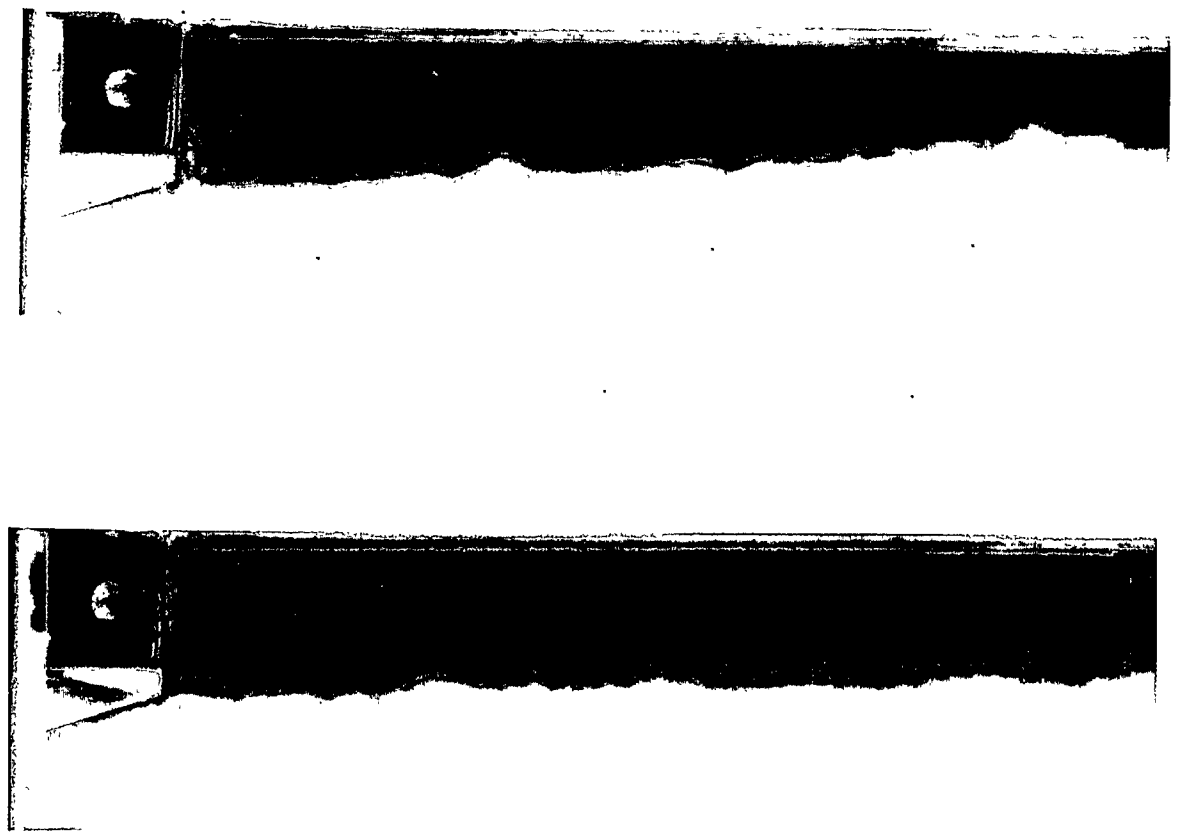

Ph. G.1. Smoke flow pattern in the homogeneous shear layer of unheated streams (top: Run 1; bottom : Run 7 -see Table F.1. for conditions) ; smoke was introduced into the bottom stream.

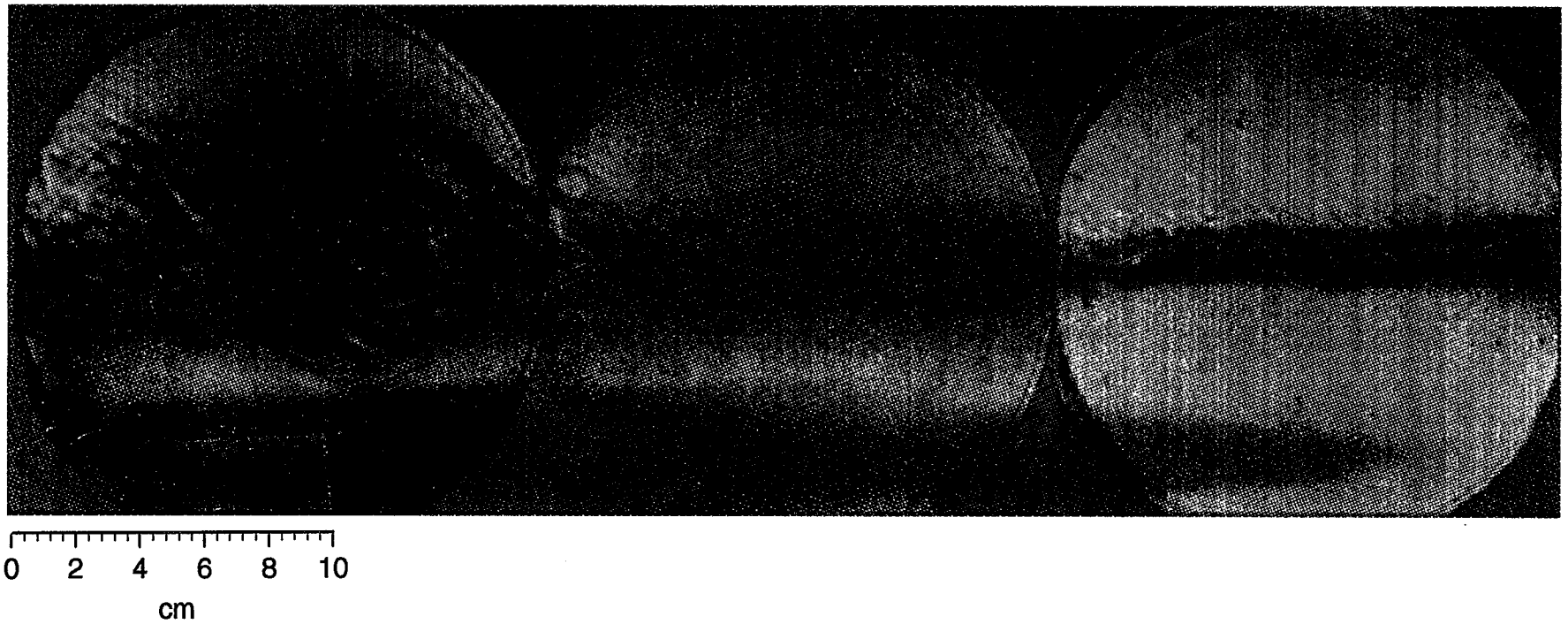

Ph. G.2. Schlieren picture of the homogeneous shear layer when the bottom stream was heated (hot run 1 -- see Table F.2 for the conditions)

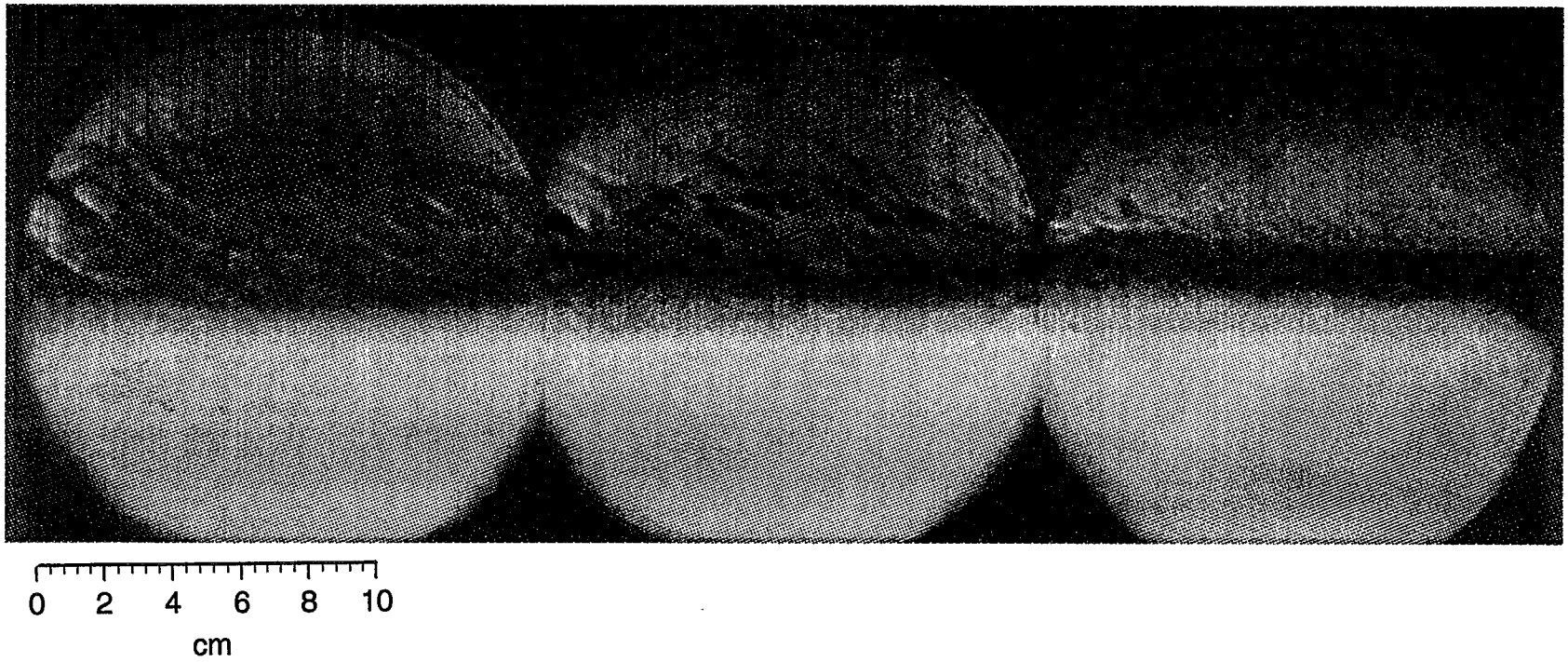

Ph. G.3. Schlieren picture of the homogeneous shear layer when the bottom stream consisted of a flame (comb run 1 -- see Table F.2 for the conditions)

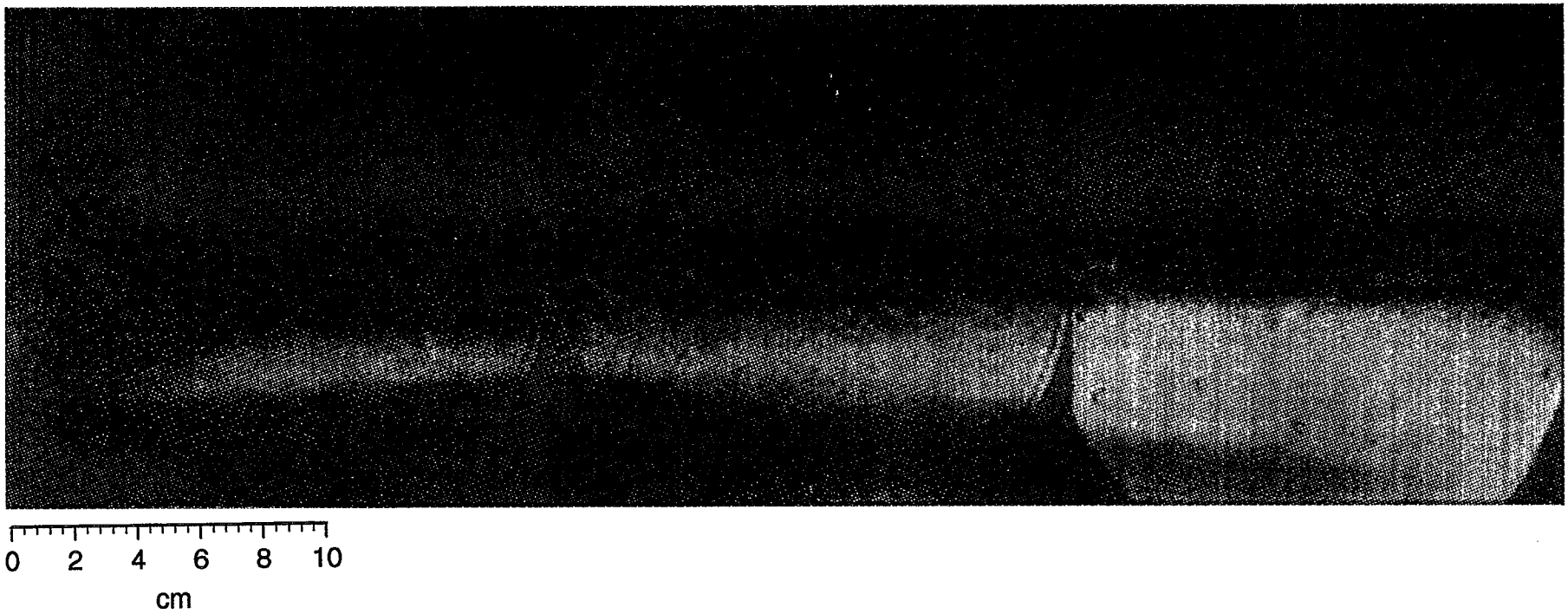

Ph. G.4. Schlieren picture of the heterogeneous shear layer when the bottom stream was heated and particles were added to the top stream (hot run 1 -- see Table F.2 for the conditions)

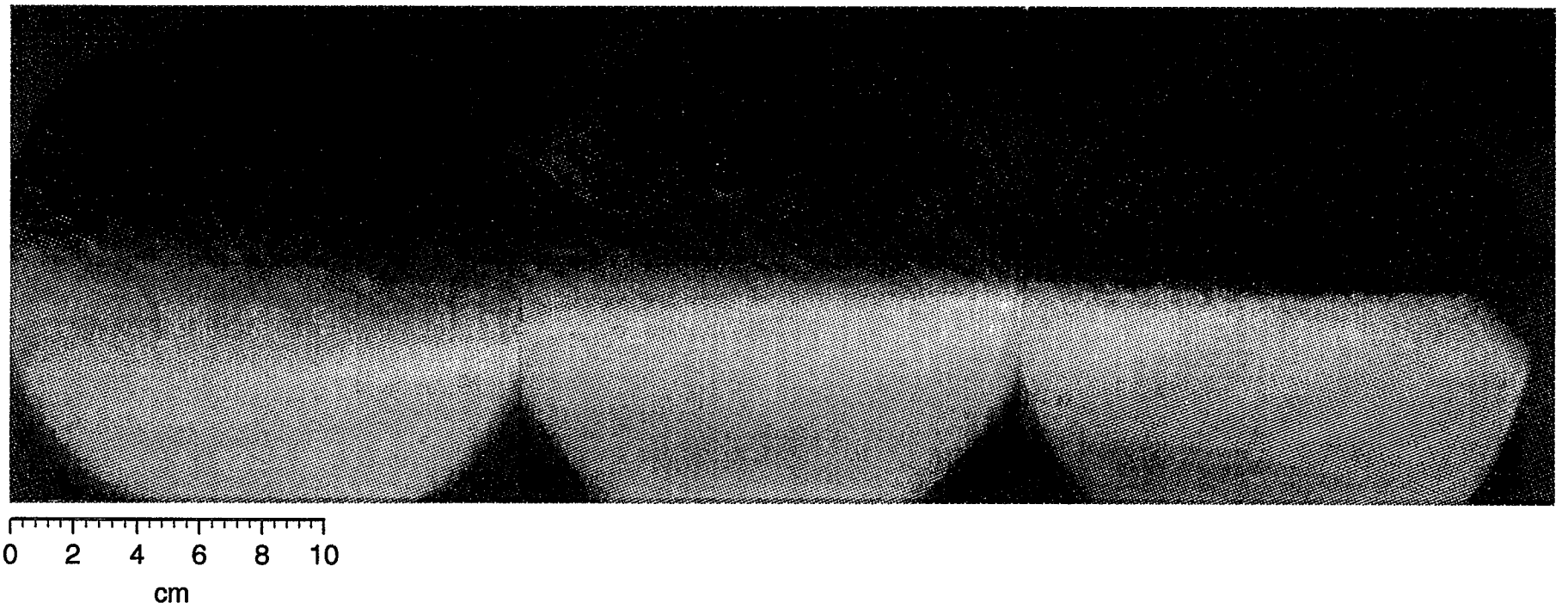

Ph. G.5. Schlieren picture of the heterogeneous shear layer when the bottom consisted of a flame and particles were added to the top stream (comb run 1 -- see Table F.2 for the conditions)

Combustion Experiments

(U1 = 12.5 m/s U2 = 5.0 m/s)

Bottom: Natural Gas Flame only t = 1 s

Bottom: Natural Gas Flame
Top: Bitminous Coal particles; 38 μm t= 1/500 s

Bottom: Natural Gas Flame
Top: Bitminous Coal particles; 38 μm t= 1/1000 s

Ph. G.6. Direct color photographs of the shear layer (top) when the bottom consisted of a flame (middle and bottom) when the bottom consisted of a flame and particles were added to the top stream (comb run 1 -- see Table F.2 for the conditions)

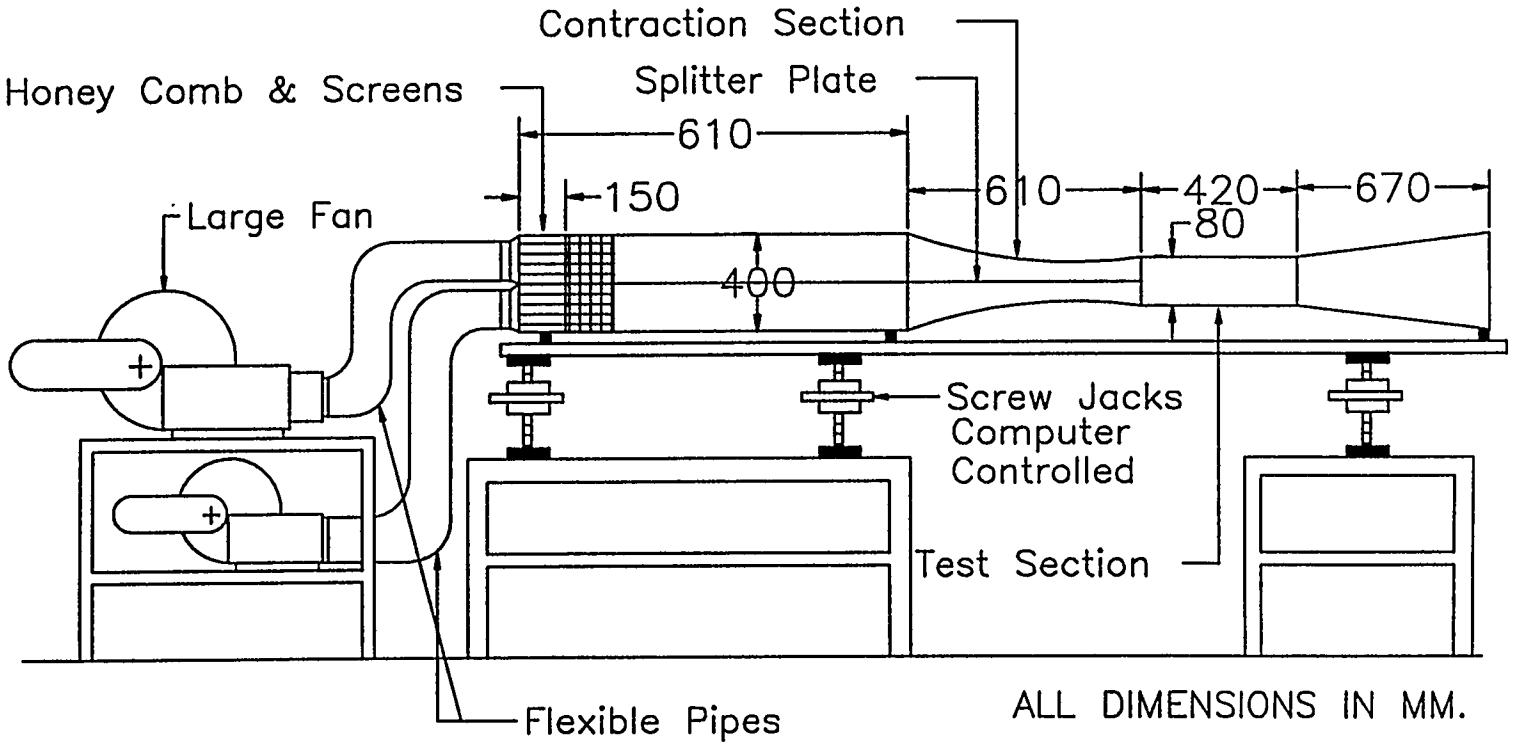

Fig. F.1. **Schematic diagram of the shear layer tunnel**

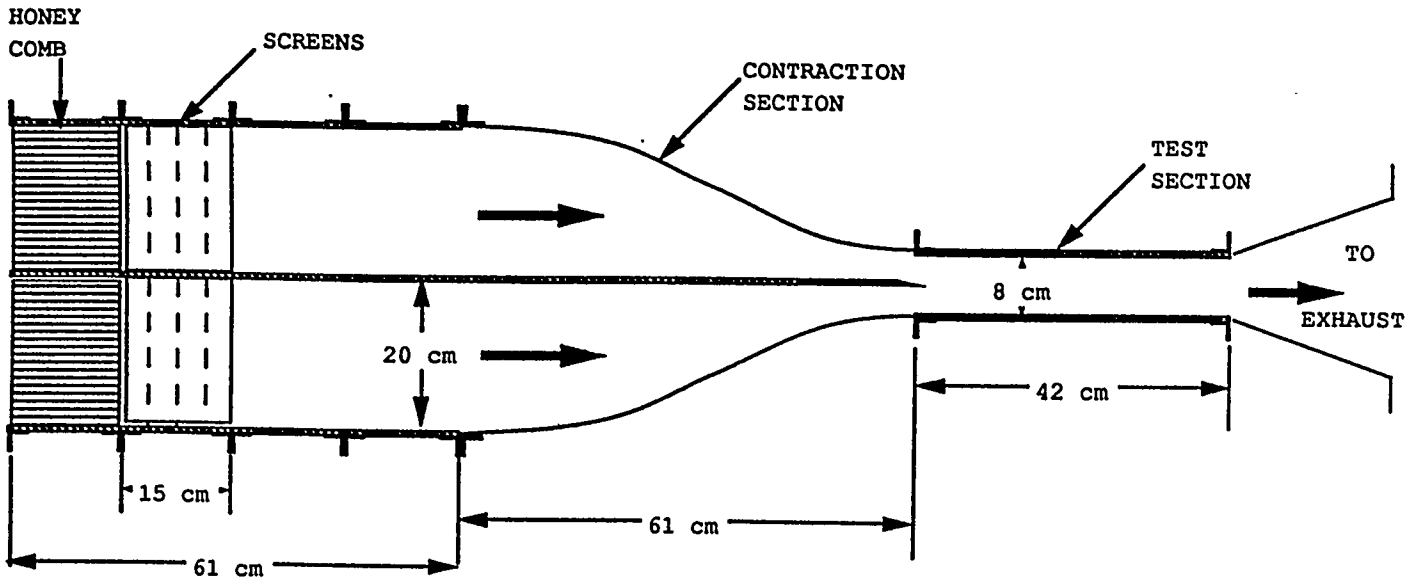

Fig. F.2. **Details of contraction and test sections of the shear layer tunnel**

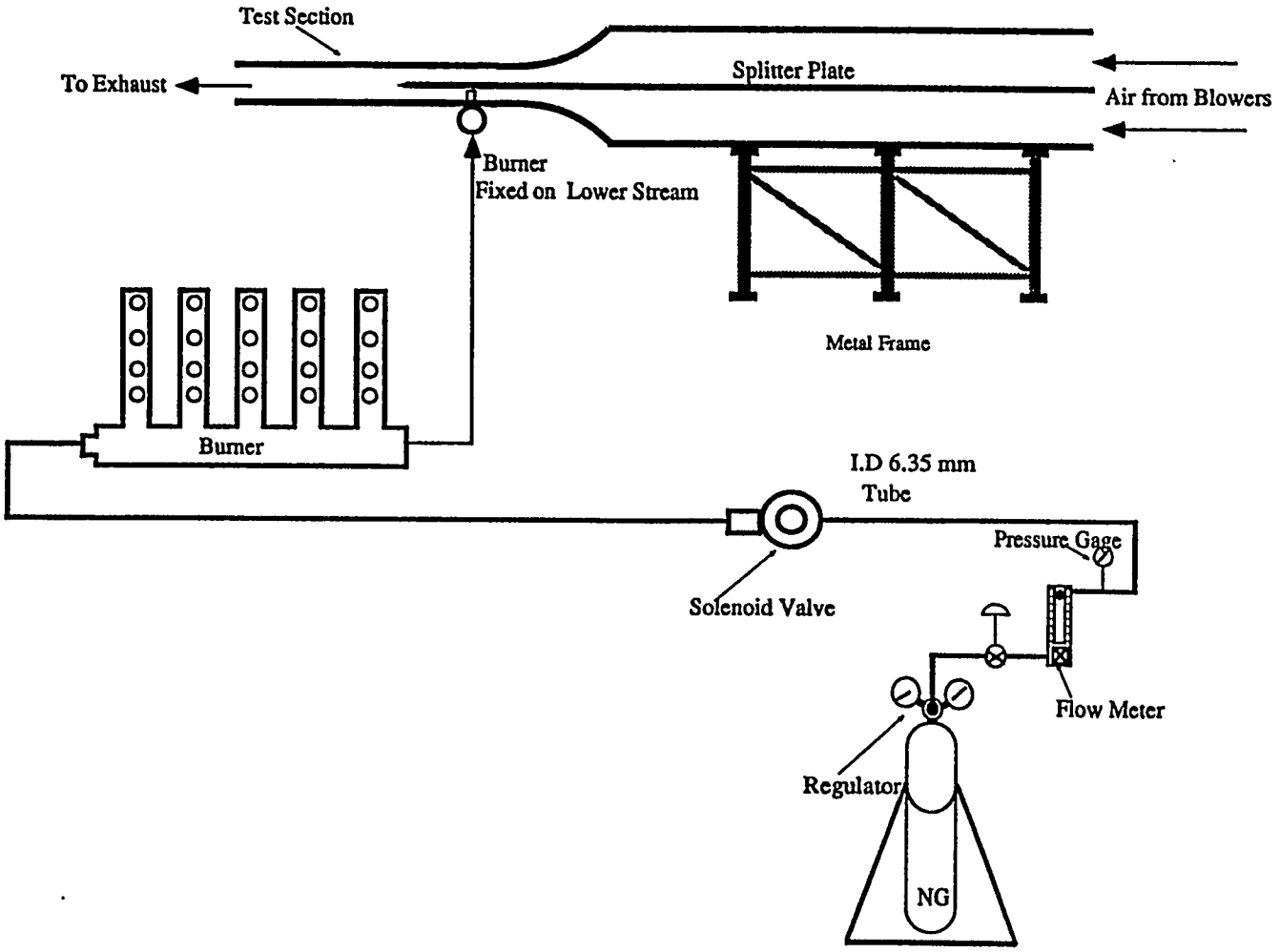

Fig. F.3. Details of the natural gas burner to heat the bottom stream

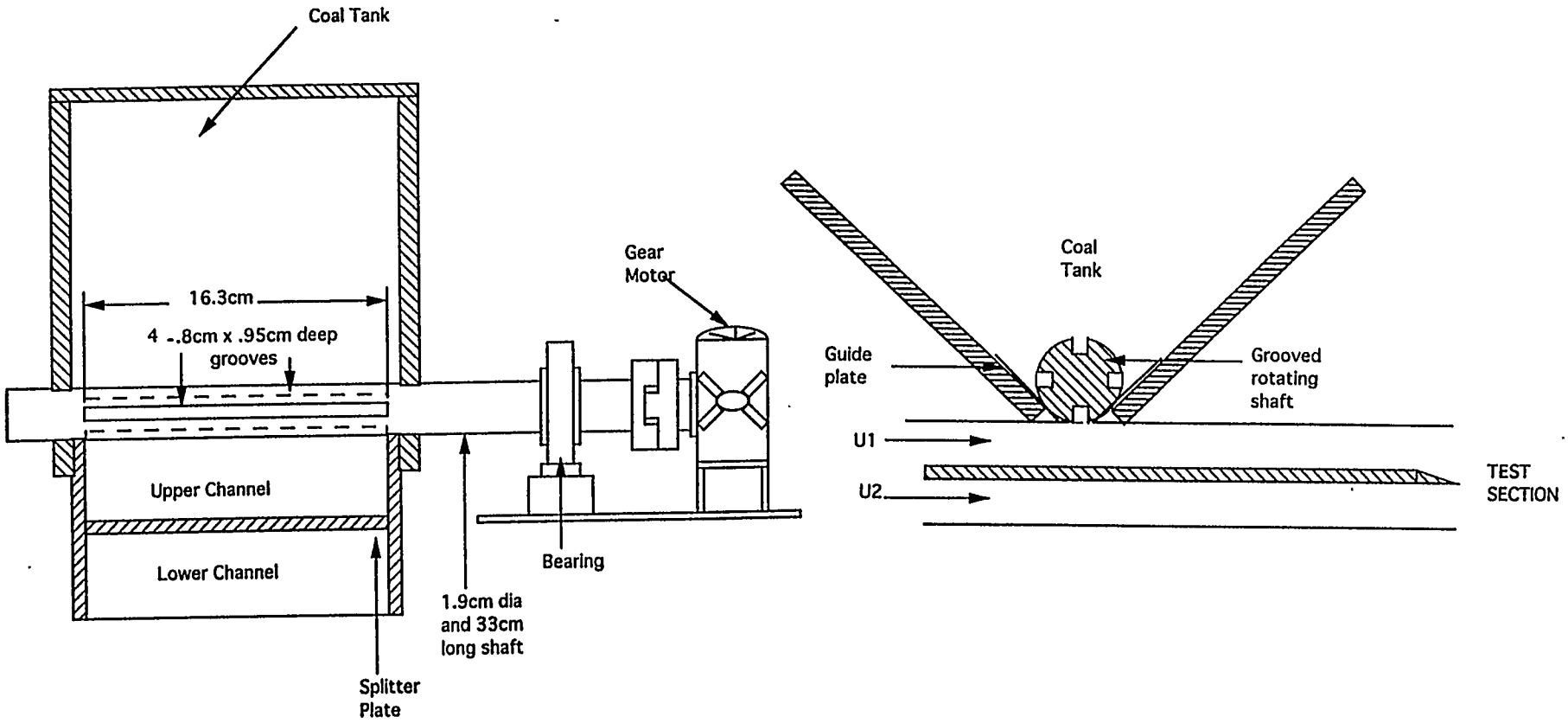

Fig. F.4. High rate particle feeder

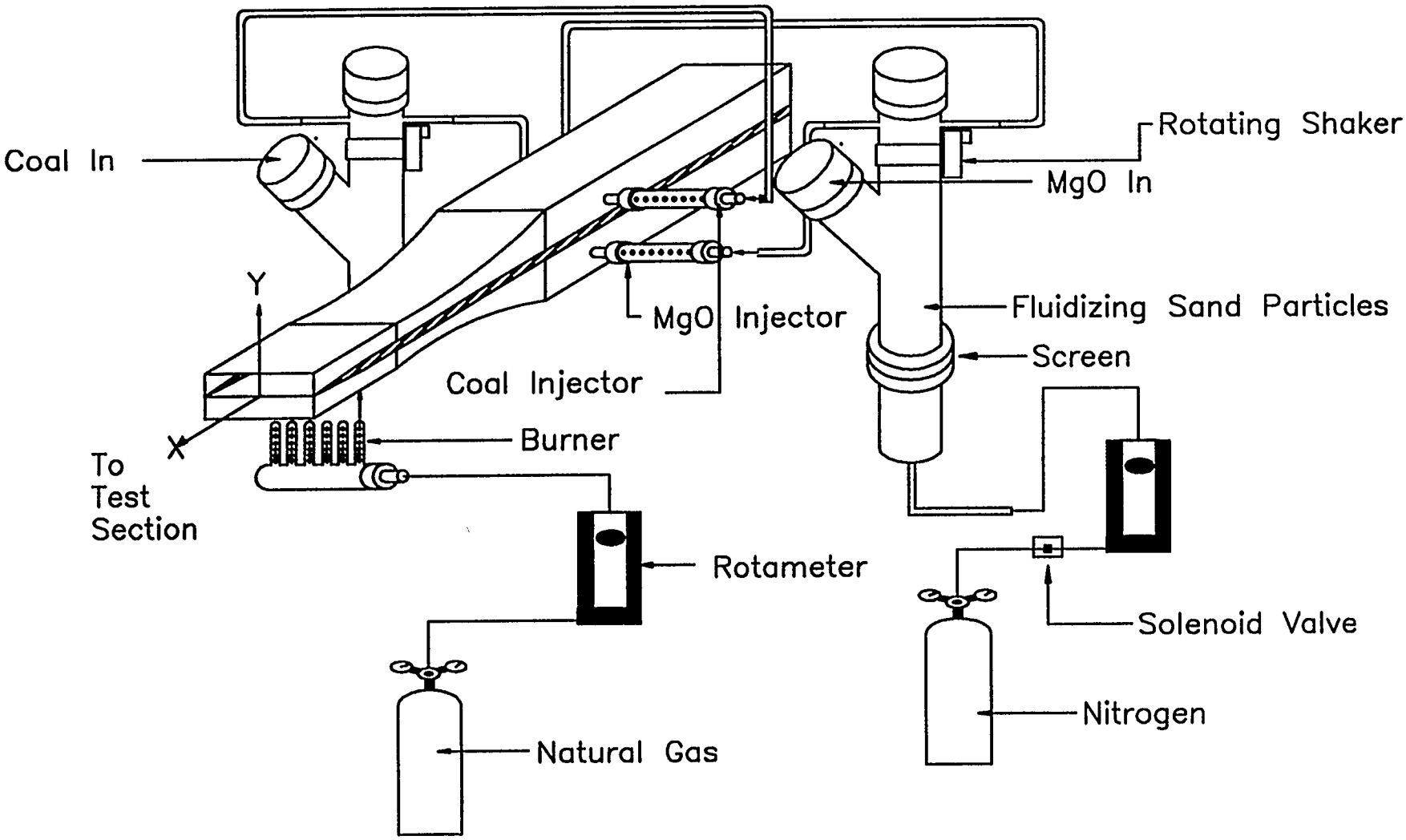

Fig. F.5 **Low rate particle feeders**

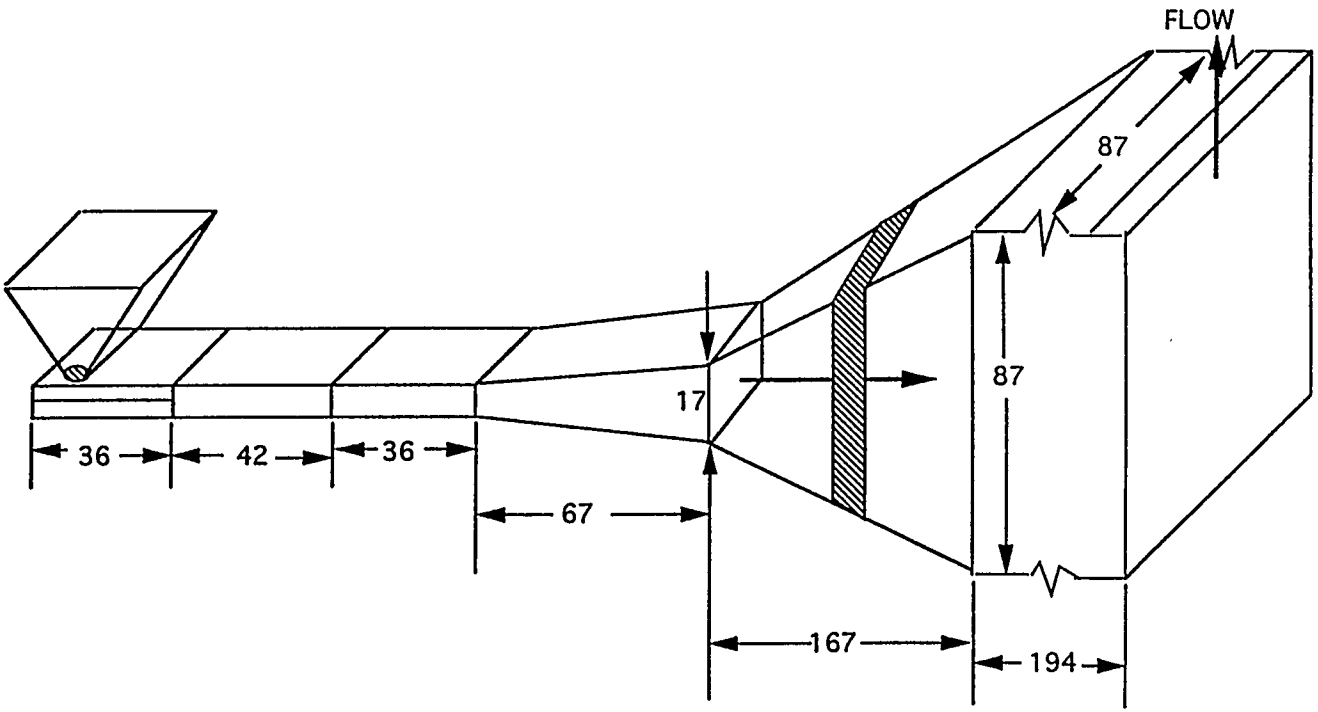

ALL ABOVE DIMENSIONS IN CM

Fig. F.6. **Exhaust and particle filtering system**

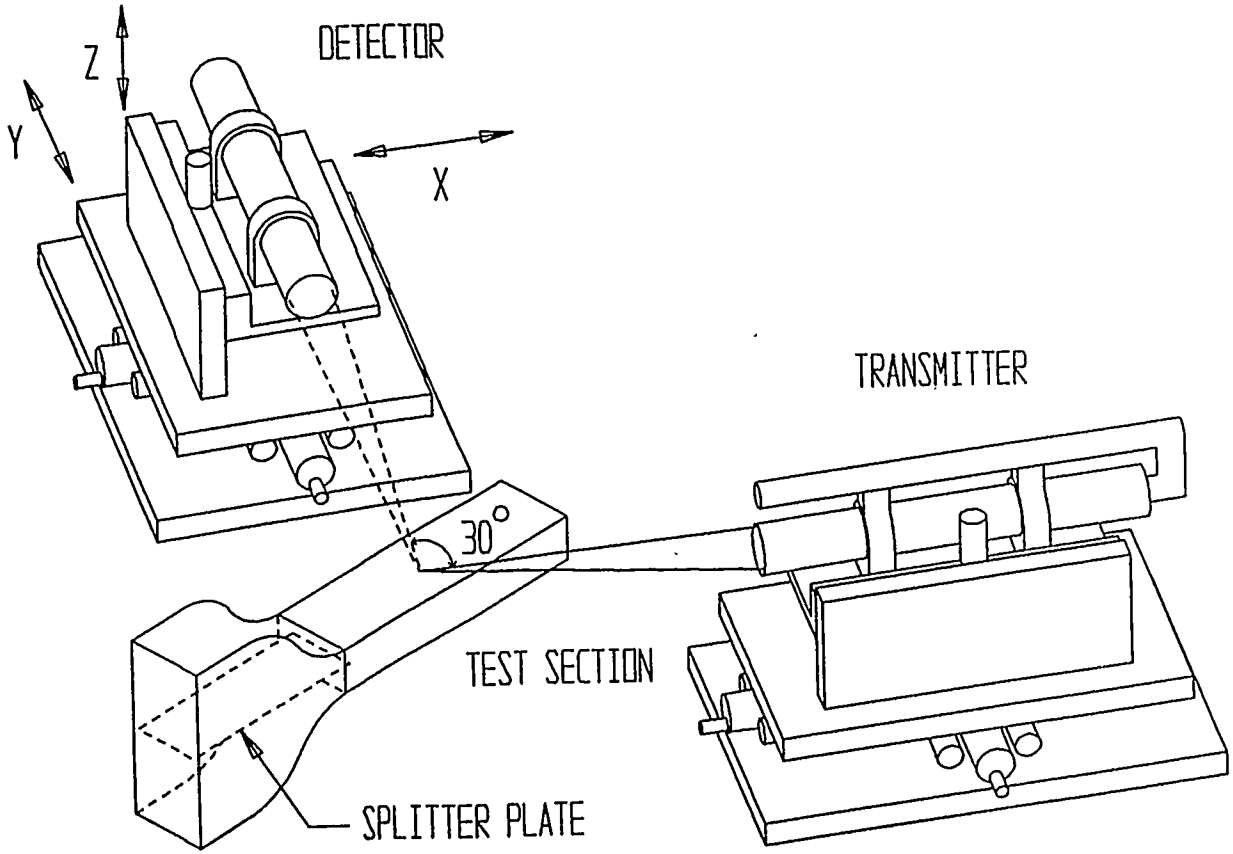

Fig. F.7. **Laser velocimetry system**

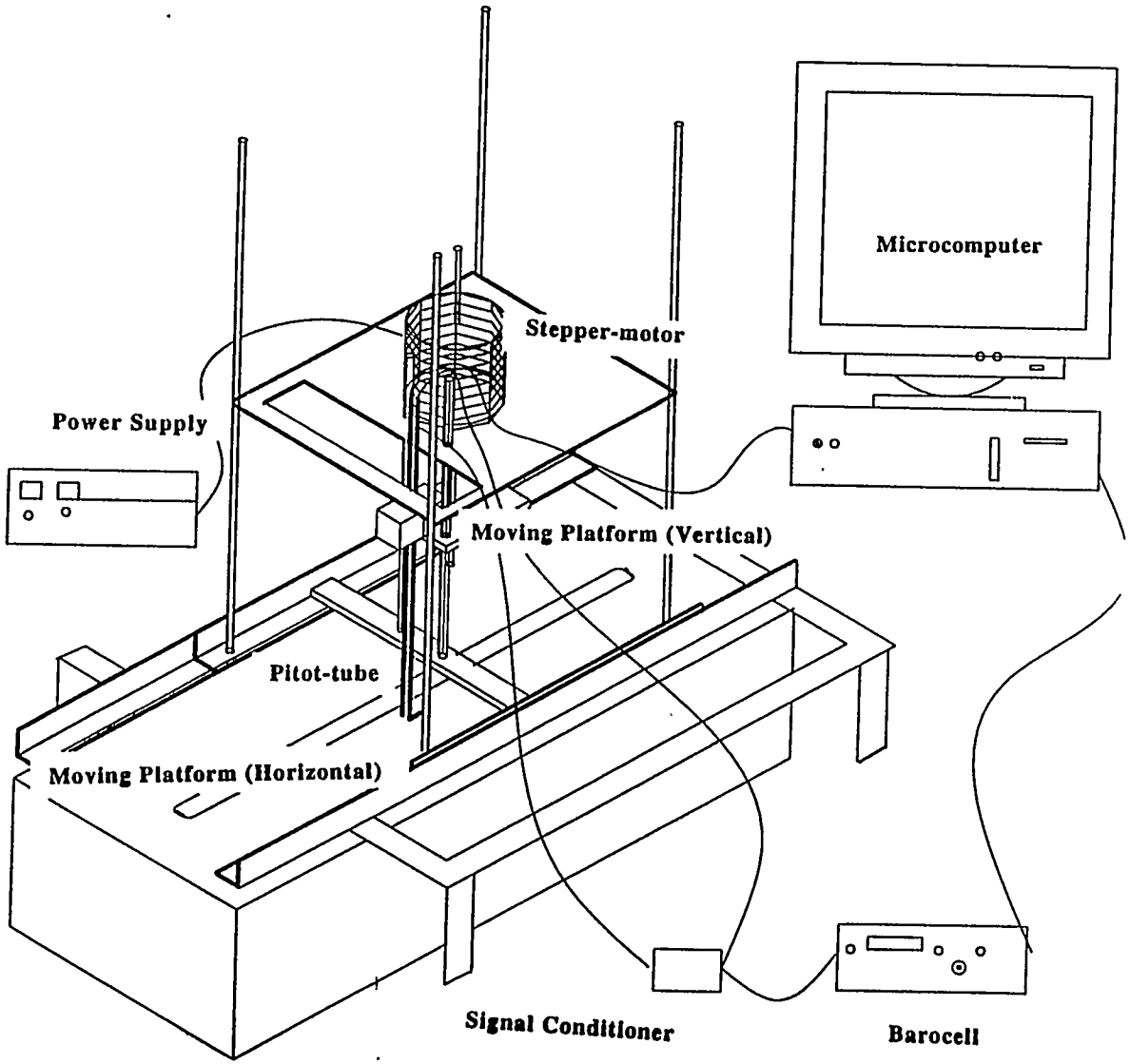

Fig. F.8. Pitot-tube and thermocouple traversing system

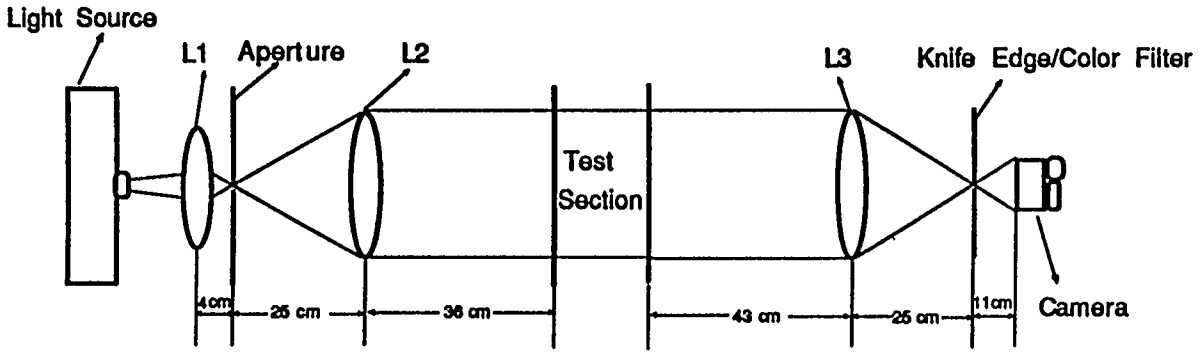

Lens	Type	Diameter	Focal Length
L1	Condenser Lens	5.7 cm	3.8 cm
L2	Collimating Lens	6 cm	25 cm
L3	Decollimating Lens	6 cm	25 cm

Fig. F.9 Schlieren flow visualization system

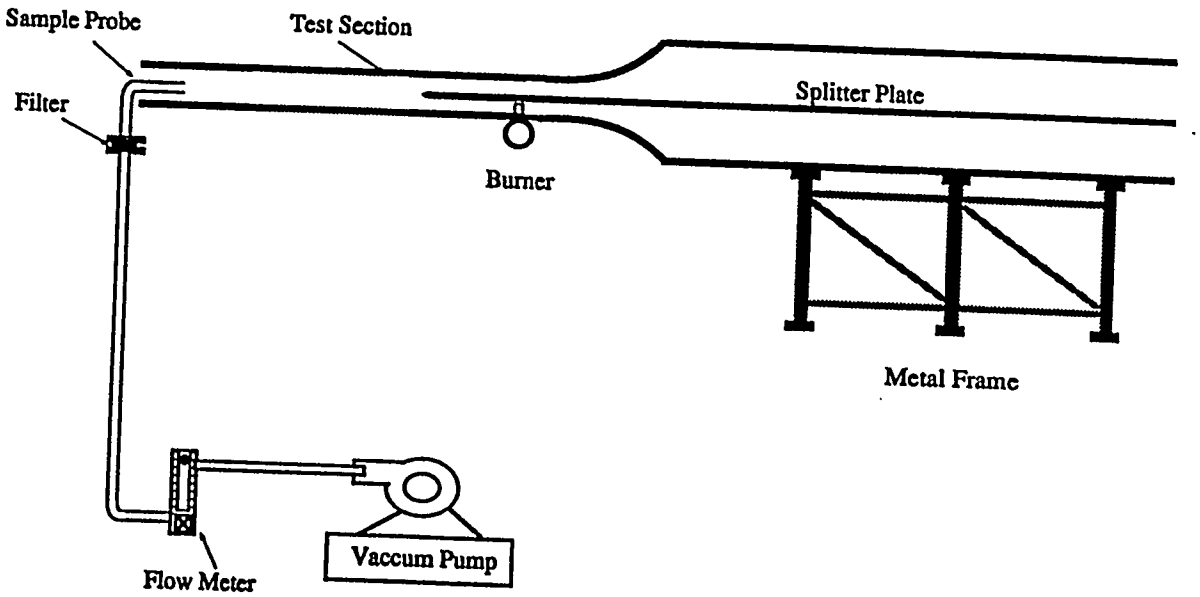

Fig. F.10. Iso-kinetic sampling system

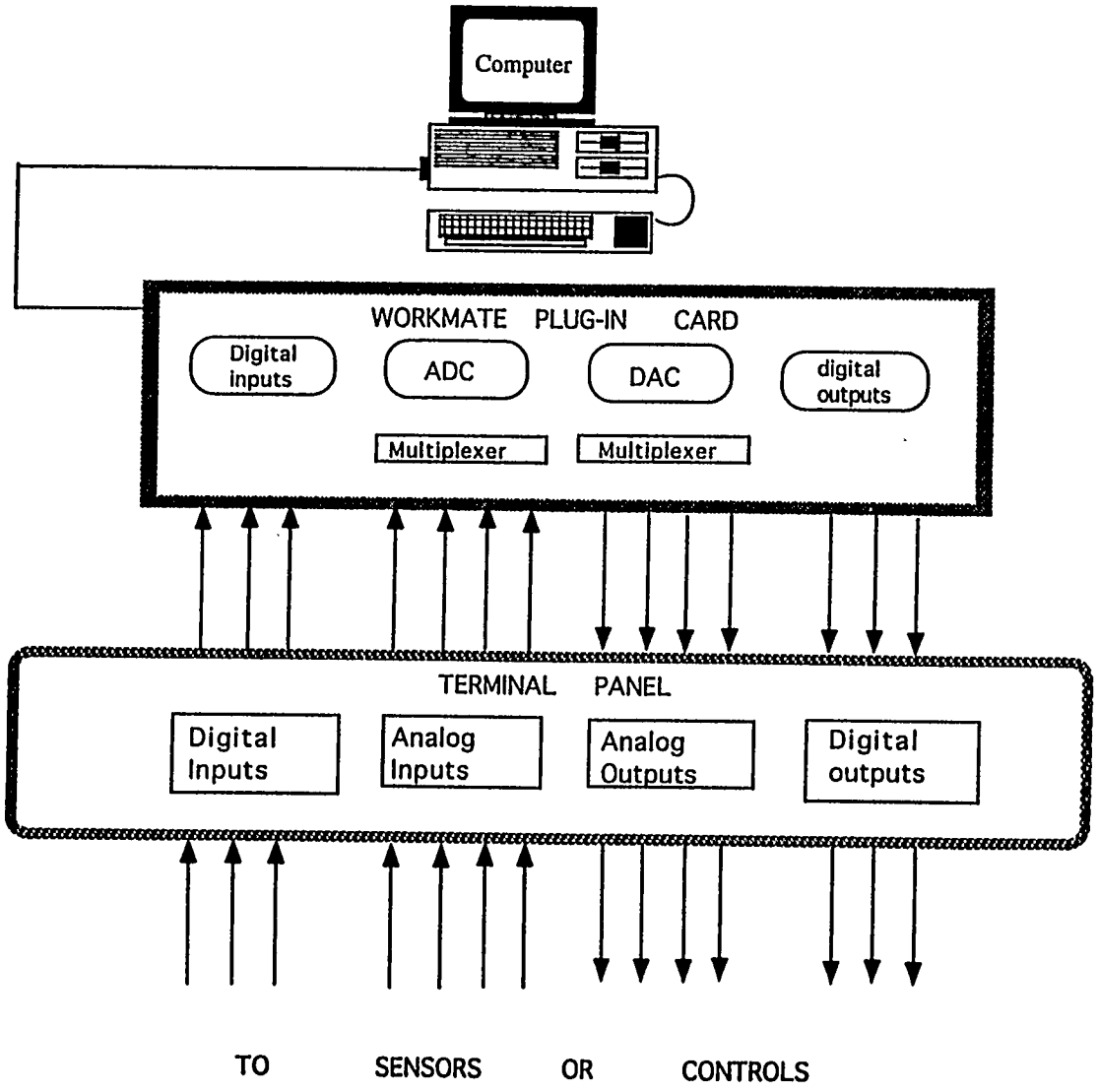

Fig. F.11. Data acquisition system

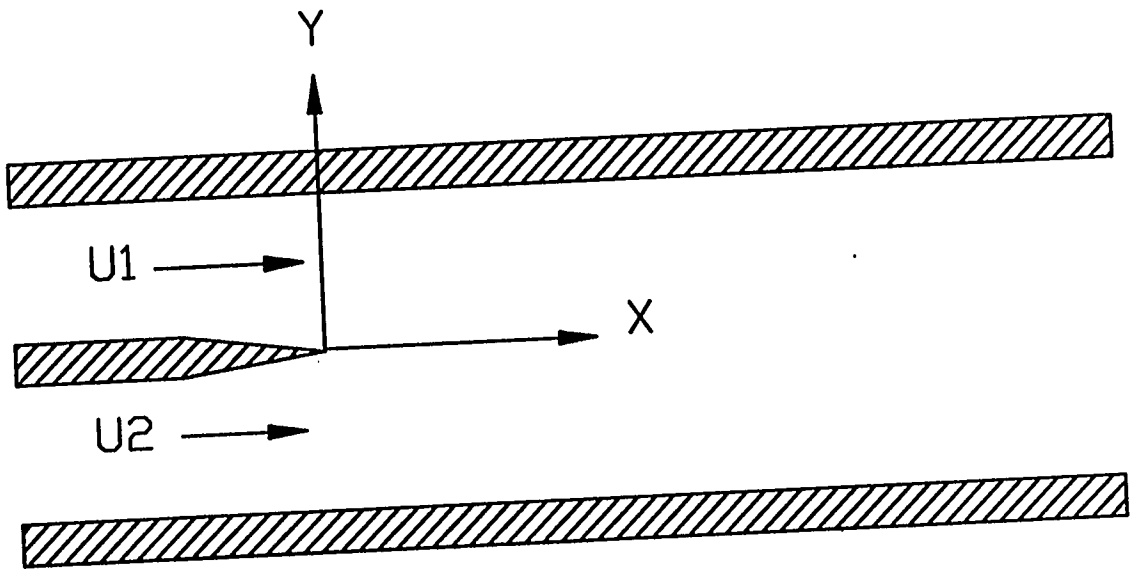

Fig. F.12. **Shear layer coordinate system**

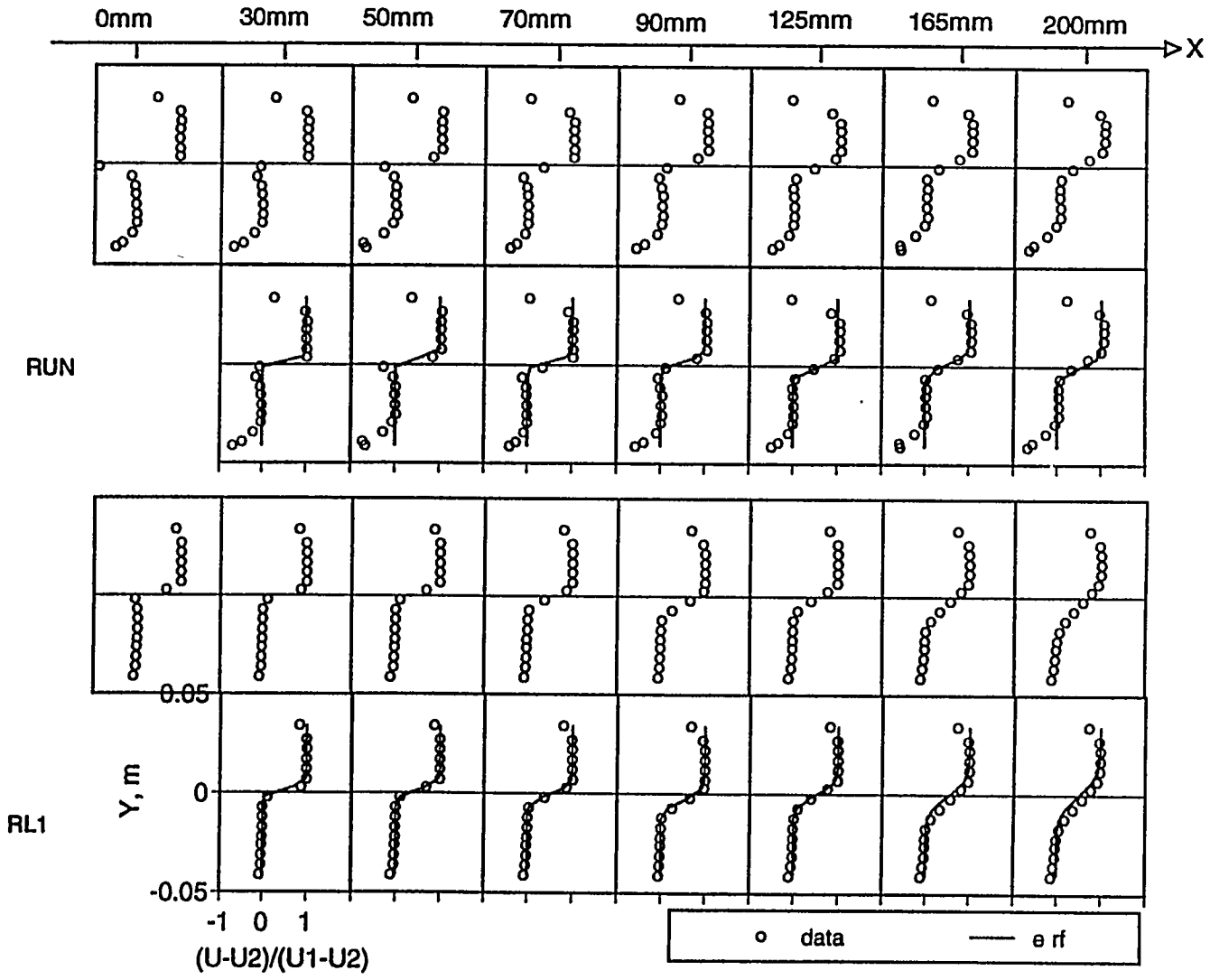

Fig. G. 1. Comparison of velocity profile development with error function variation in the homogeneous shear layer formed by unheated streams (top rows: data only; bottom rows: data are shown by circles and the error function fit shown by a continuous line)

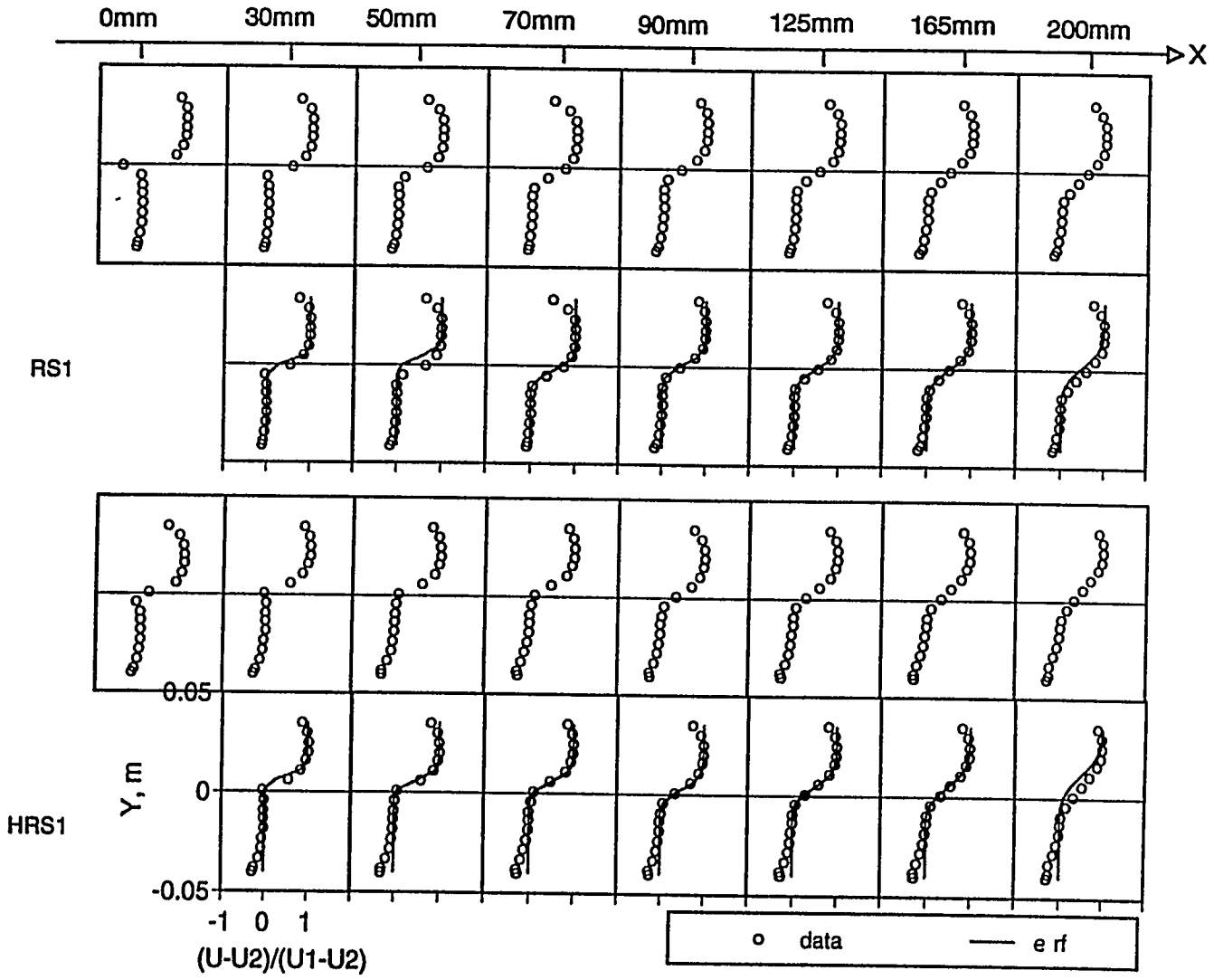

Fig. G.2. Comparison of velocity profile development with error function variation in the homogeneous shear layer when the top stream was heated (top row: data only; bottom row: (data shown by circles and the error function fits shown by a continuous line)

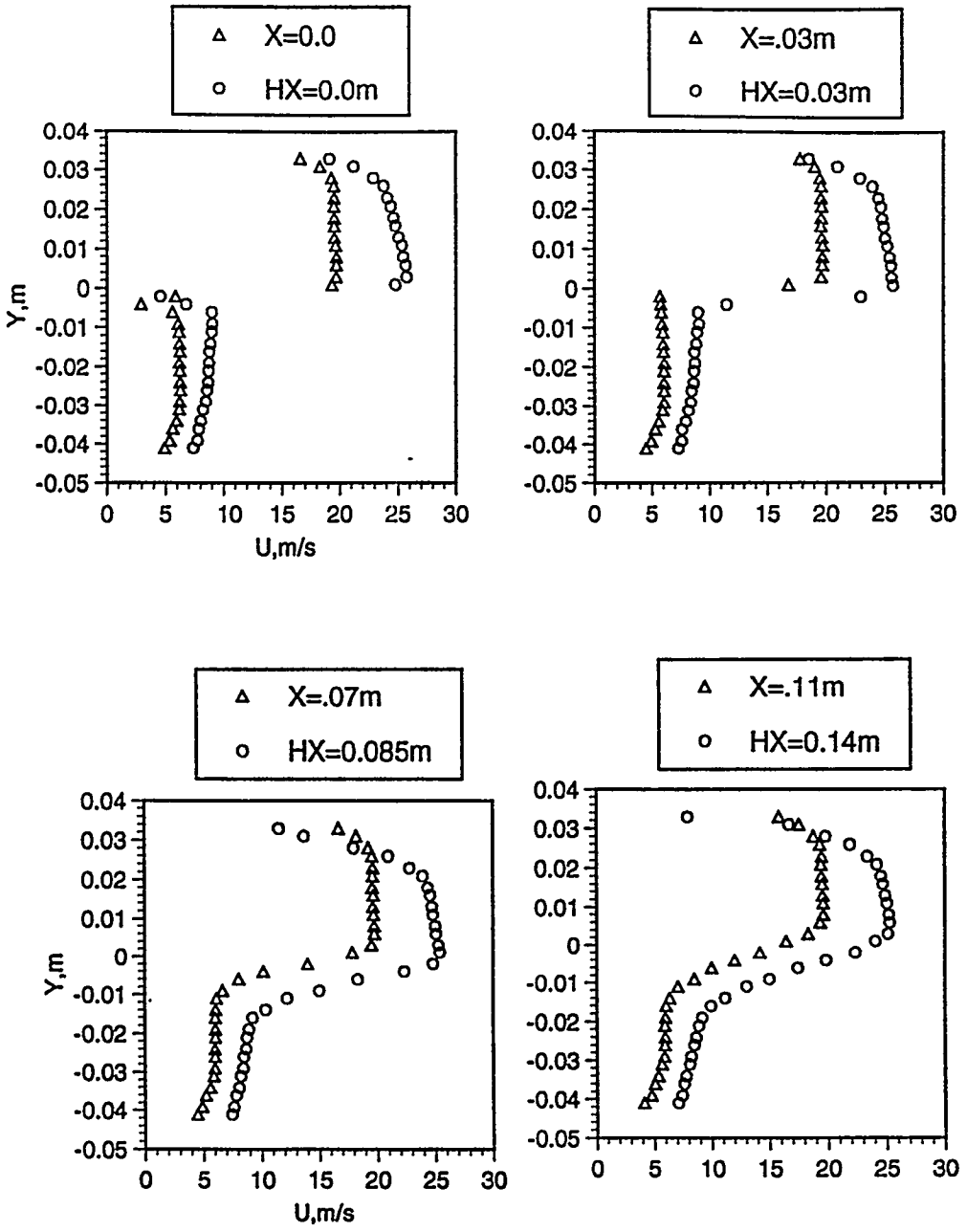

Fig. G.3. Comparison of velocity profile development in homogeneous shear layer with both streams unheated (triangles -run 1) and when only the top stream was heated (circles run 2)

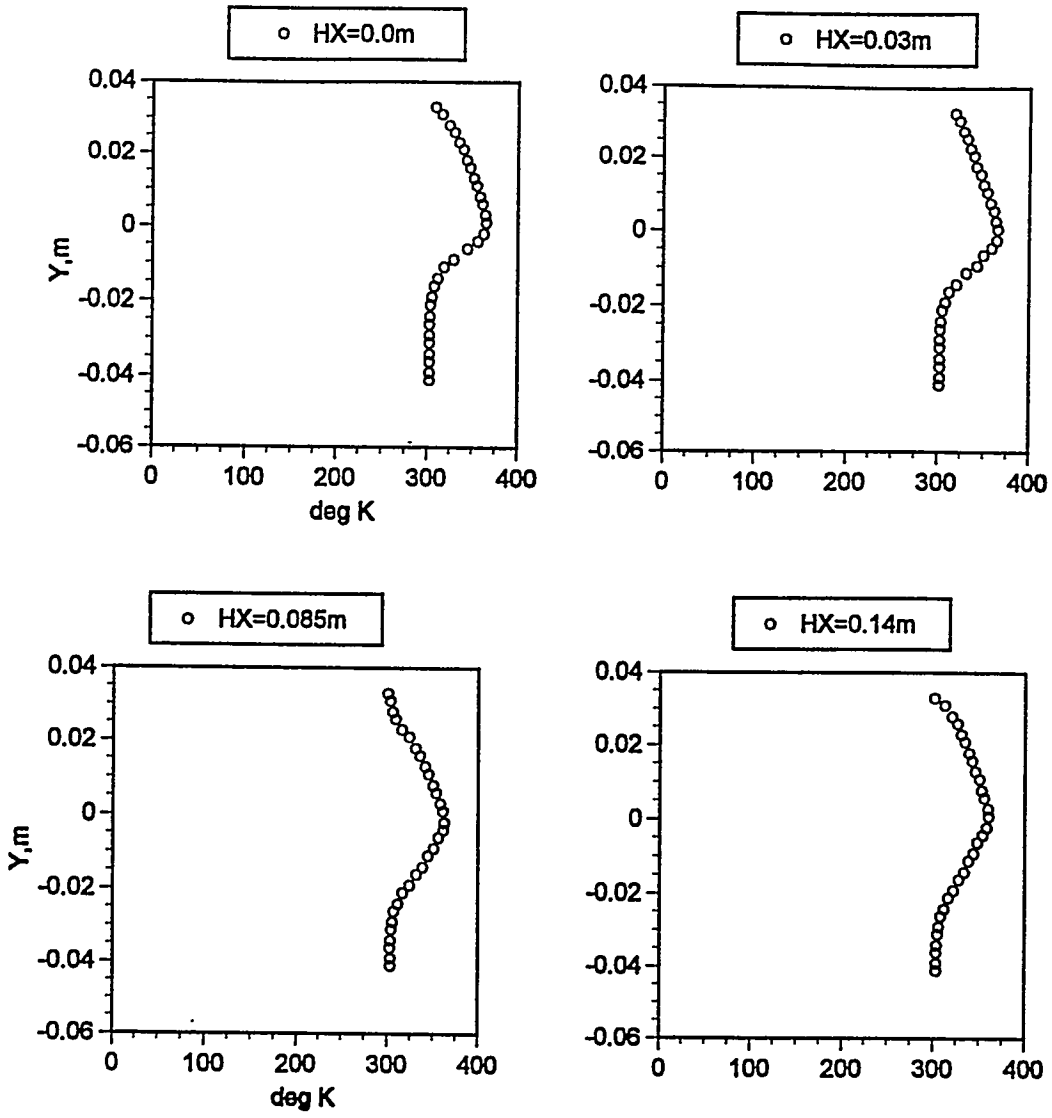

Fig. G.4. Development of temperature profiles in the homogeneous shear layer with only the top stream heated (run 2)

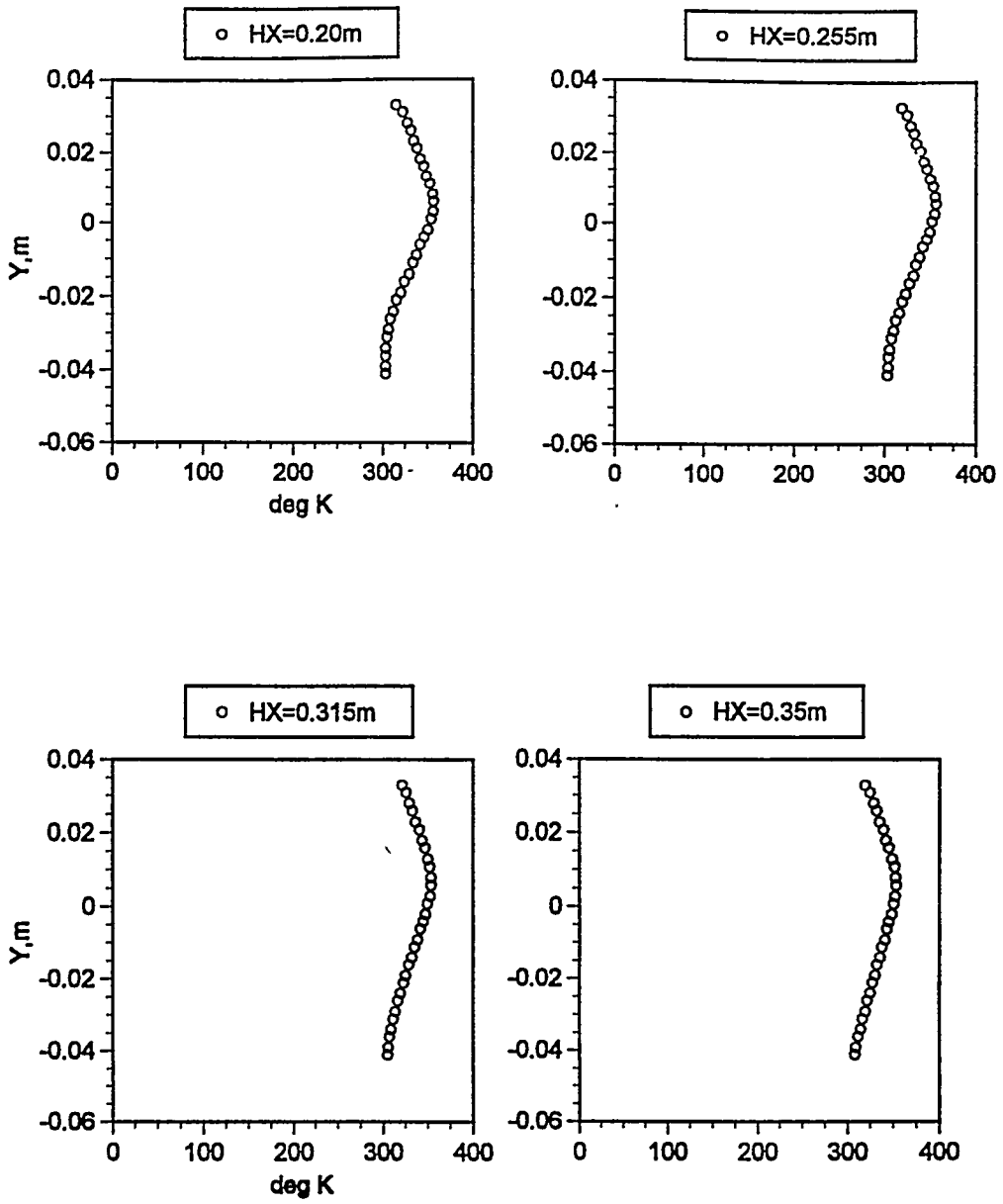

Fig. G.4. Development of temperature profiles in the homogeneous shear layer with only the top stream heated (run 2)

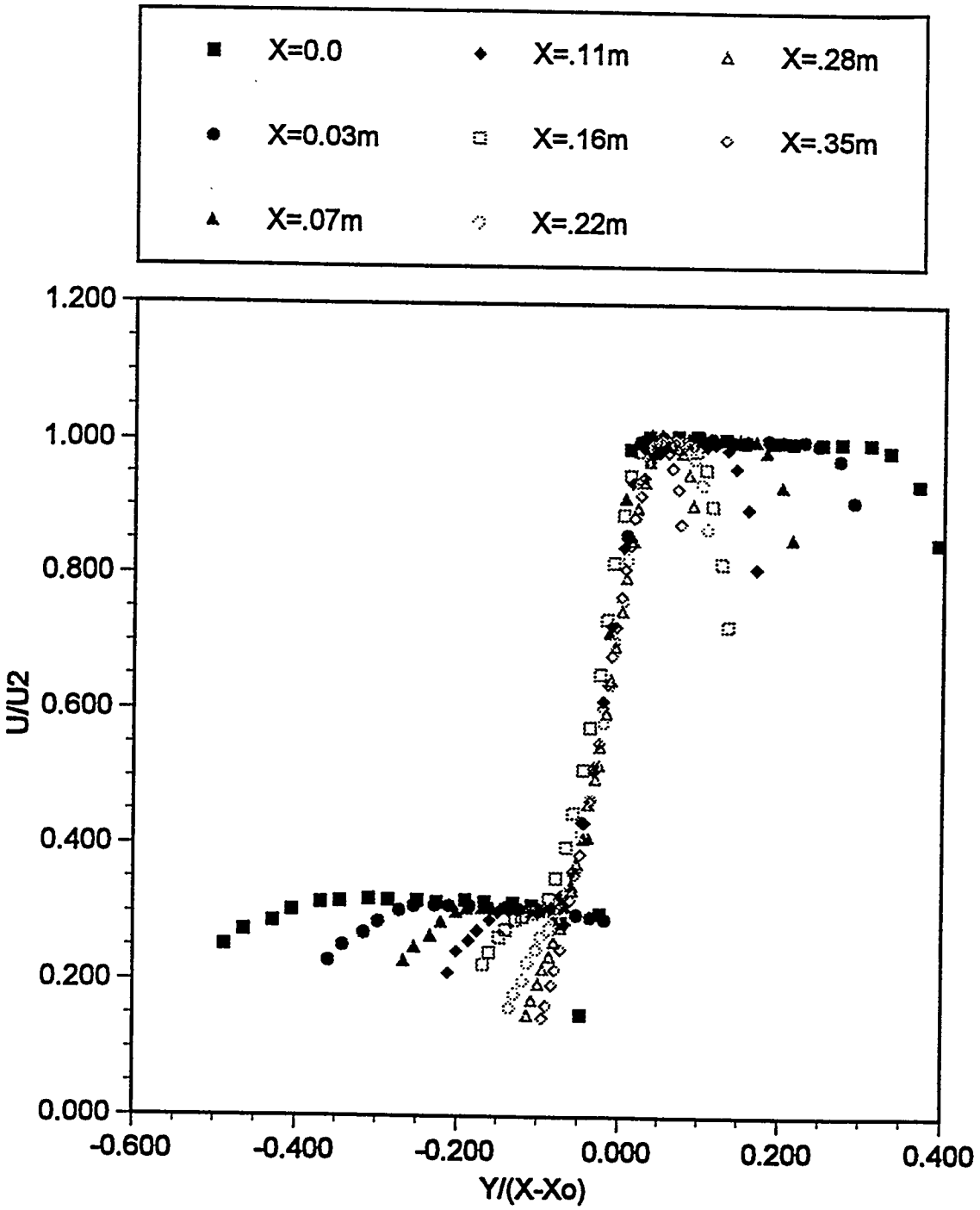

Fig. G.5. Similarity of velocity profiles in the homogeneous shear layers in the unheated case (run 1)

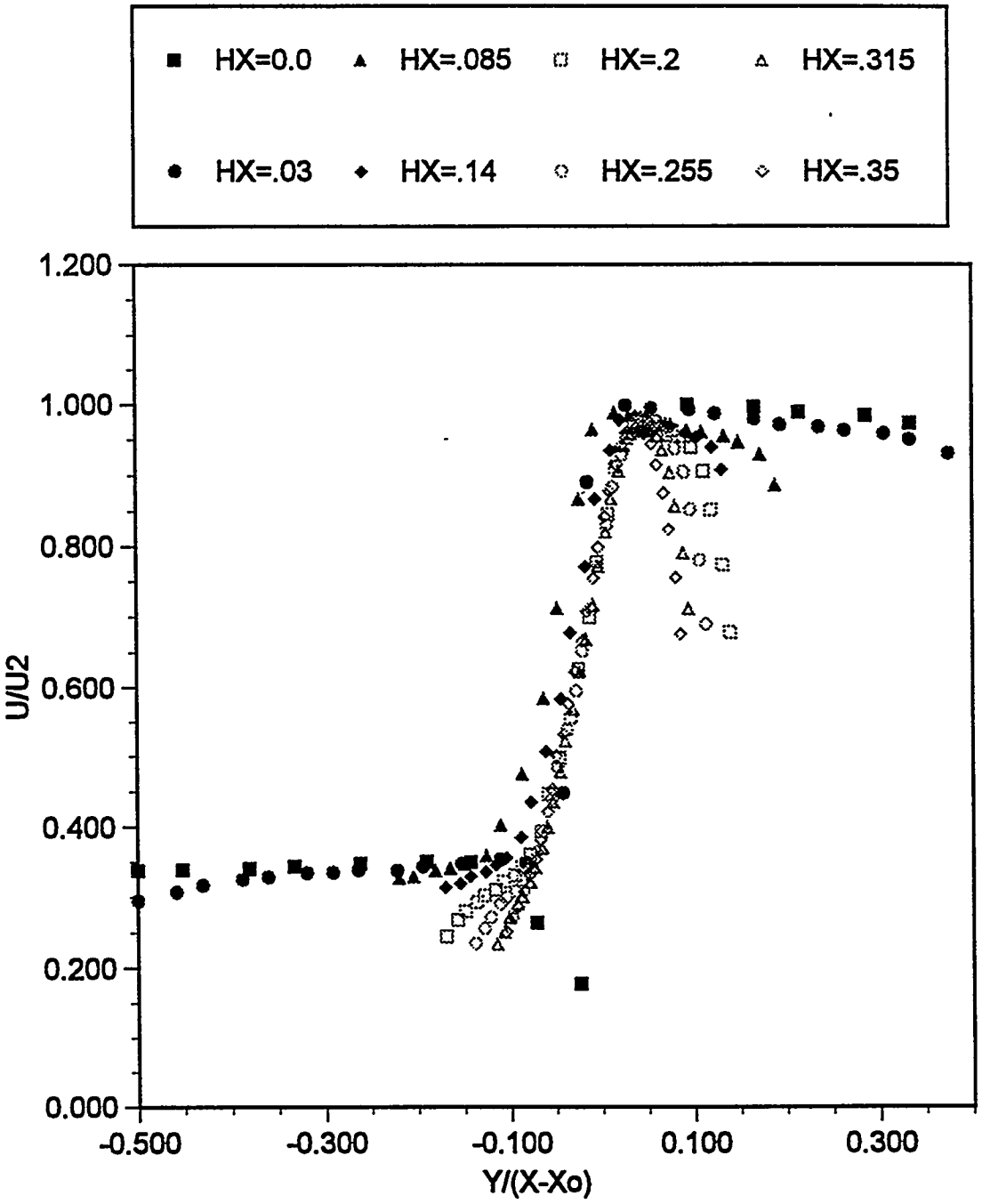

Fig. G.6. Similarity of velocity profiles in the homogeneous shear layers when the top stream was heated (run 2)

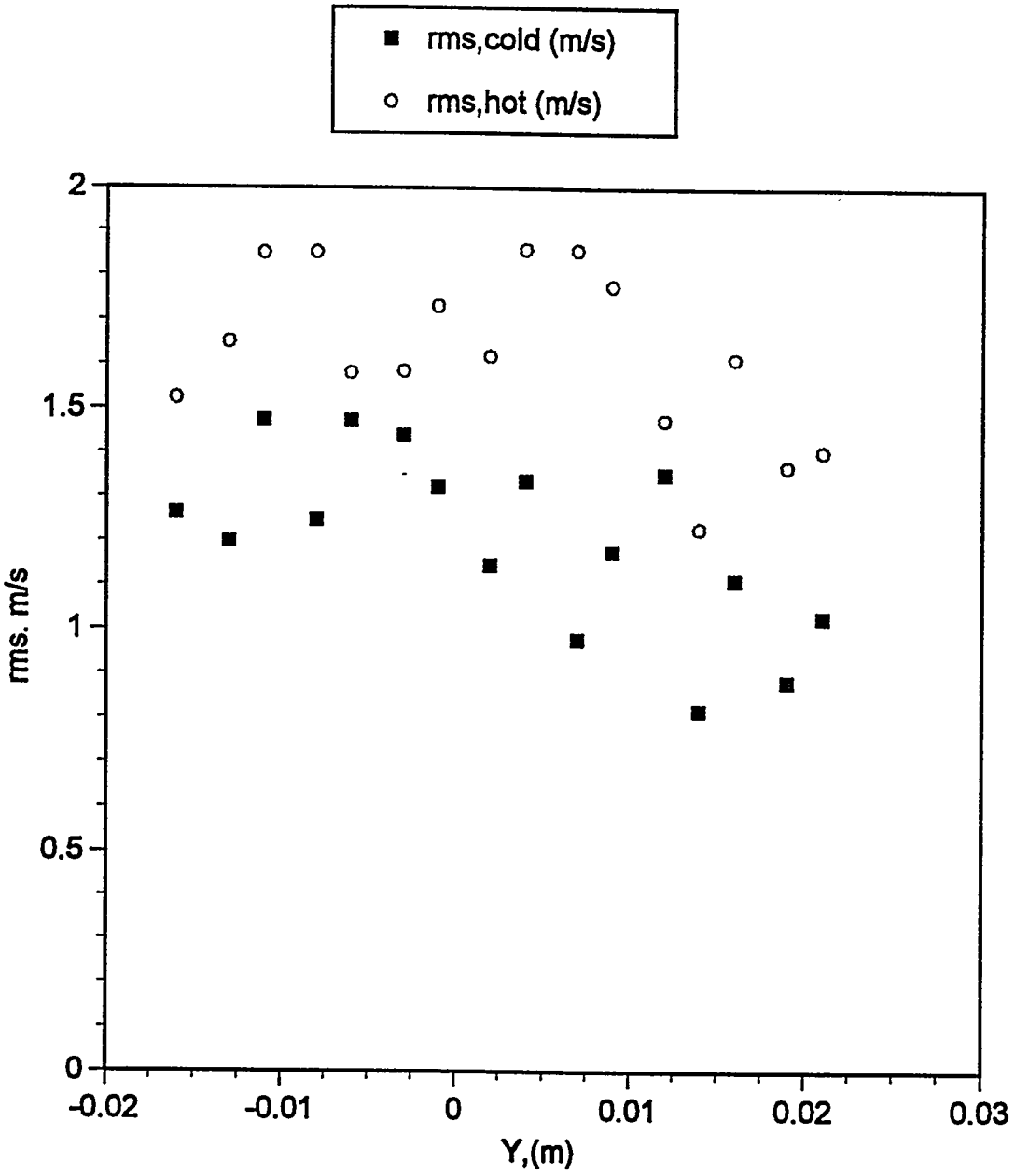

Fig. G.7. Comparison of the fluctuating component of velocity in unheated and heated shear layers (runs 1 and 2)

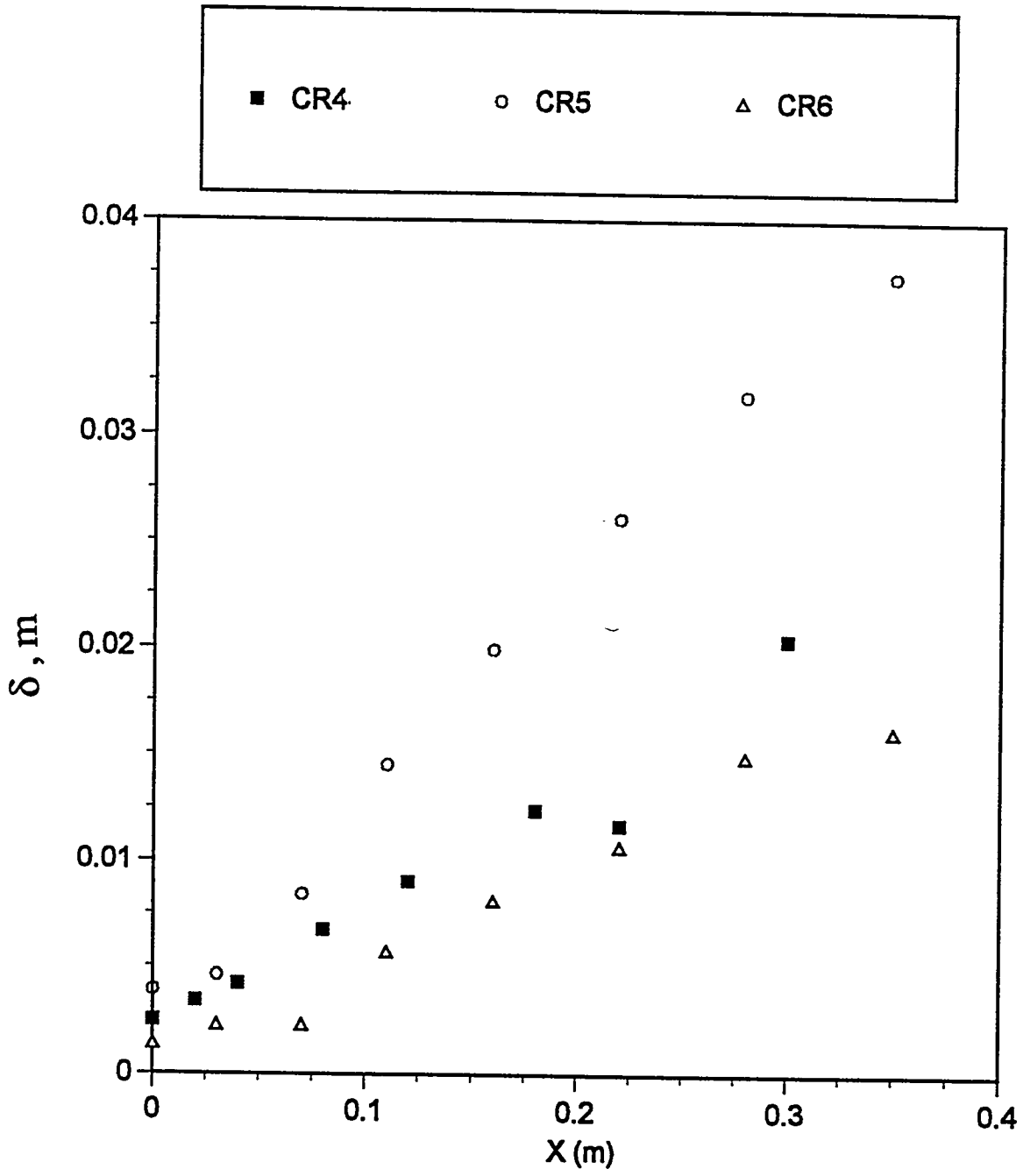

Fig. G.8. Growth of vorticity thickness in the homogeneous shear layers of unheated streams

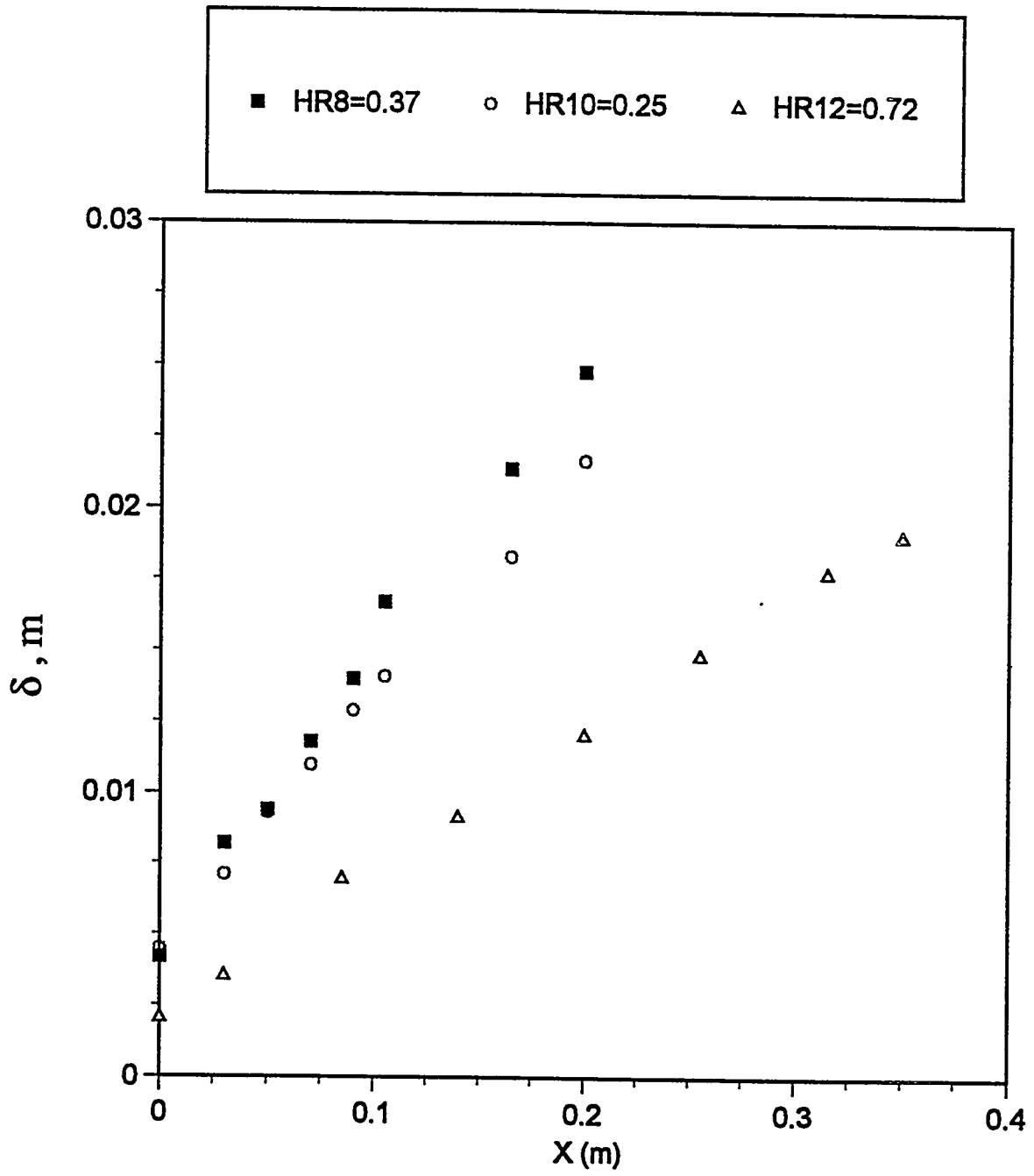

Fig. G.9. Growth of vorticity thickness in the homogeneous shear layers when the top stream was heated

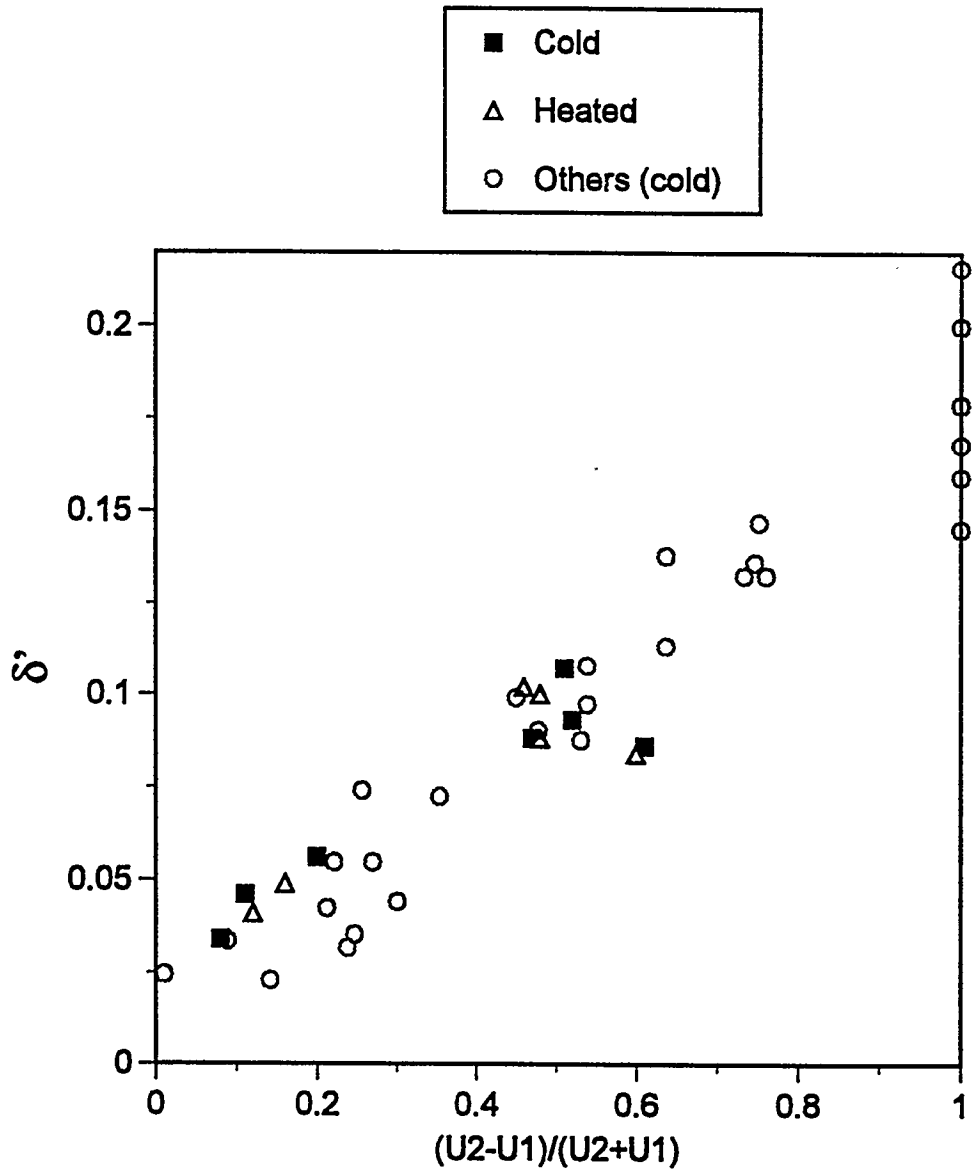

Fig. G.10 Comparison of the growth rate parameter with dimensionless velocity parameter for homogeneous shear layers

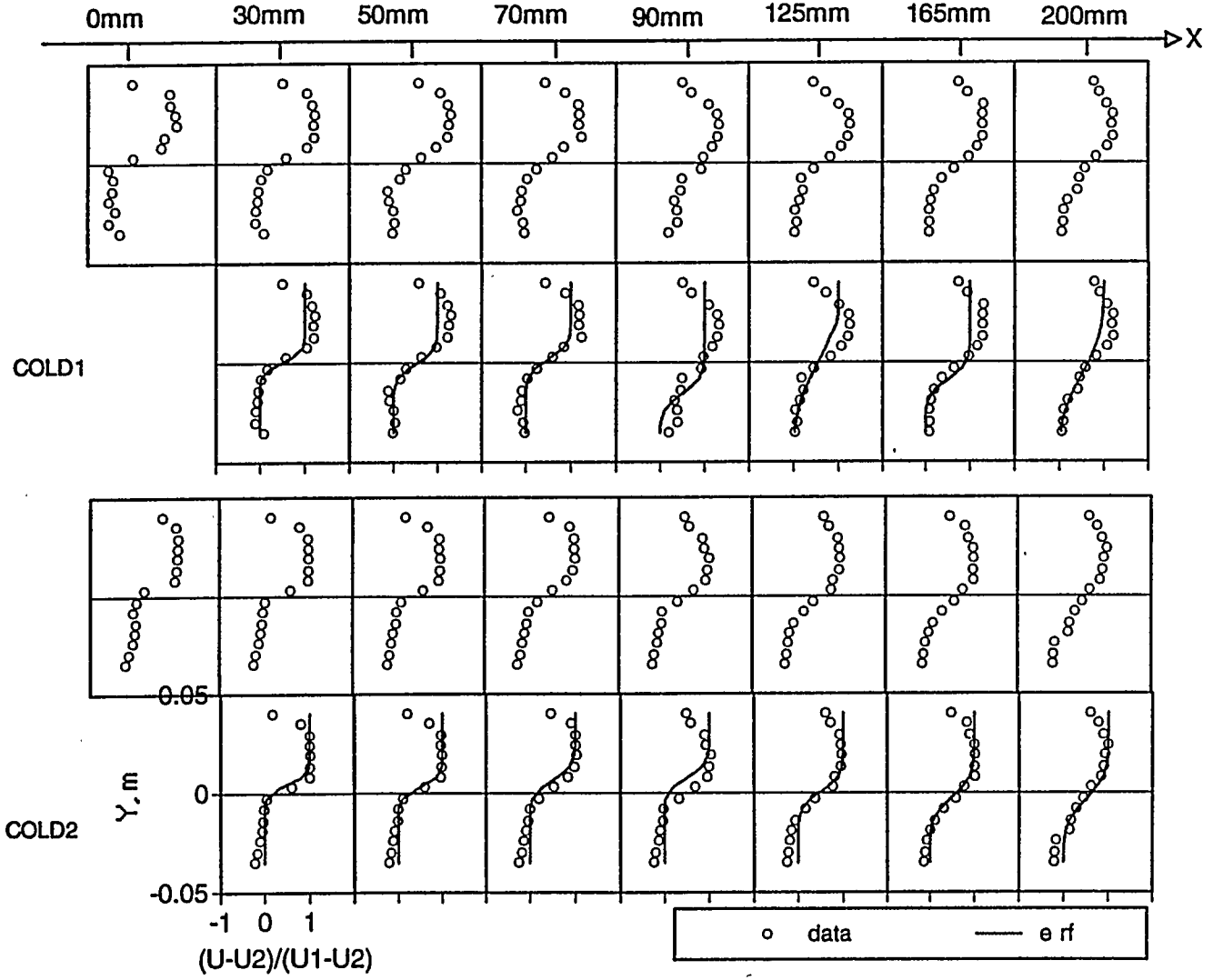

Fig. G.11 Velocity profile development in the perturbed unheated shear layers (runs: cold 1 and cold 2)

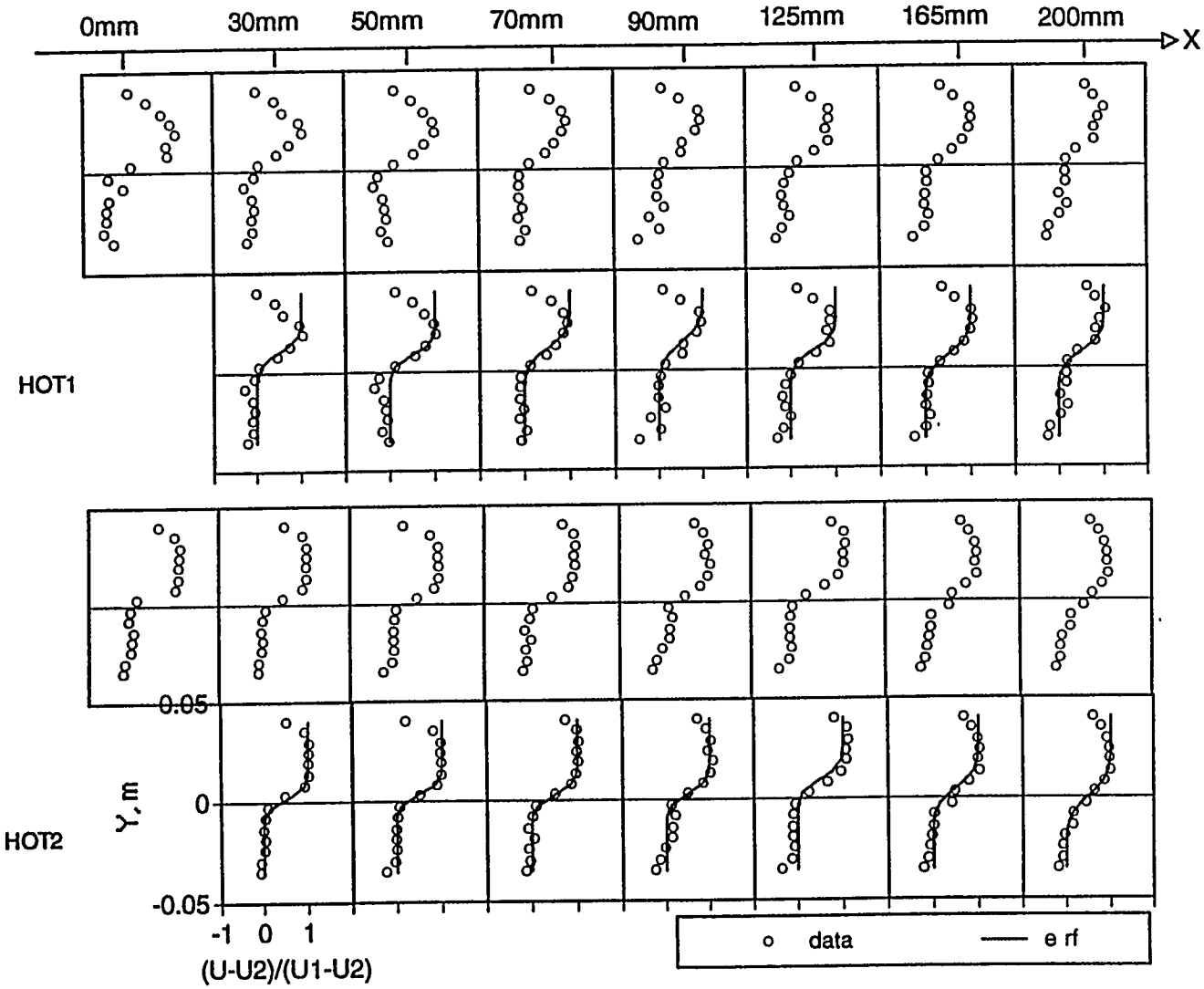

Fig. G.12 Velocity profile development in the perturbed heated shear layers (runs: hot 1 and hot 2)

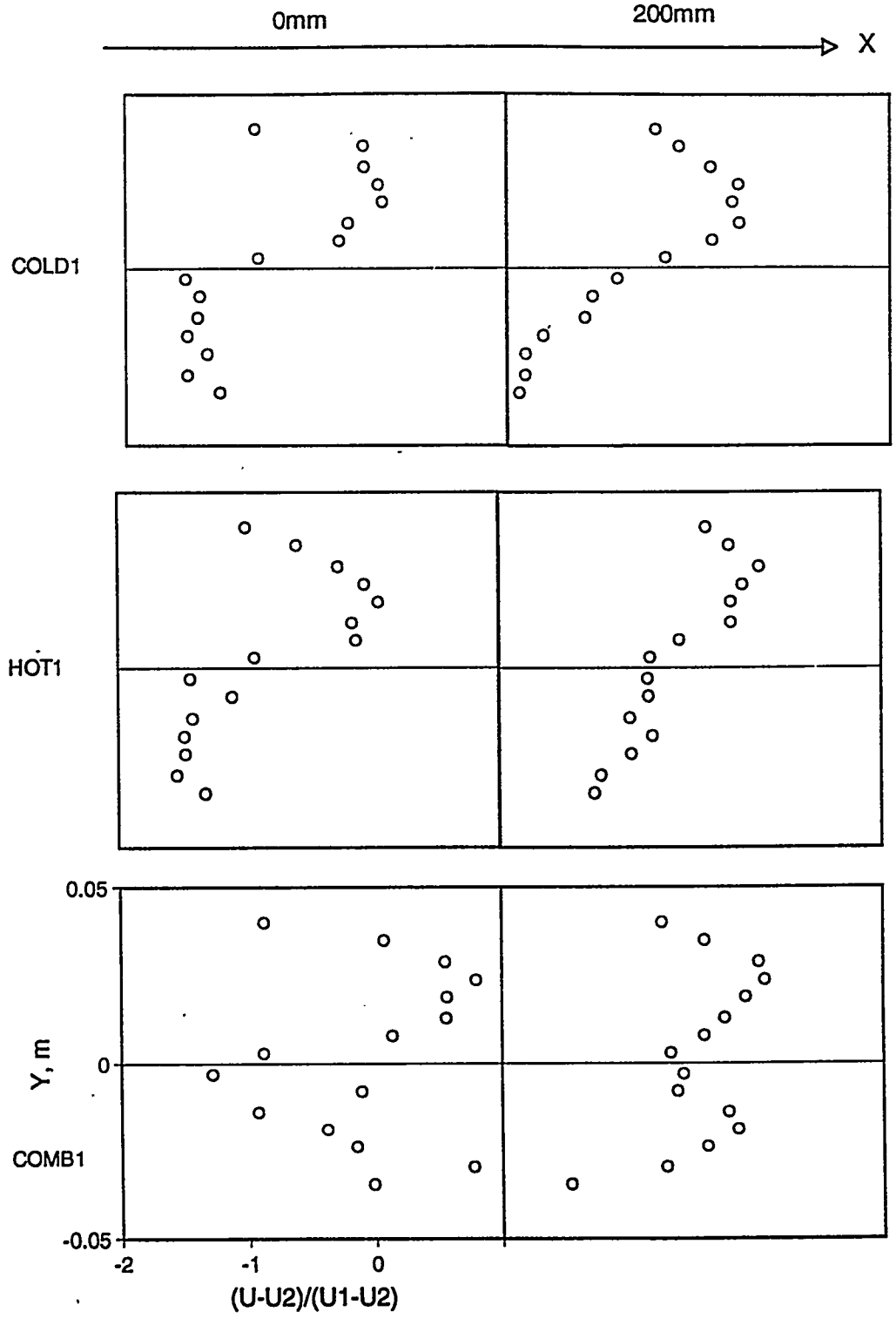

Fig. G. 13a Comparison of velocity profiles in shear layers where both streams unheated (top), the lower stream heated (middle), and the lower stream consisted of natural gas flame (bottom); (runs: cold 1, hot 1, comb 1)

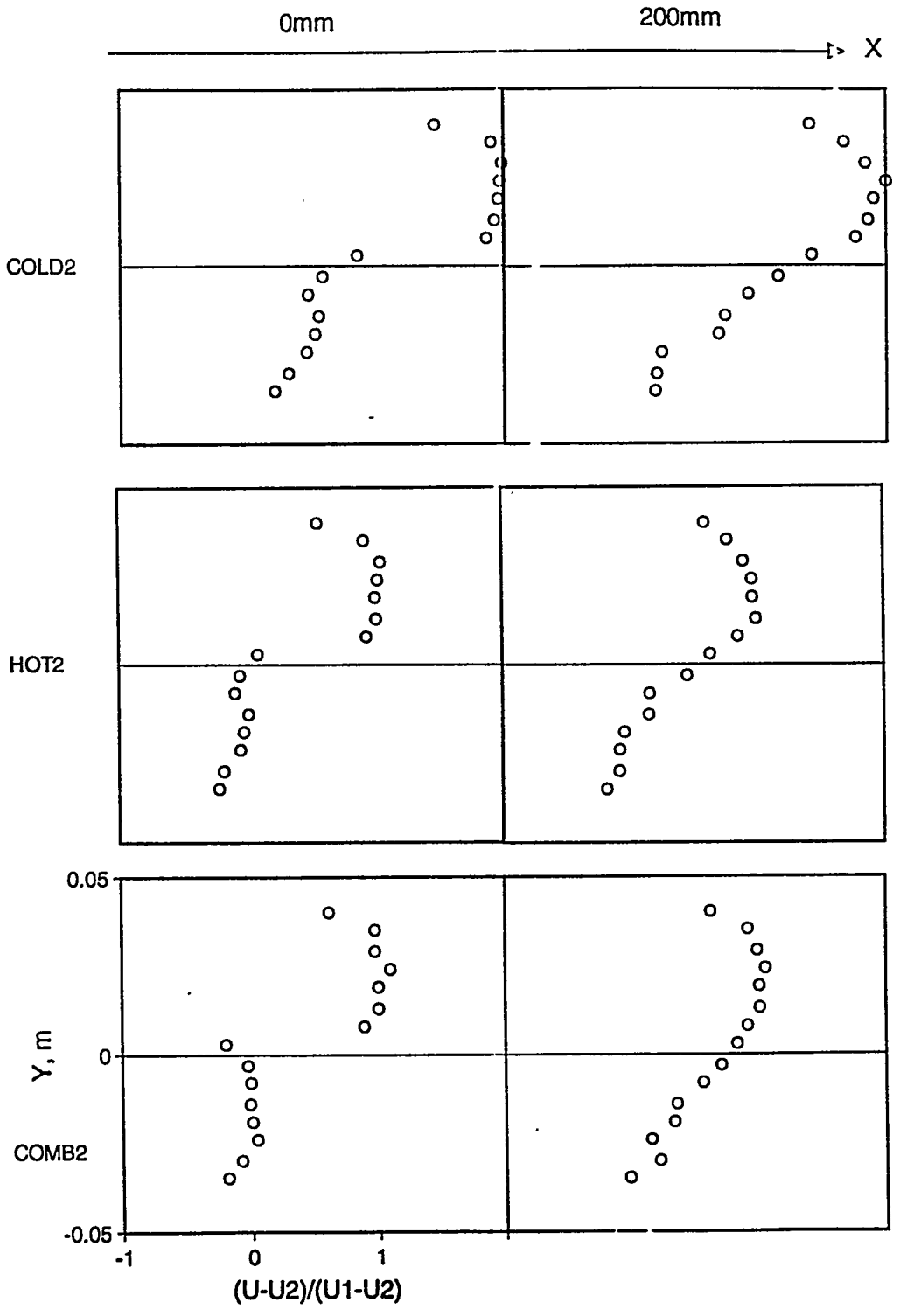

Fig. G. 13b Comparison of velocity profiles in shear layers where both streams unheated (top), the lower stream heated (middle), and the lower stream consisted of natural gas flame (bottom); (runs: cold 2, hot 2, comb 2)

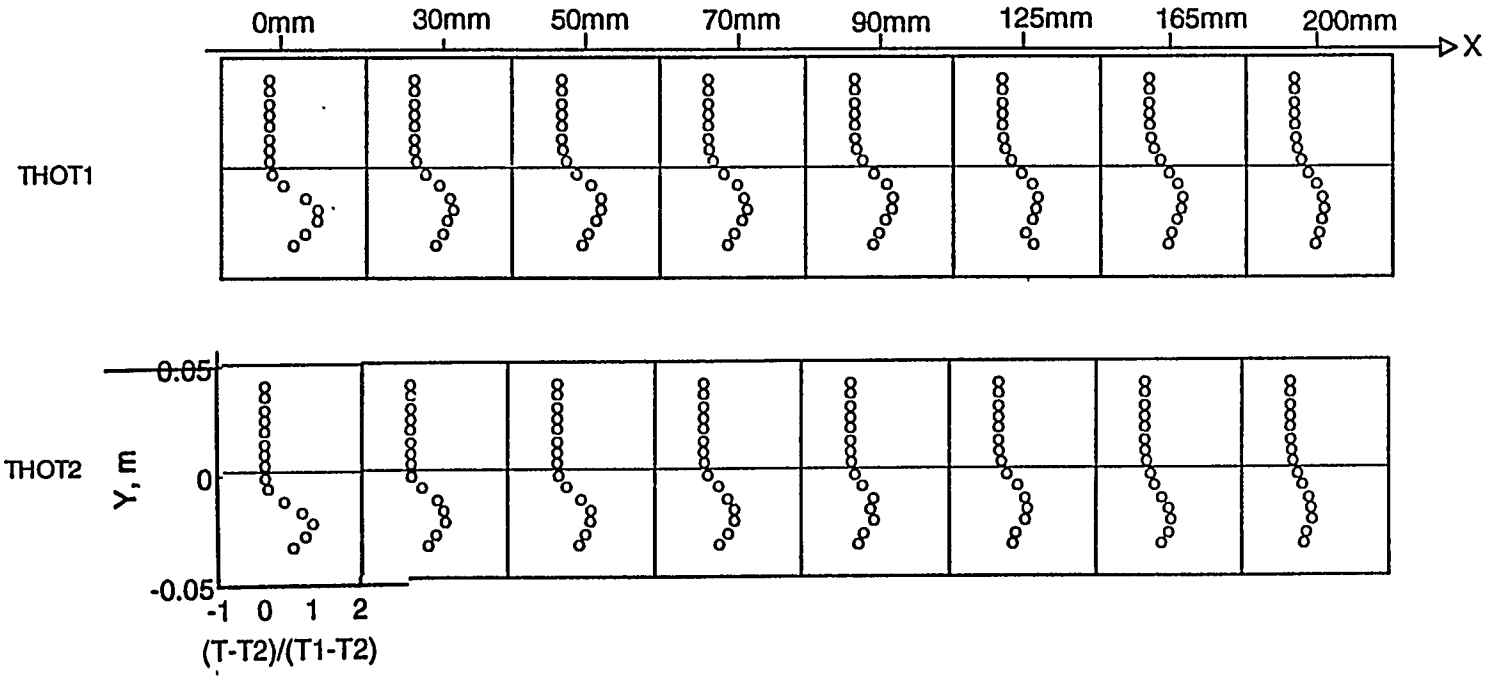

Fig. G. 14 Normalized temperature profiles in shear layer where the bottom stream was heated (runs: hot 1and hot 2)

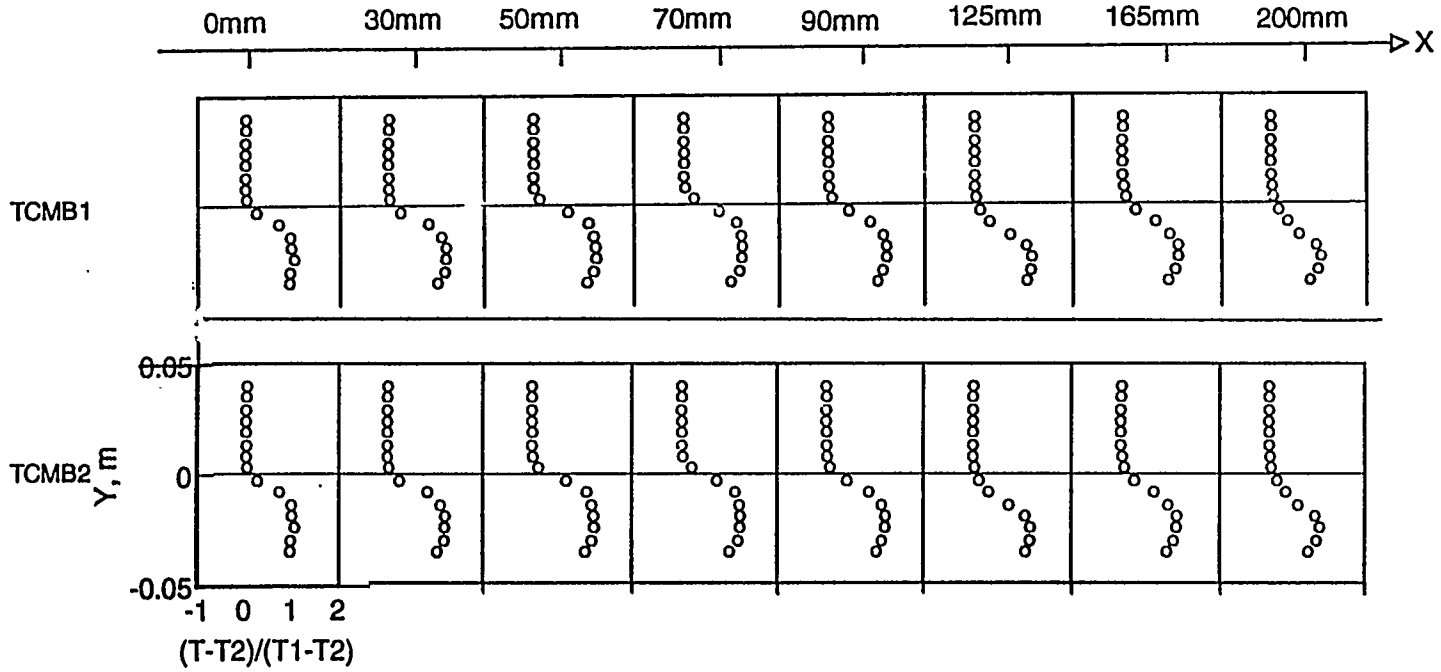

Fig. G.15 Normalized temperature profiles in the shear layer where a flame was present in the bottom stream (runs: comb1 and comb 2)

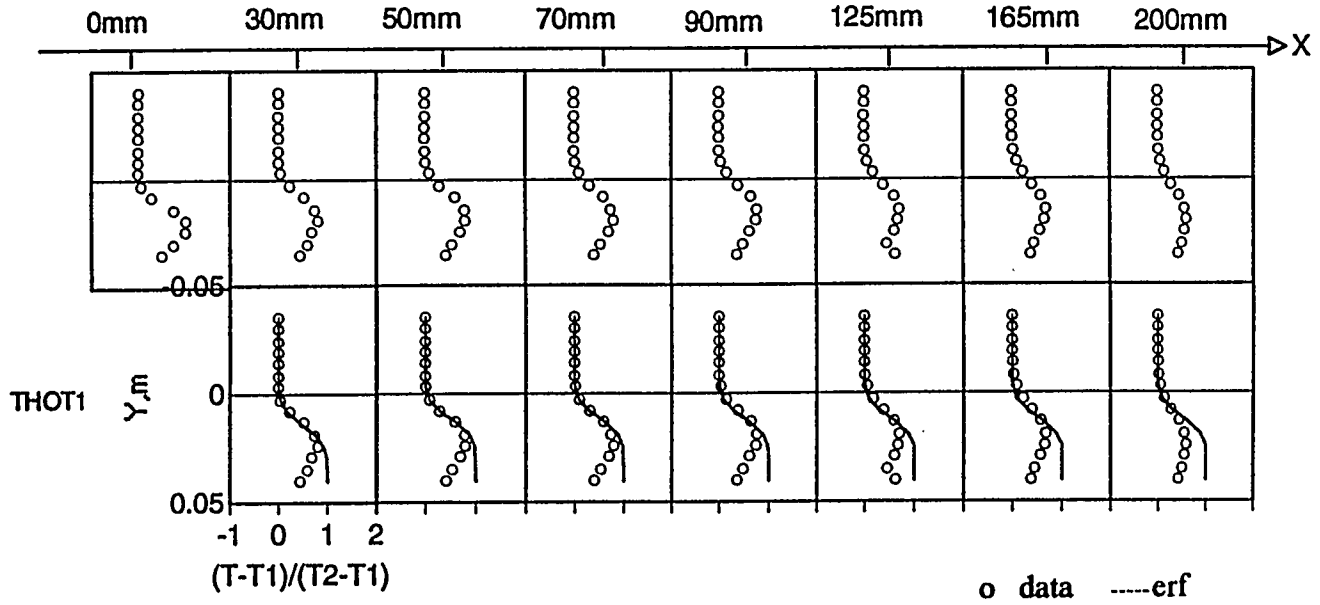

Fig. G.16a Error function description of temperature profiles in the shear layer where the bottom stream was heated (run: hot 1)

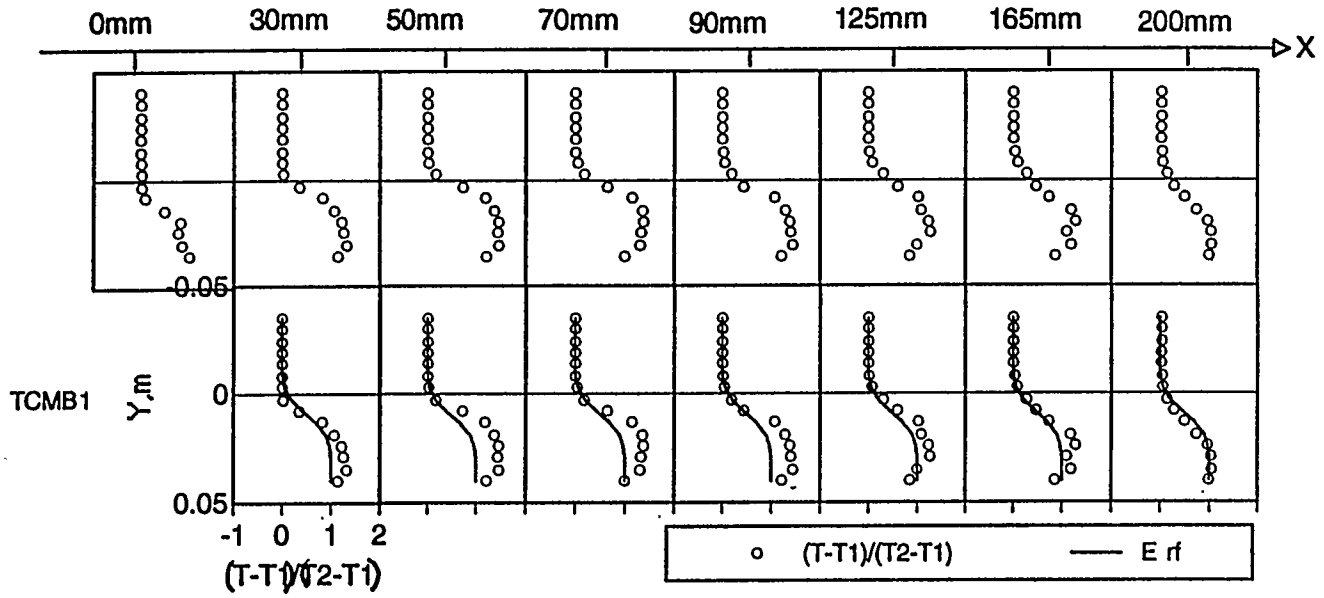

Fig. G.16b Error function description of temperature profiles in the shear layer where a flame was present in the bottom stream (run: comb 1)

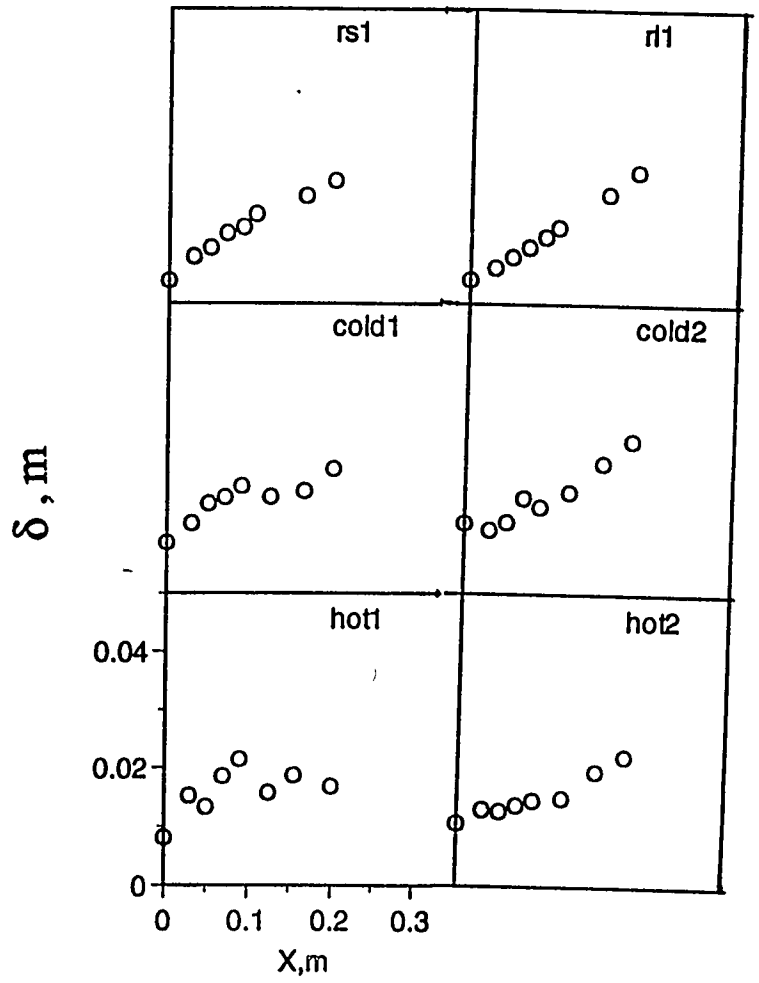

Fig. G. 17 Growth of shear layer thickness based on velocity data in the unperturbed, perturbed and heated cases (see Tables F.1. and F.2 for run conditions).

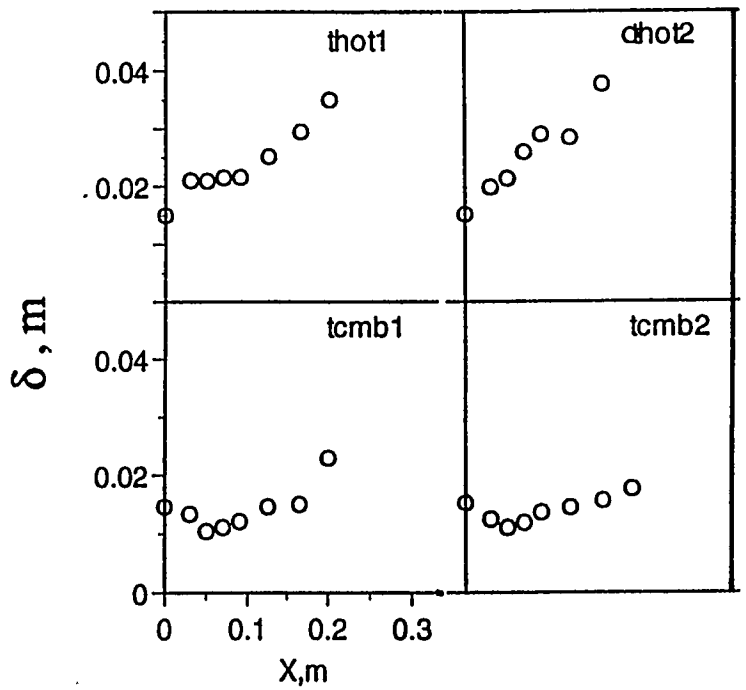

Fig. G.18 Growth of shear layer thickness based on temperature data in the heated and combustion cases (runs: hot 1 and comb 1)

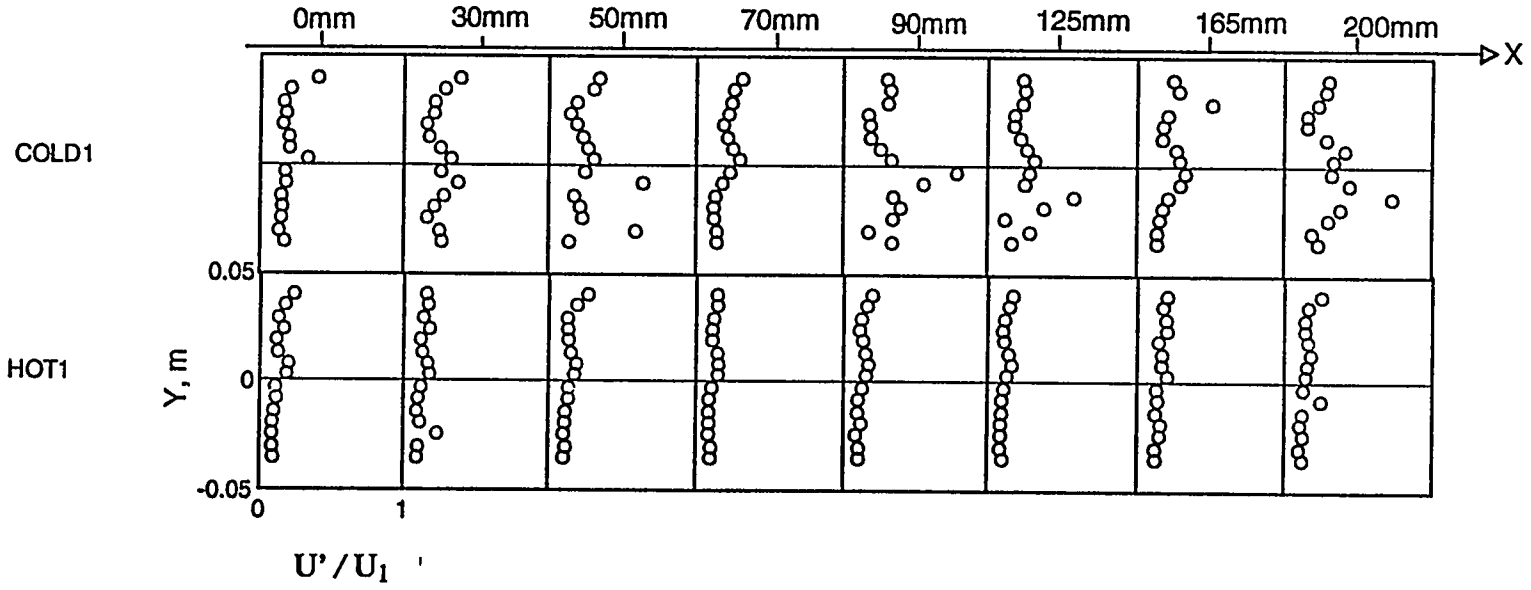

Fig. G.19 Profiles of the fluctuating component of the streamwise velocity in shear layers where both streams were unheated and the bottom stream was heated (runs: cold 1 and hot 1)

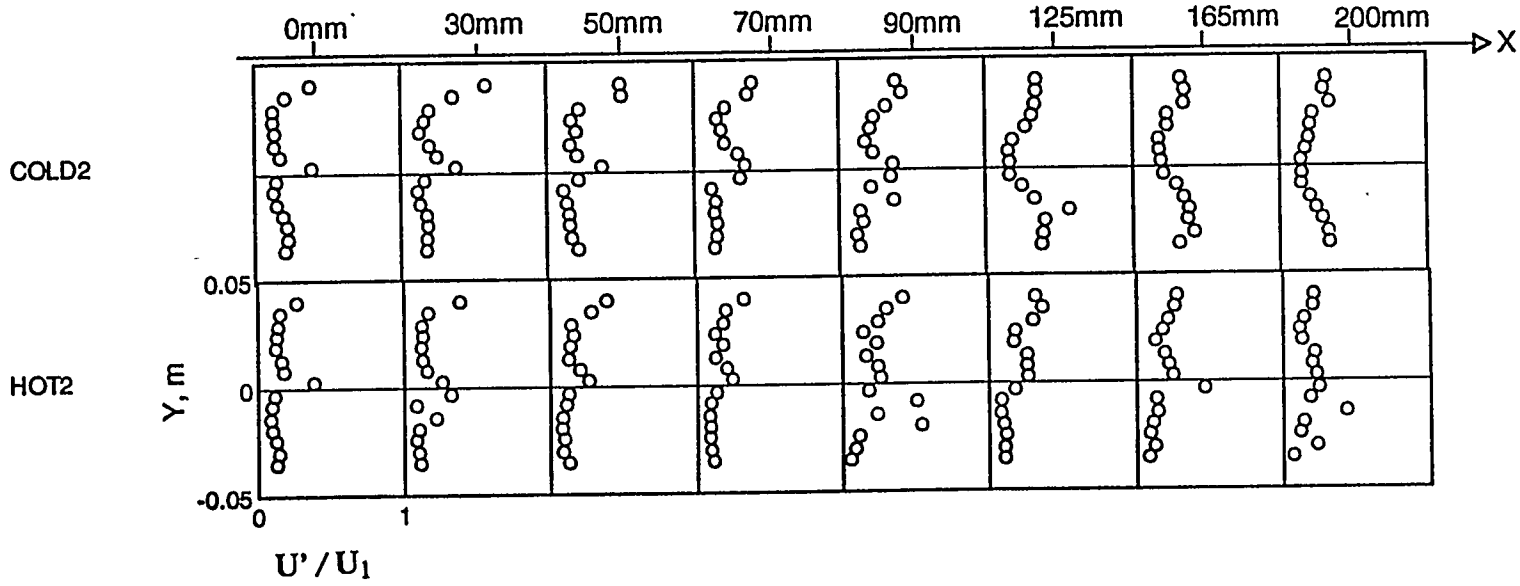

Fig. G.20 Profiles of the fluctuating component of the streamwise velocity in shear layers where both streams were unheated and the bottom stream was heated (runs: cold 2 and hot 2).

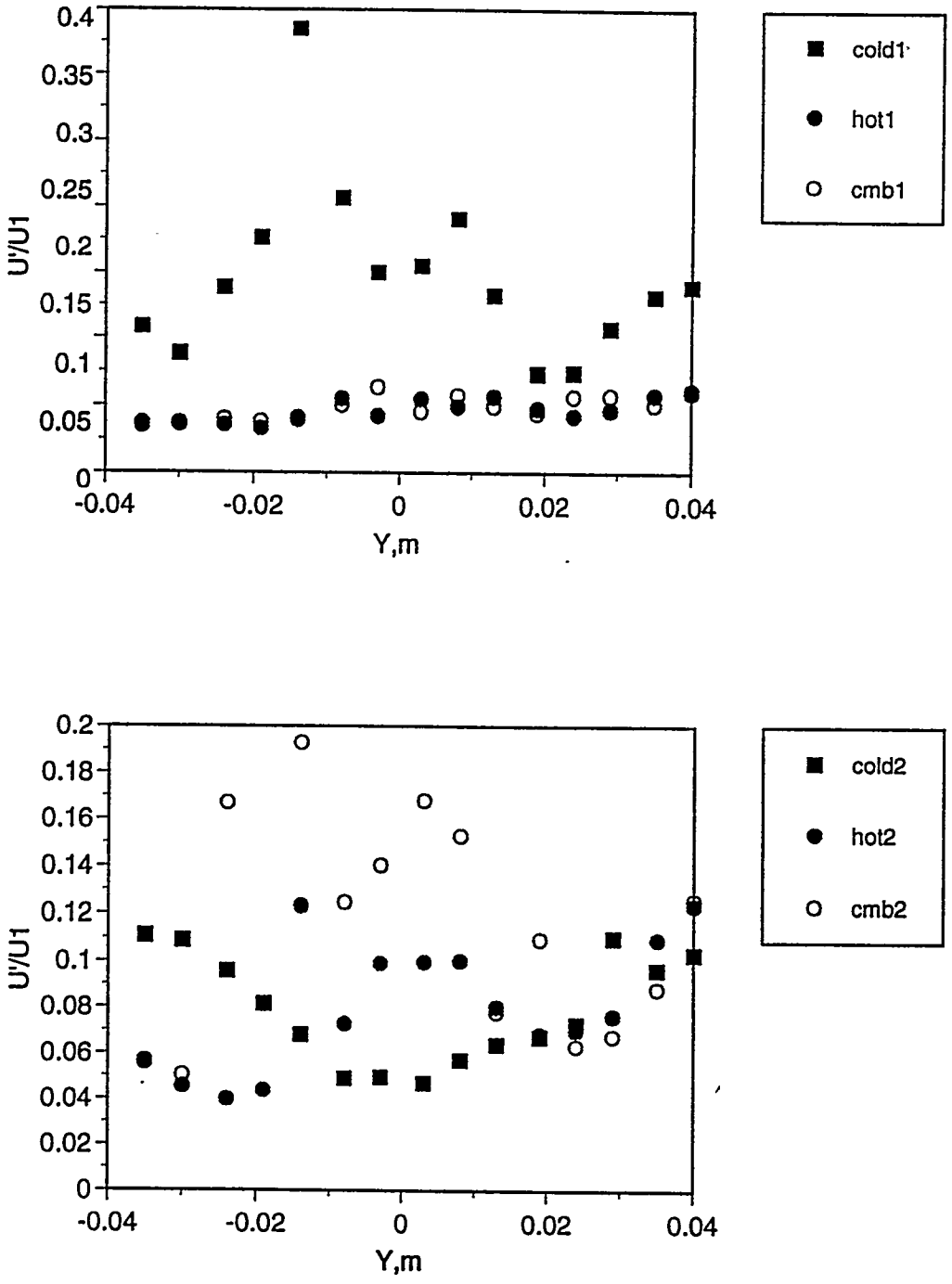

Fig. G. 21 Comparison of the fluctuating component of the streamwise velocity in shear layers at x= 200 mm where both streams unheated, the bottom stream heated, and the bottom stream had a flame (runs: cold 1, hot 1, and comb 1)

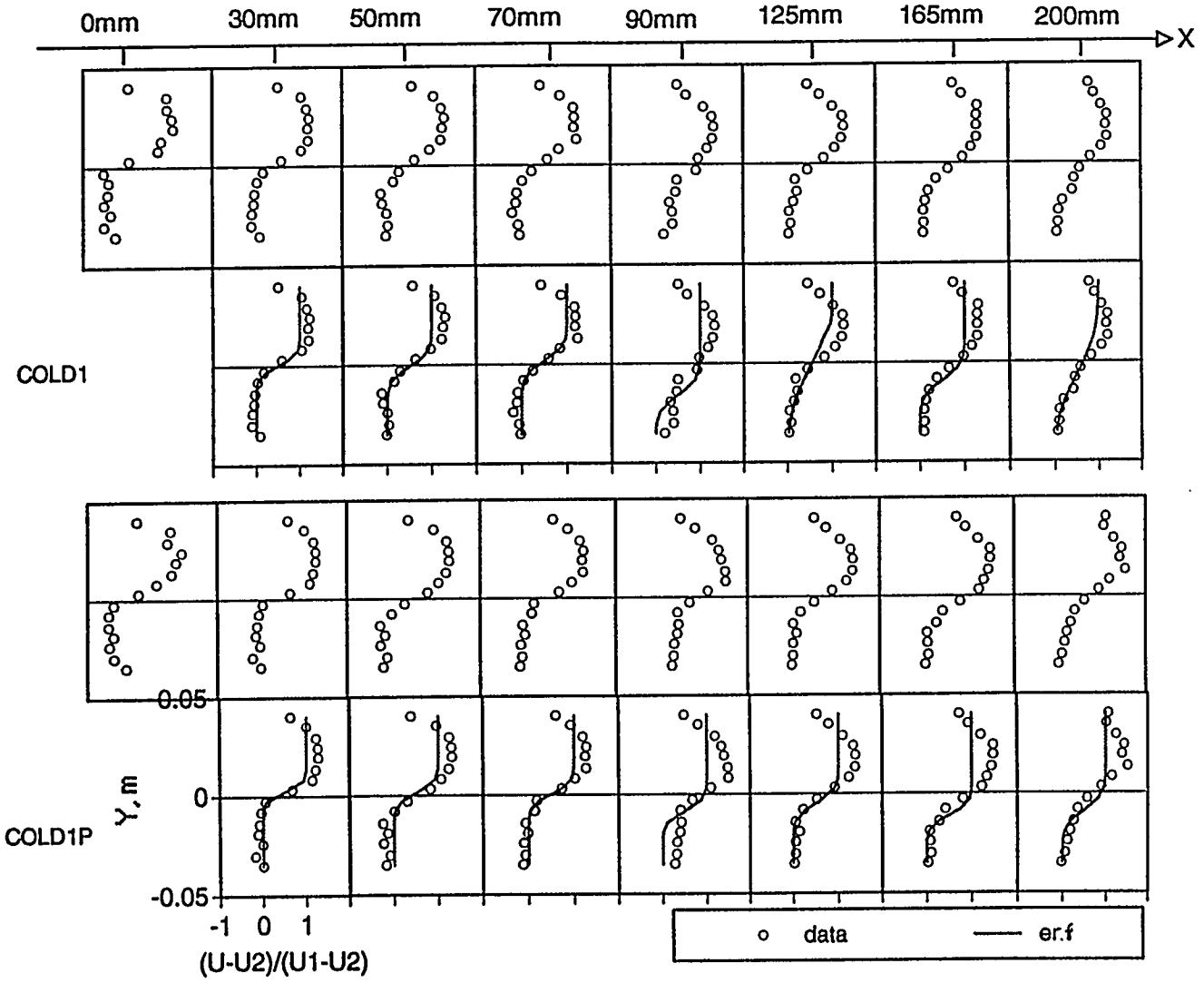

Fig. G.22 Comparison of the streamwise velocity profile development in unheated shear layers in which particles were present in the top stream (run: cold 1)

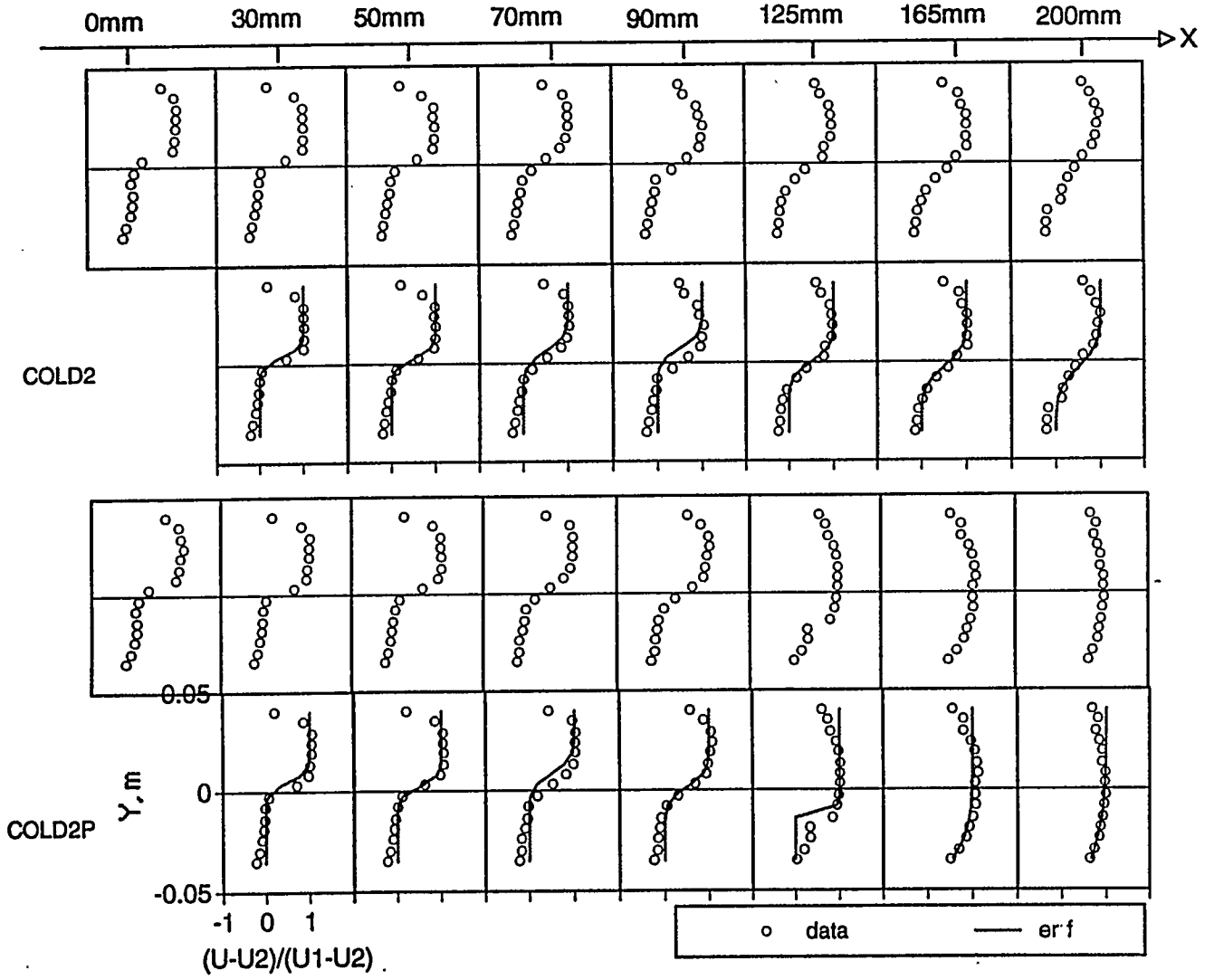

Fig. G.23 Comparison of the streamwise velocity profile development in unheated shear layers in which particles were present in the top stream (run: cold 2)

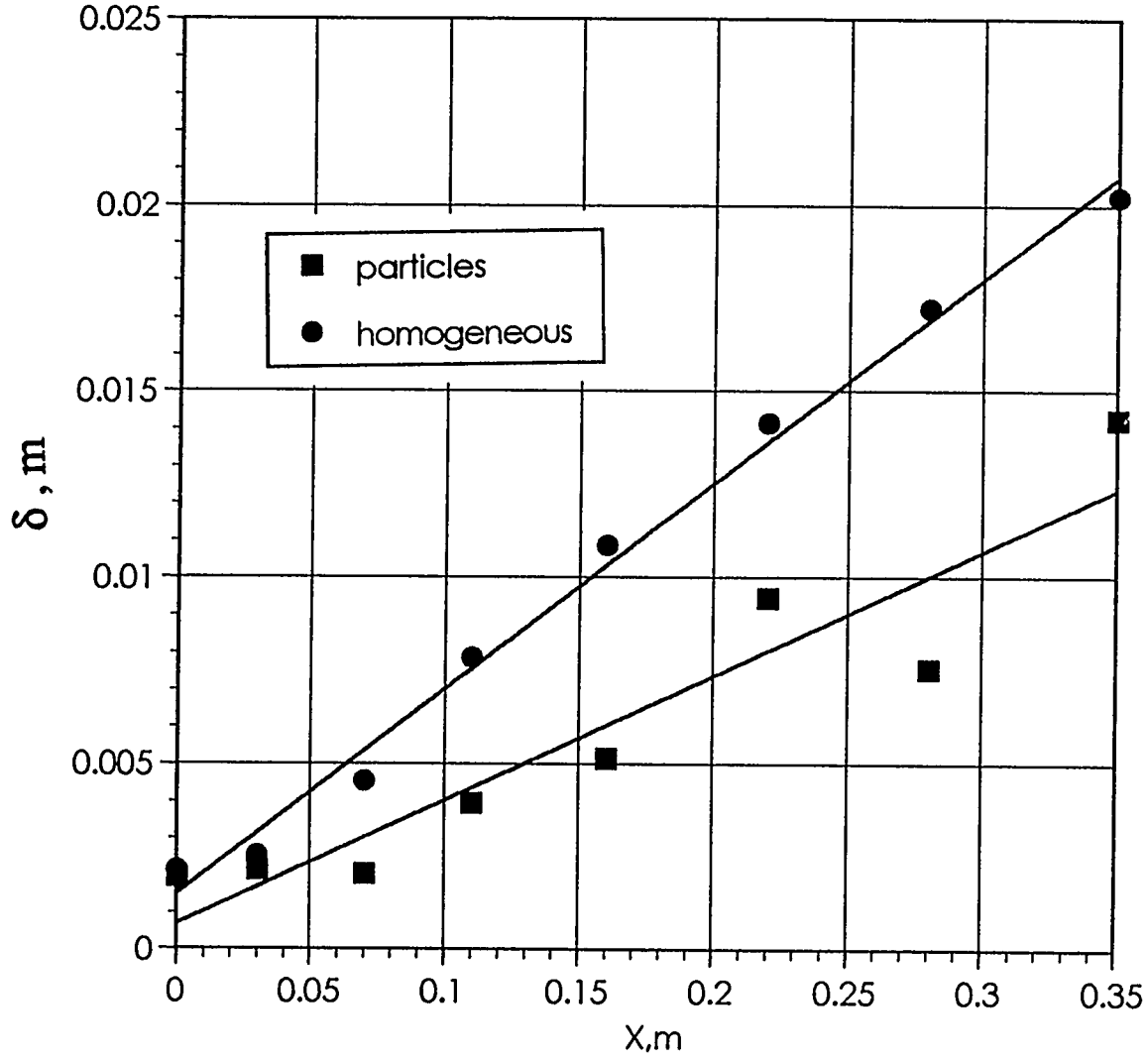

Fig. G.24 **Effect of particles in the upper stream on the growth of unheated and unperturbed shear layer.**

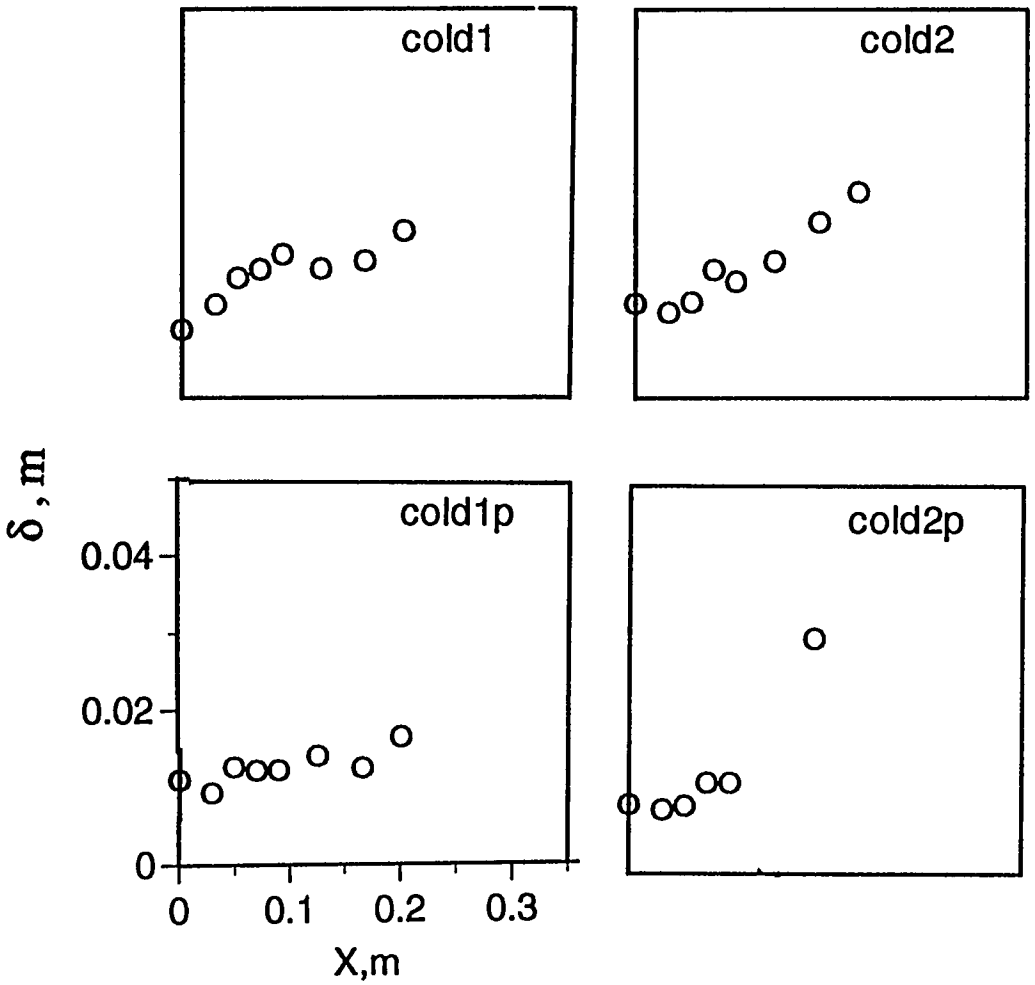

Fig. G.25 Effect of particles in the upper stream on the growth of perturbed shear layers at various conditions.

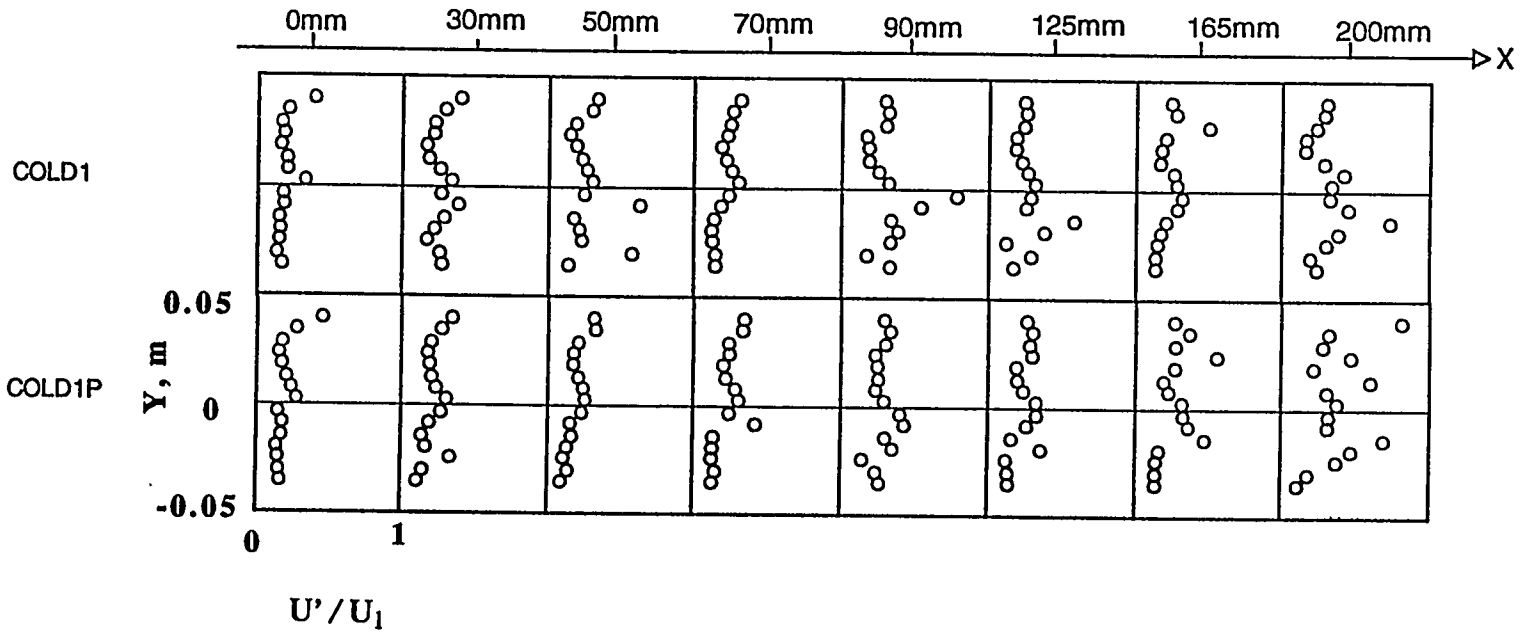

Fig. G.26 Effect of particles in the upper stream on the development of turbulent intensity profiles in the unheated perturbed shear layer (run: cold 1)

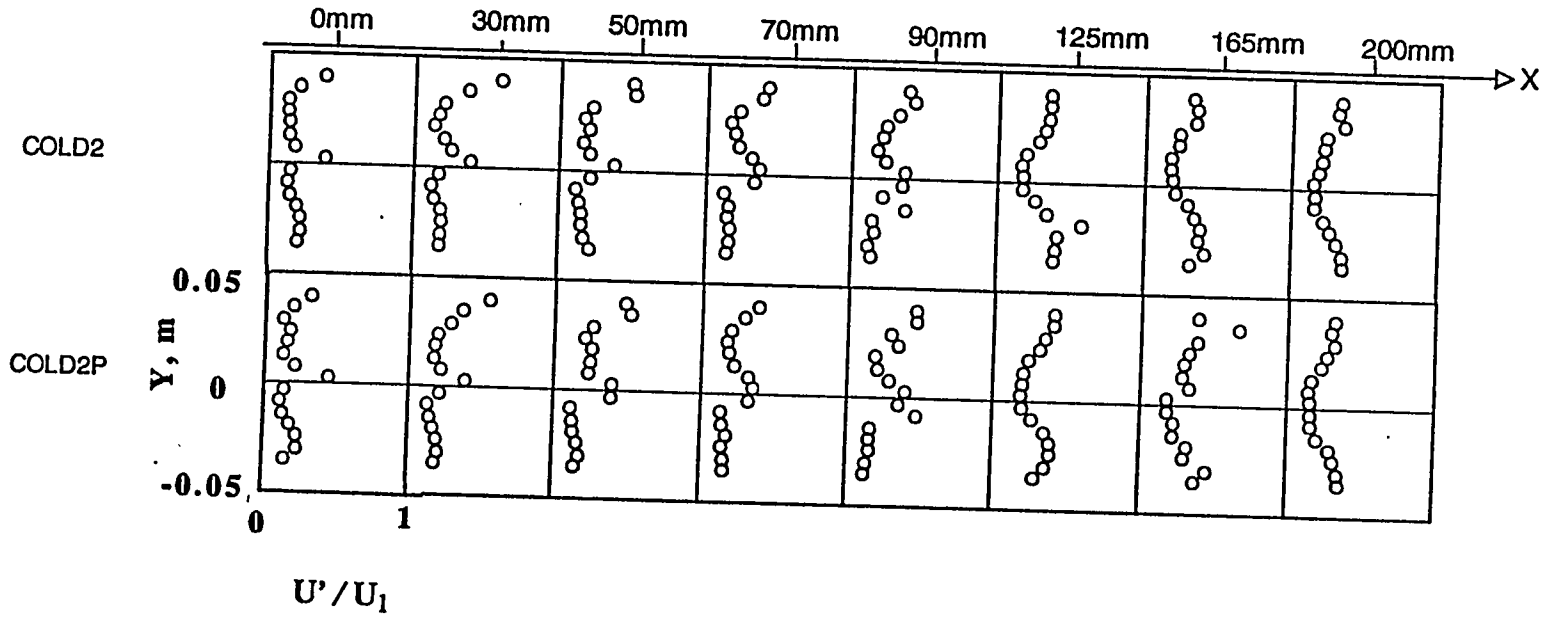

Fig. G.27 Effect of particles in the upper stream on the development of turbulent intensity profiles in the unheated perturbed shear layer (run: cold 2)

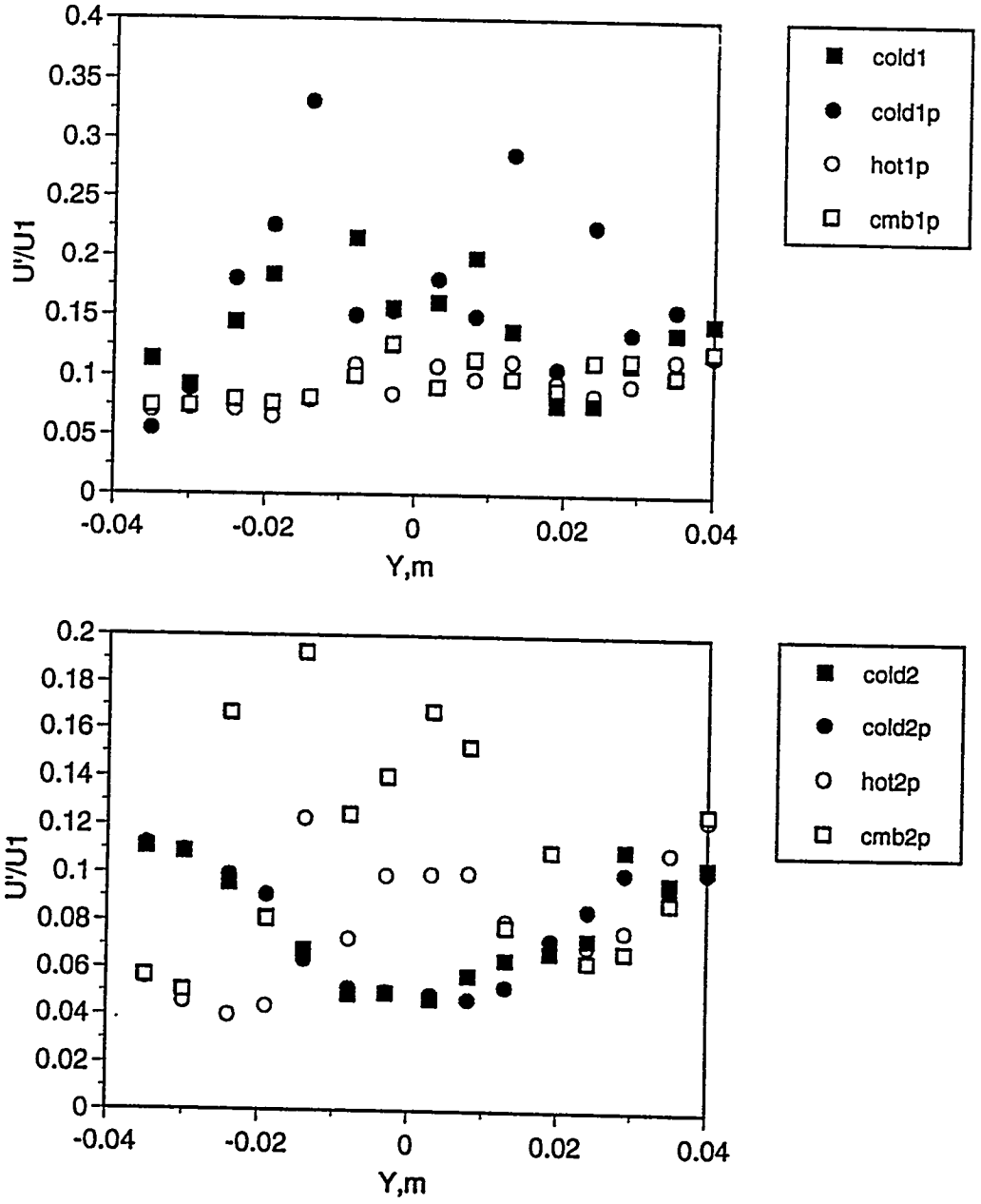

Fig. G.28 Turbulent intensity profiles at x =200 mm with and without particles

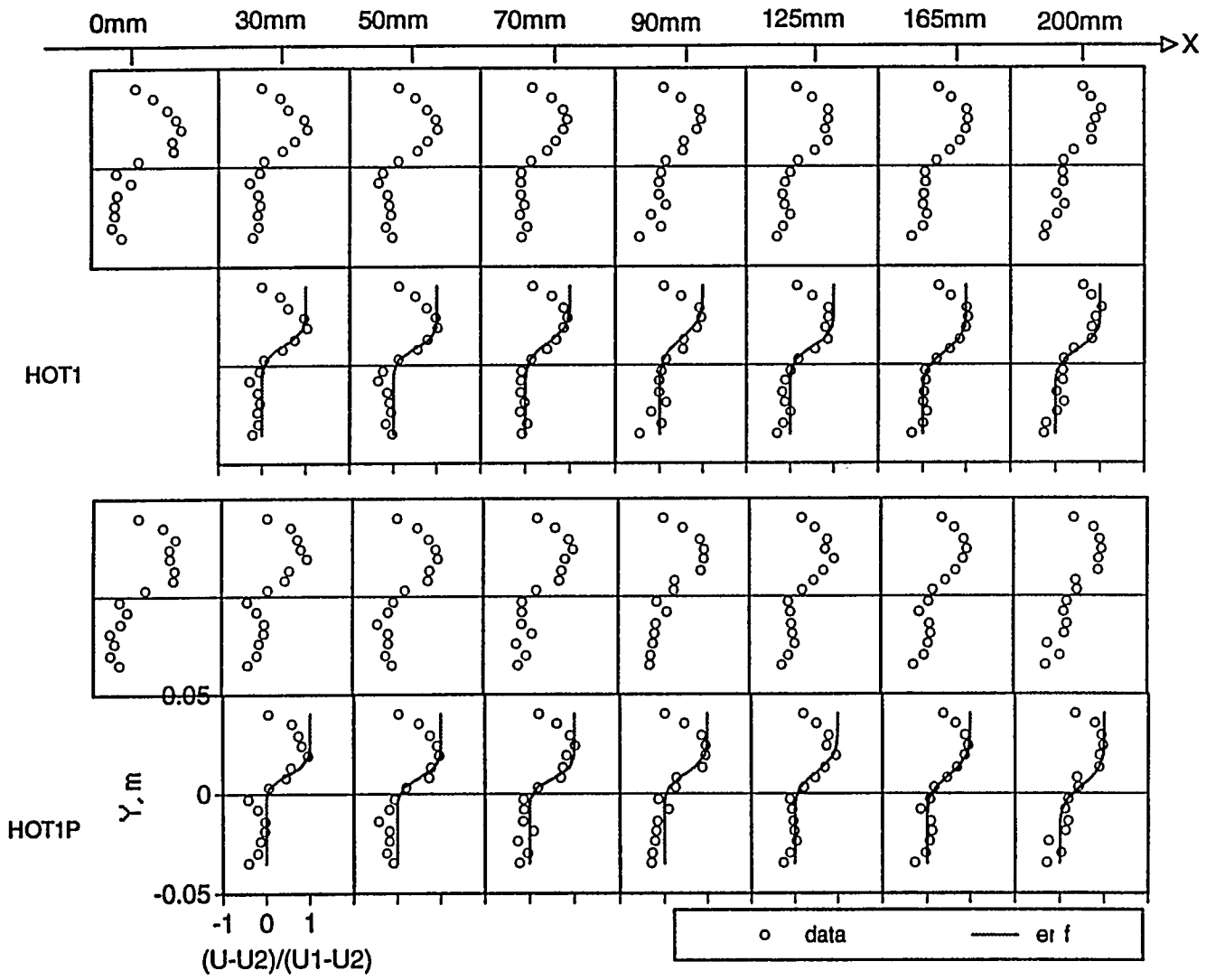

Fig. G.29 Effect of pyrolyzing particles on the development of velocity profiles (run: hot 1)

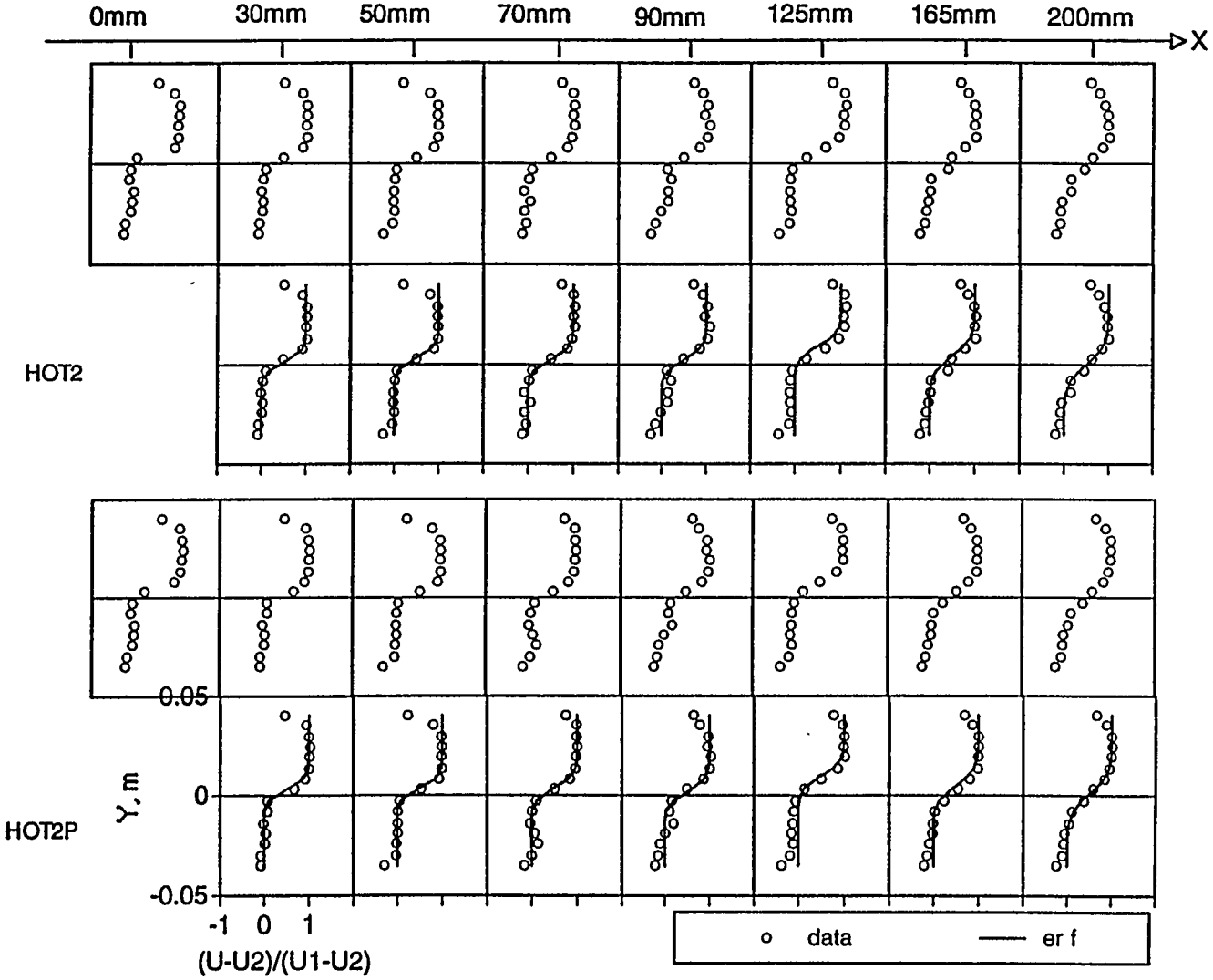

Fig. G.30 Effect of pyrolyzing particles on the development of velocity profiles (run: hot 2)

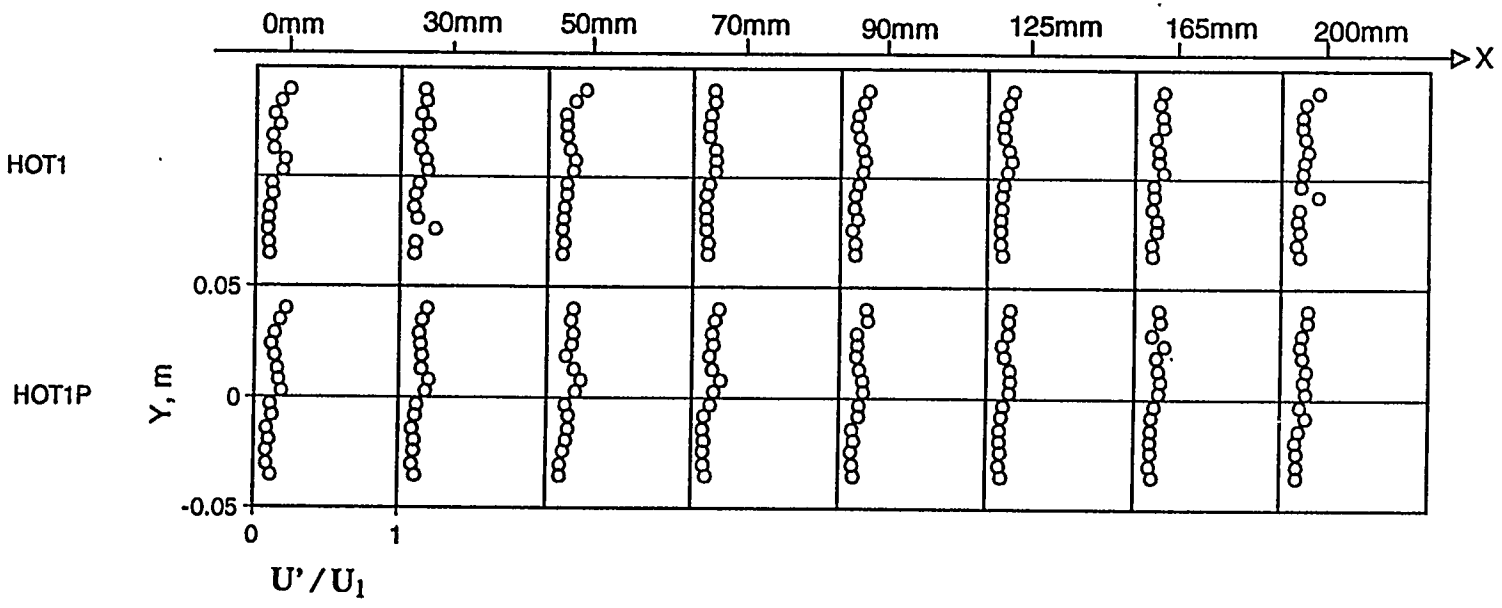

Fig. G.31 Effect of pyrolyzing particles on the development of turbulent intensity profiles (run: hot 1)

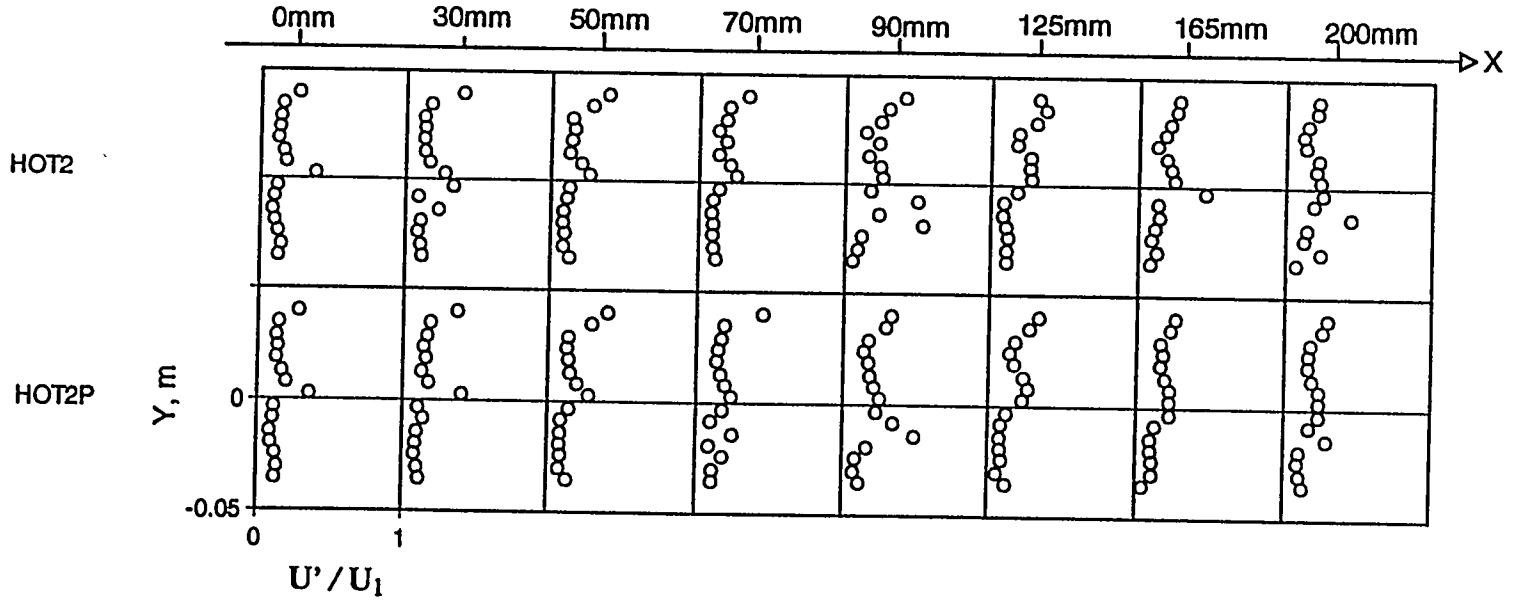

Fig. G.32 **Effect of pyrolyzing particles on the development of turbulent intensity profiles (run: hot 2)**

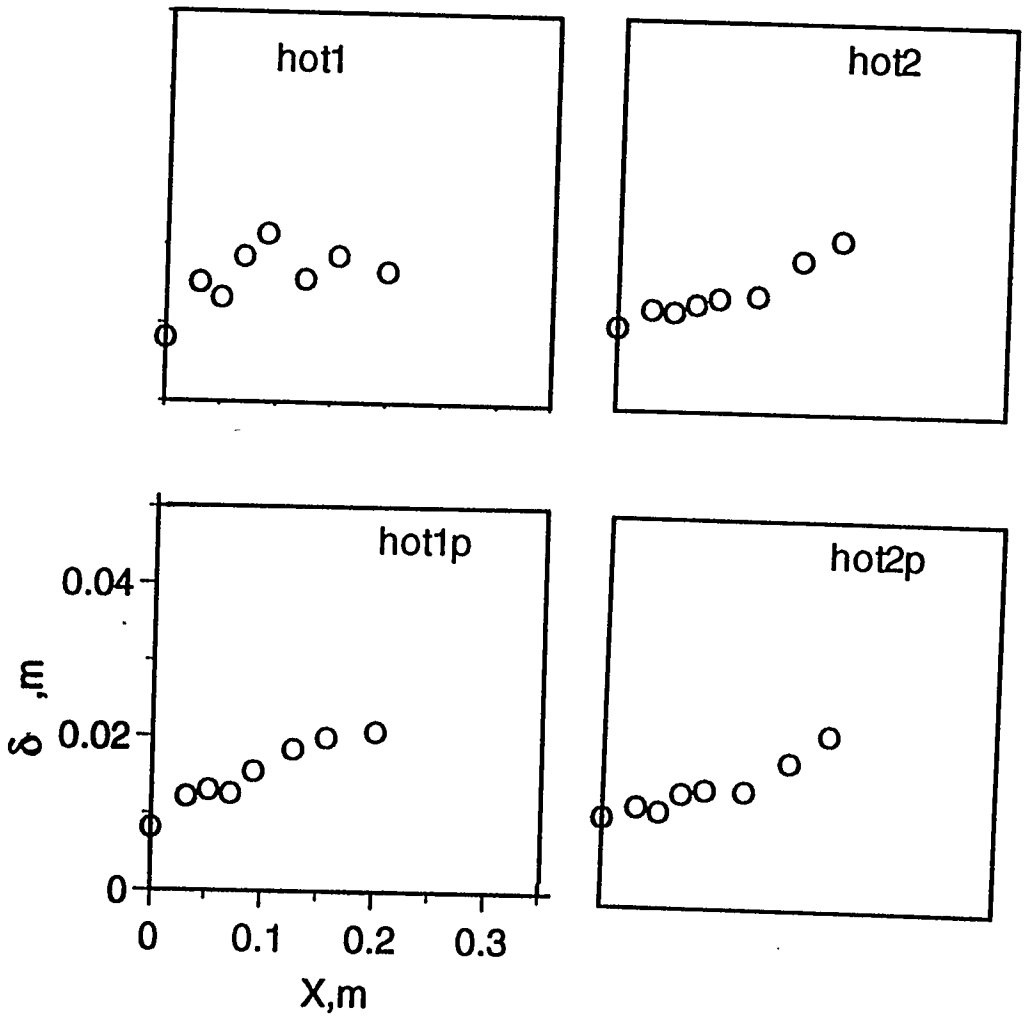

Fig. G.33 Effect of pyrolyzing particles on the growth of shear layer

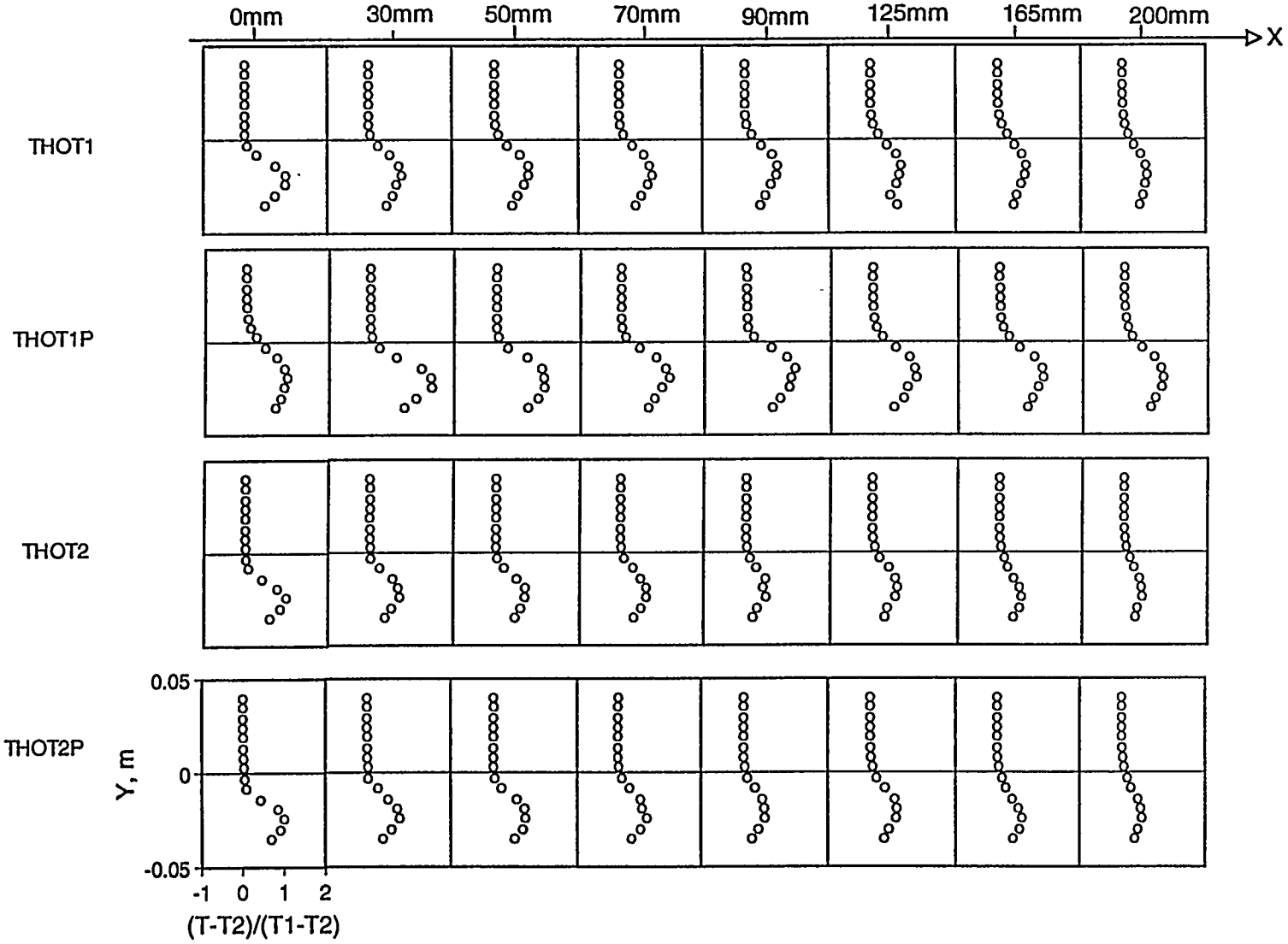

Fig. G.34 Temperature profiles in shear layers with pyrolyzing particles (run: hot 1 and hot 2)

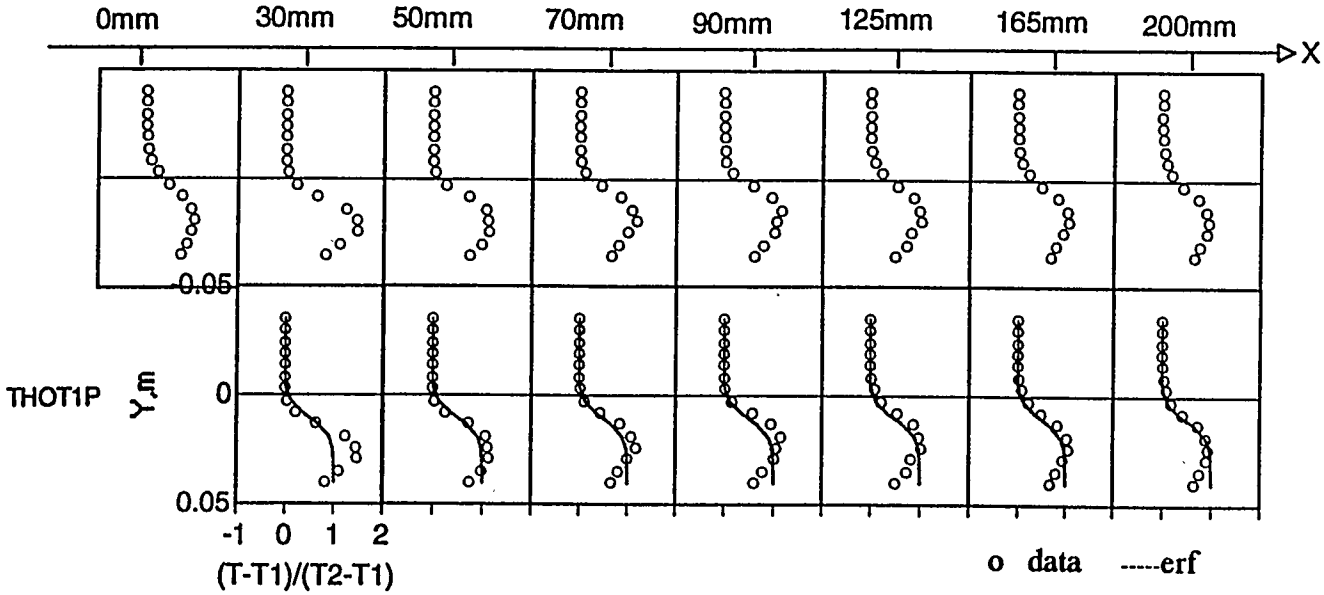

Fig. G. 35 Error function fit to the temperature profiles in the shear layer with pyrolyzing particles (run: comb 1)

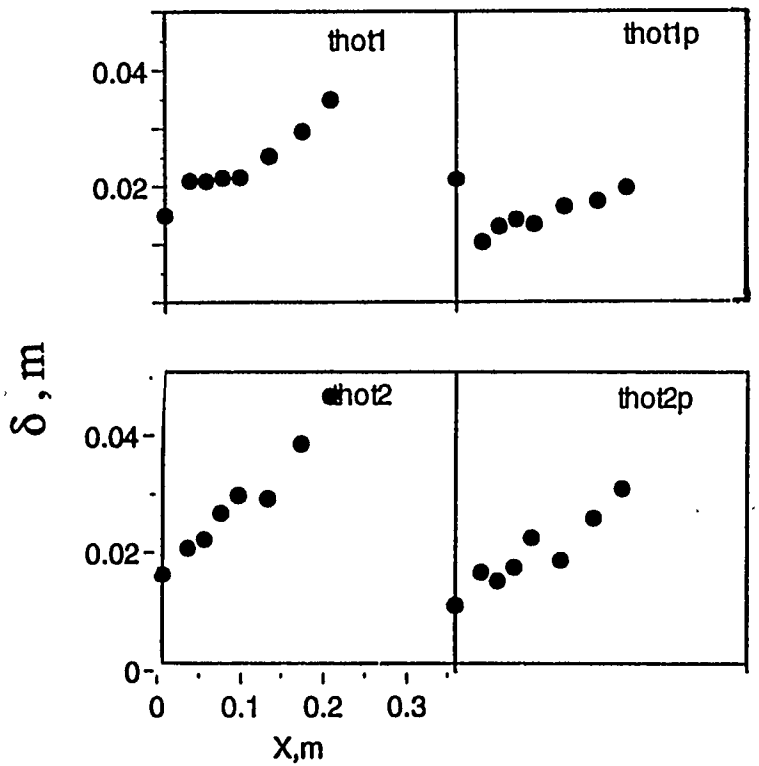

Fig. G.36 Effects of pyrolyzing particles on the thermal thickness of the shear layer

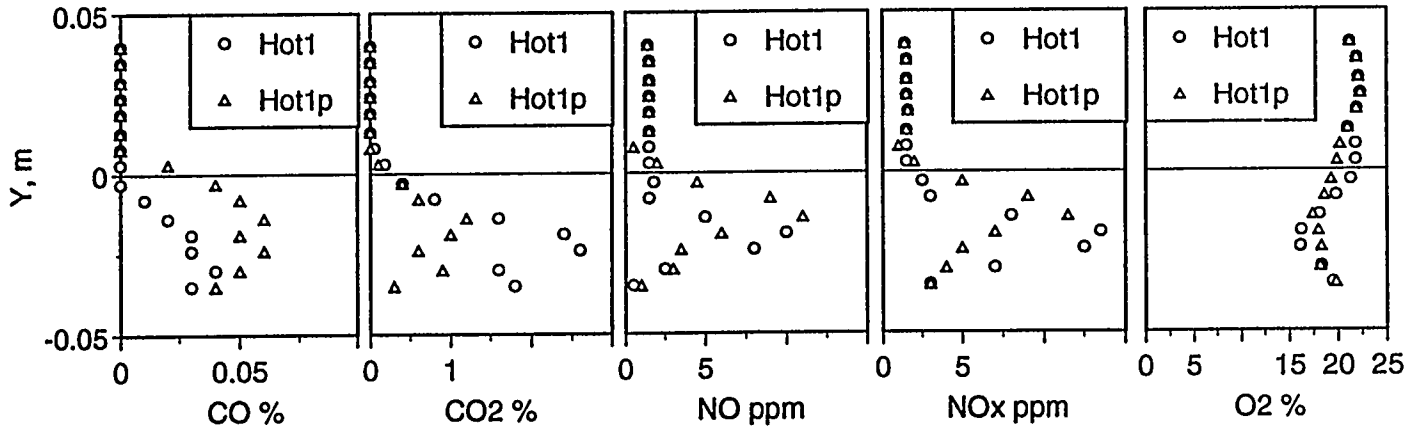

Fig. G.37 Effects of pyrolyzing particles on the concentration profiles of product species in the shear layer (run: hot 1)

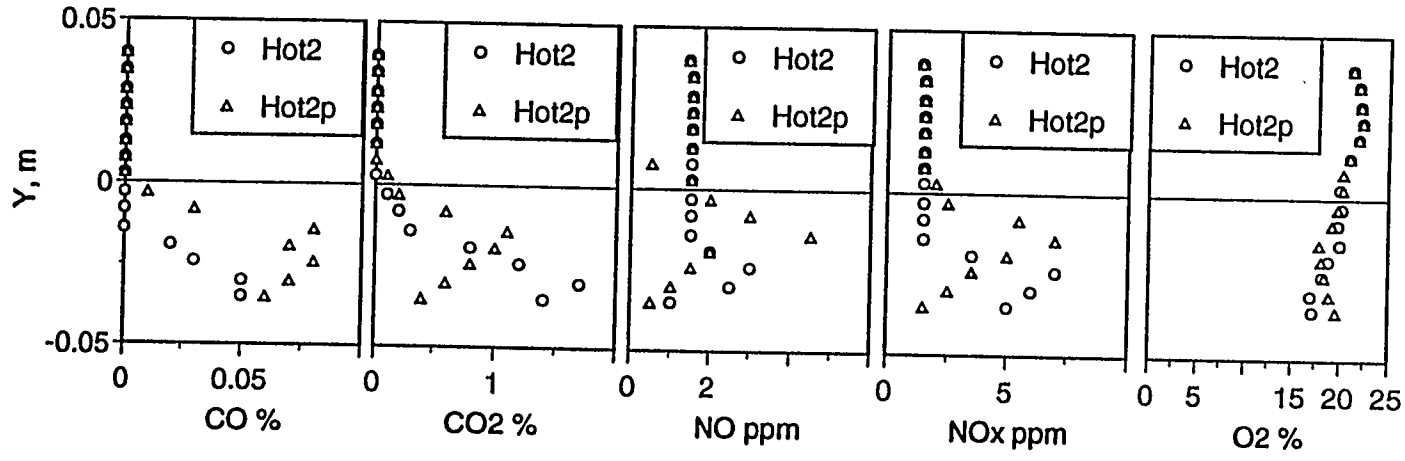

Fig. G.38 Effects of pyrolyzing particles on the concentration profiles of product species in the shear layer (run: hot 2)

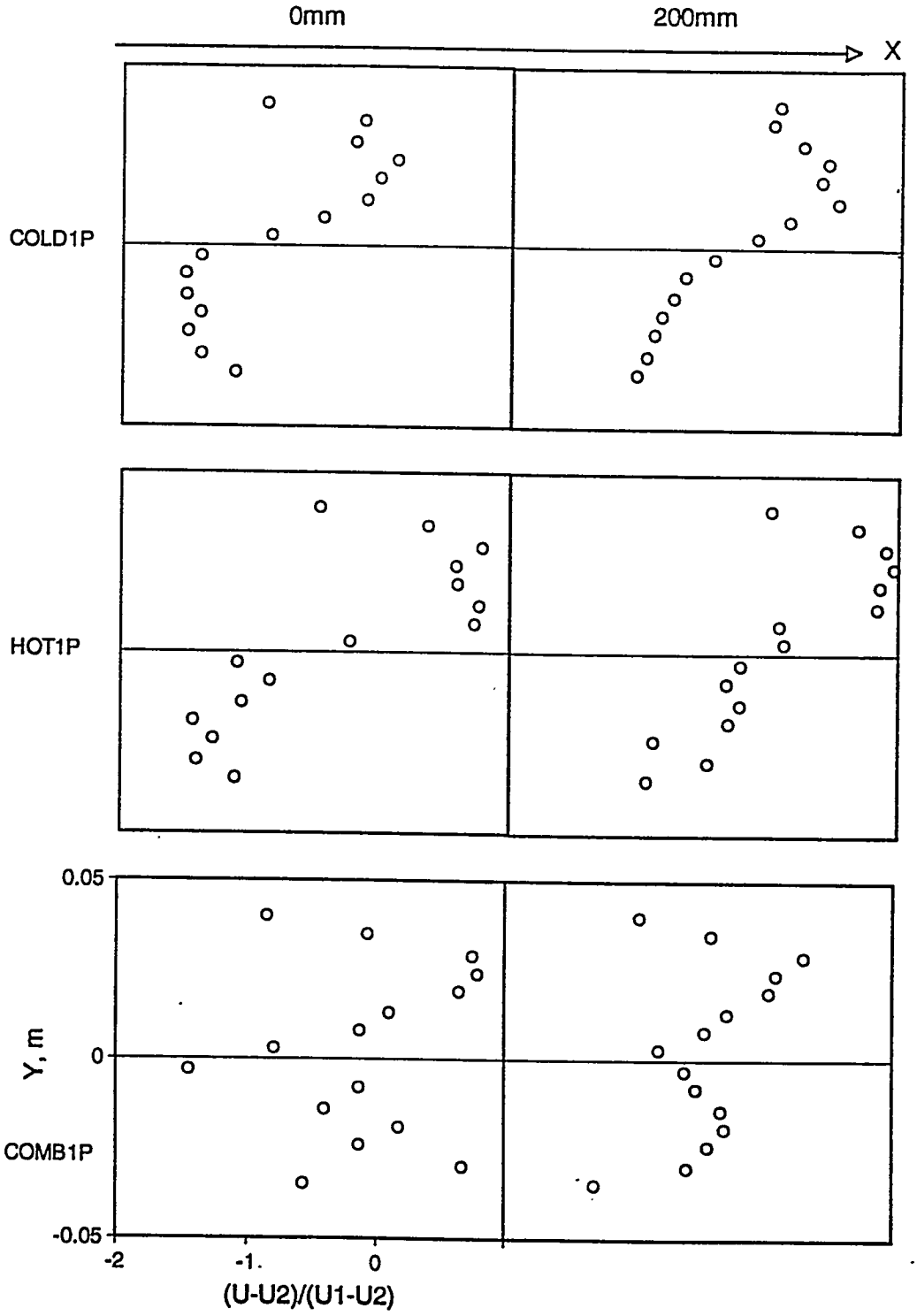

Fig. G.39 Comparison of the velocity profiles at x = 0 mm and x = 200 mm in shear layer with inert, pyrolyzing, and burning particles (runs: cold 1, hot 1 and comb 1)

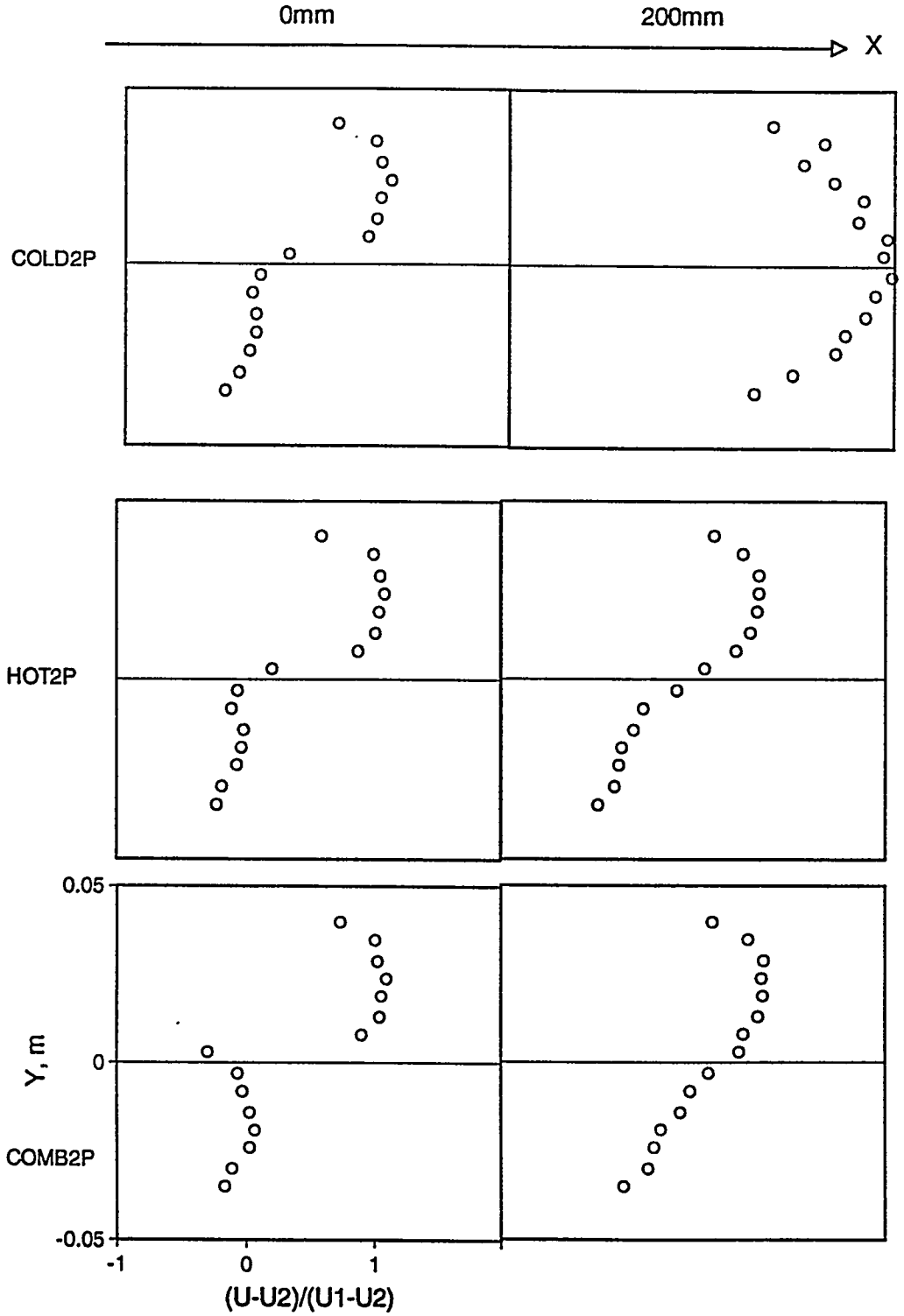

Fig. G.40 Comparison of the velocity profiles at x = 0 mm and x = 200 mm in shear layer with inert, pyrolyzing, and burning particles (runs: cold 2, hot 2 and comb 2)

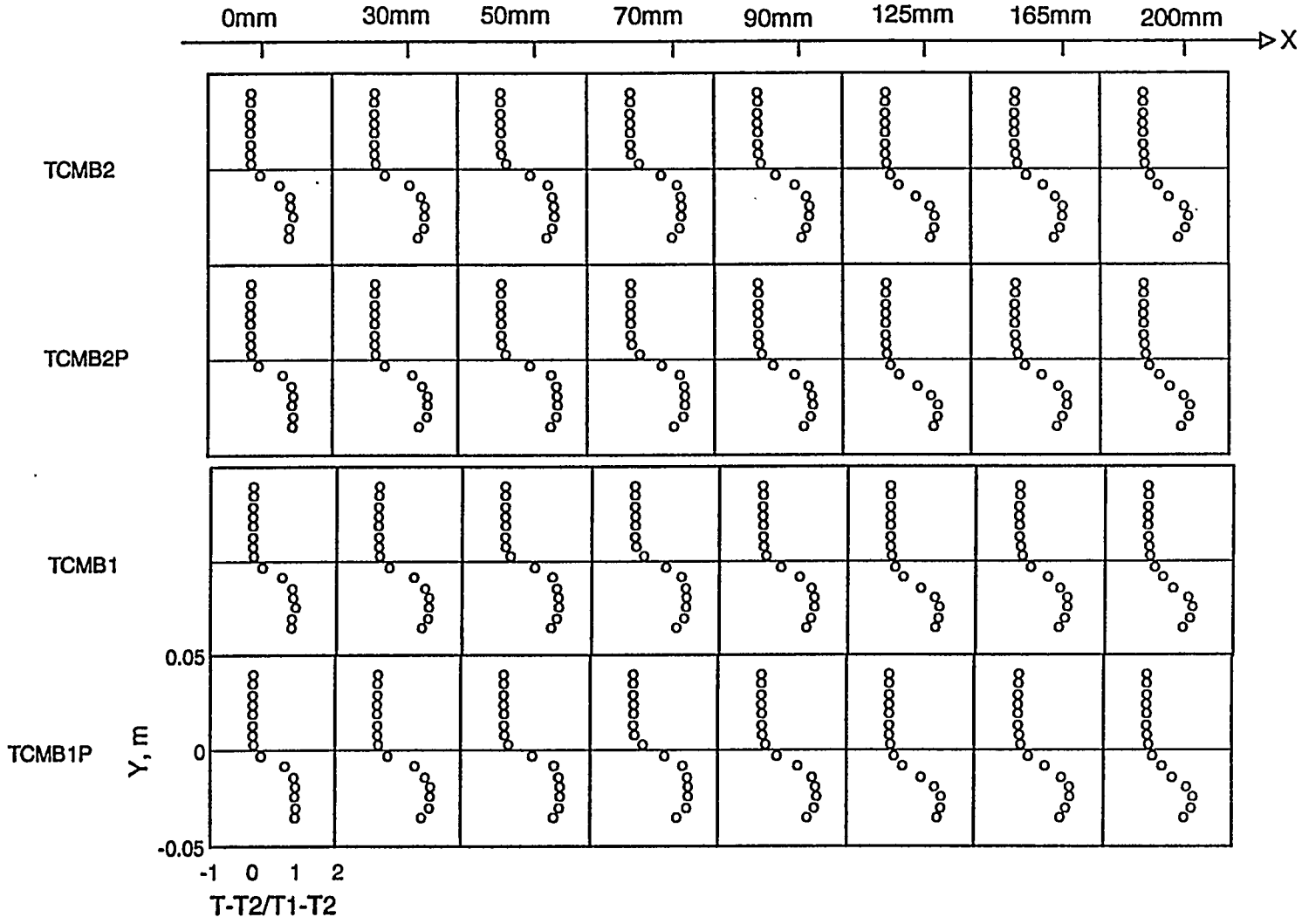

Fig. G.41 **Temperature profiles in shear layers with burning particles (runs: comb1 and comb 2)**

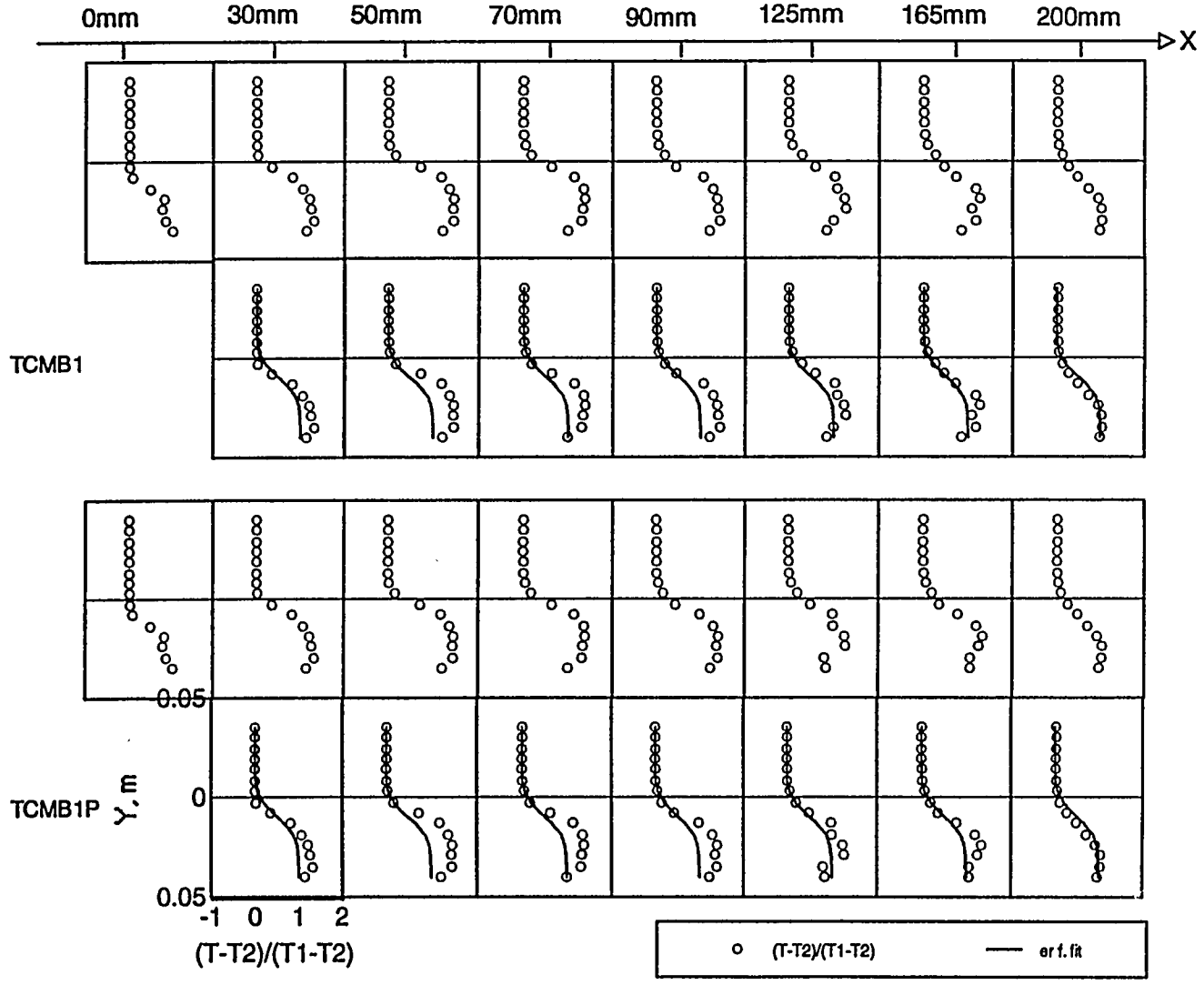

Fig. G.42 Error function fit to the temperature profiles in the shear layer with burning particles (run: comb 1)

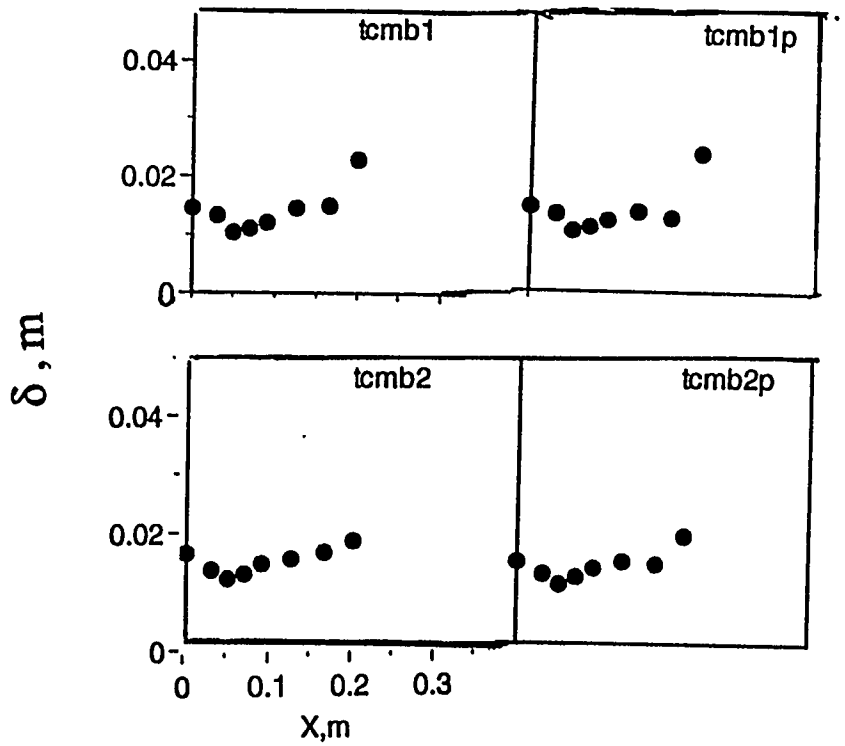

Fig. G.43 Effects of burning particles on the thermal thickness of the shear layer

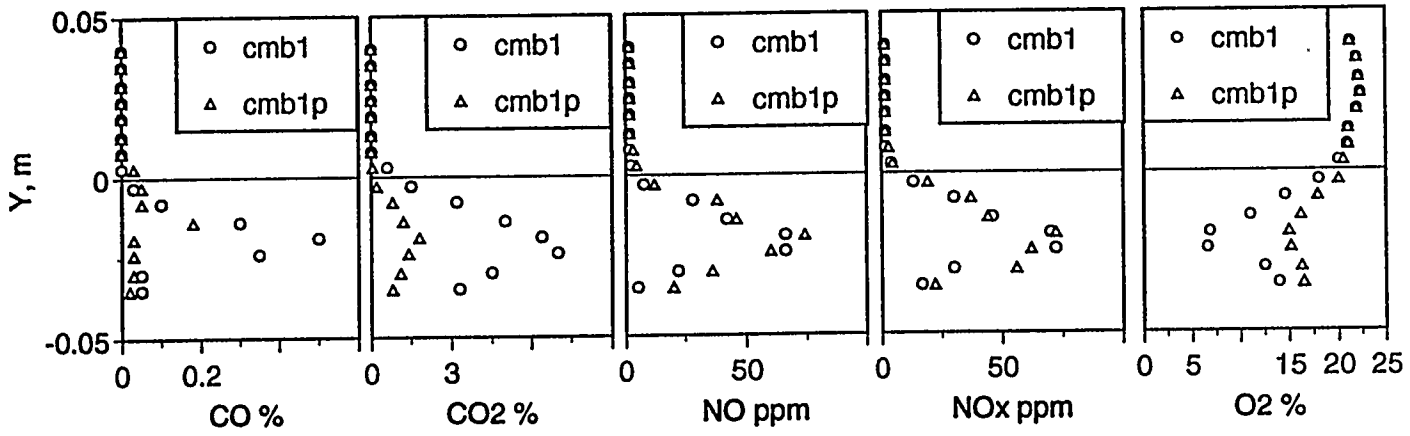

Fig. G.44 Effects of burning particles on the concentration profiles of product species in the shear layer (run: comb 1)

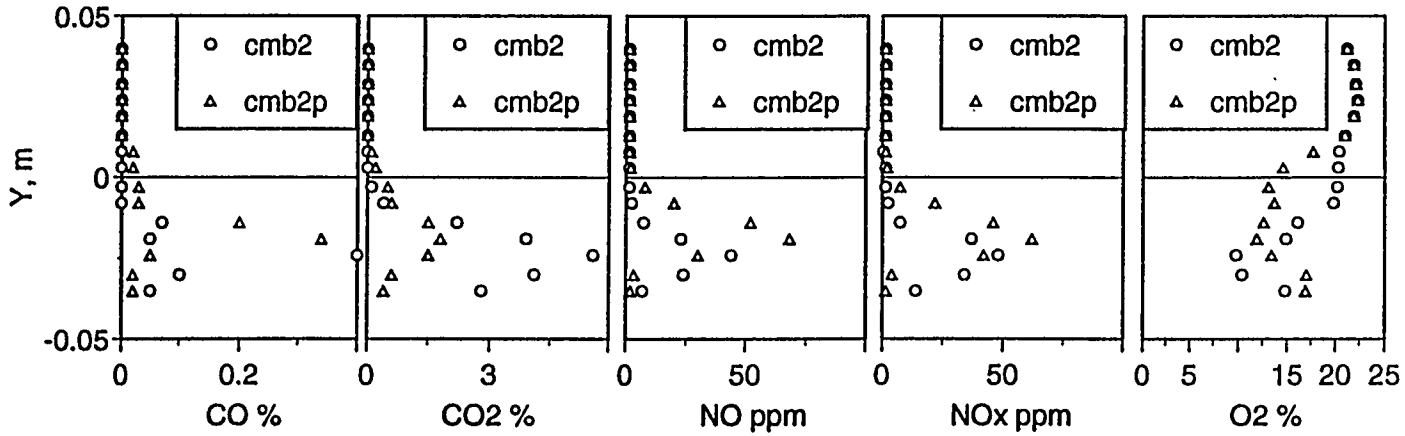

Fig. G.45 **Effects of burning particles on the concentration profiles of product species in the shear layer (run: comb 2)**

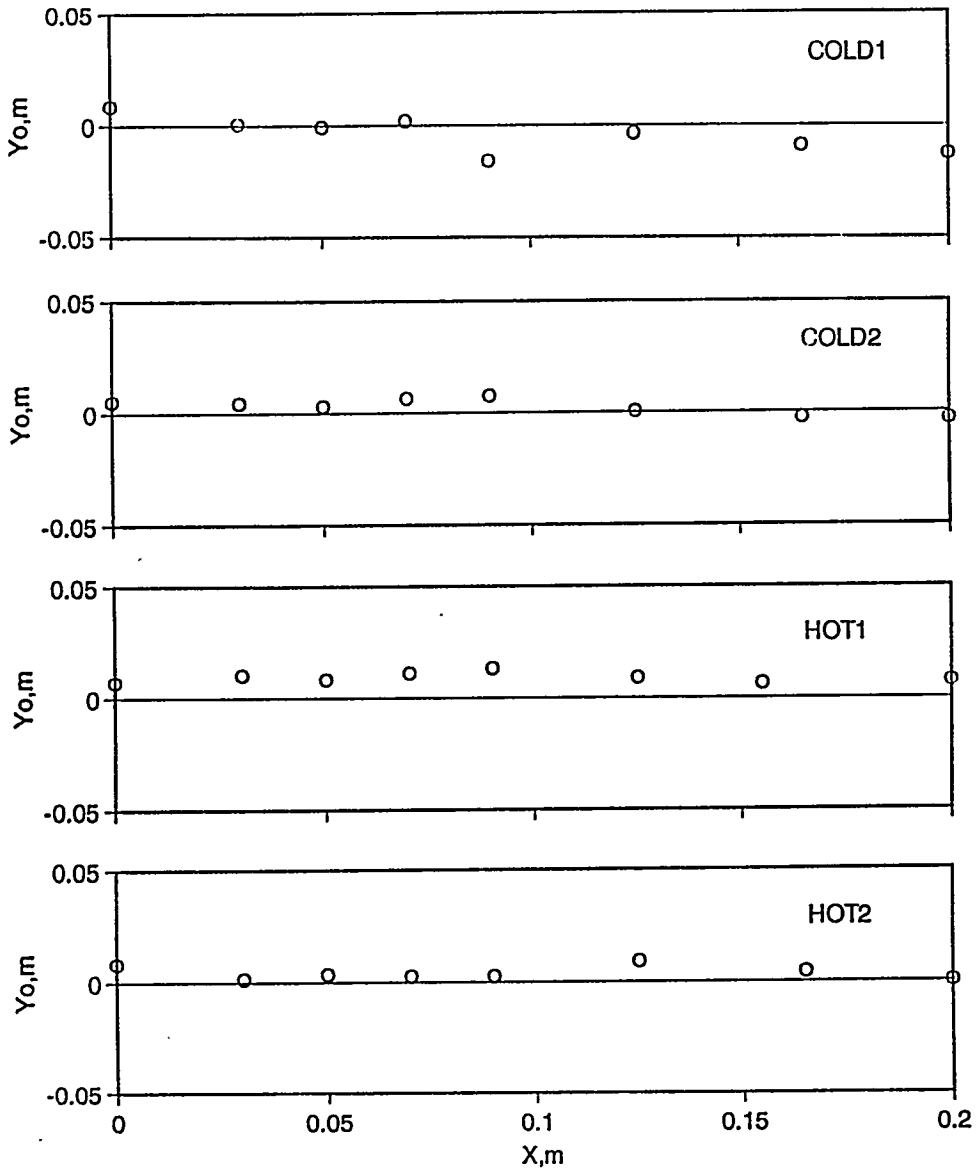

Fig. G.46 Plot of displacement of the centr l plane (yo) in the streamwise direction in homogeneous shear layers

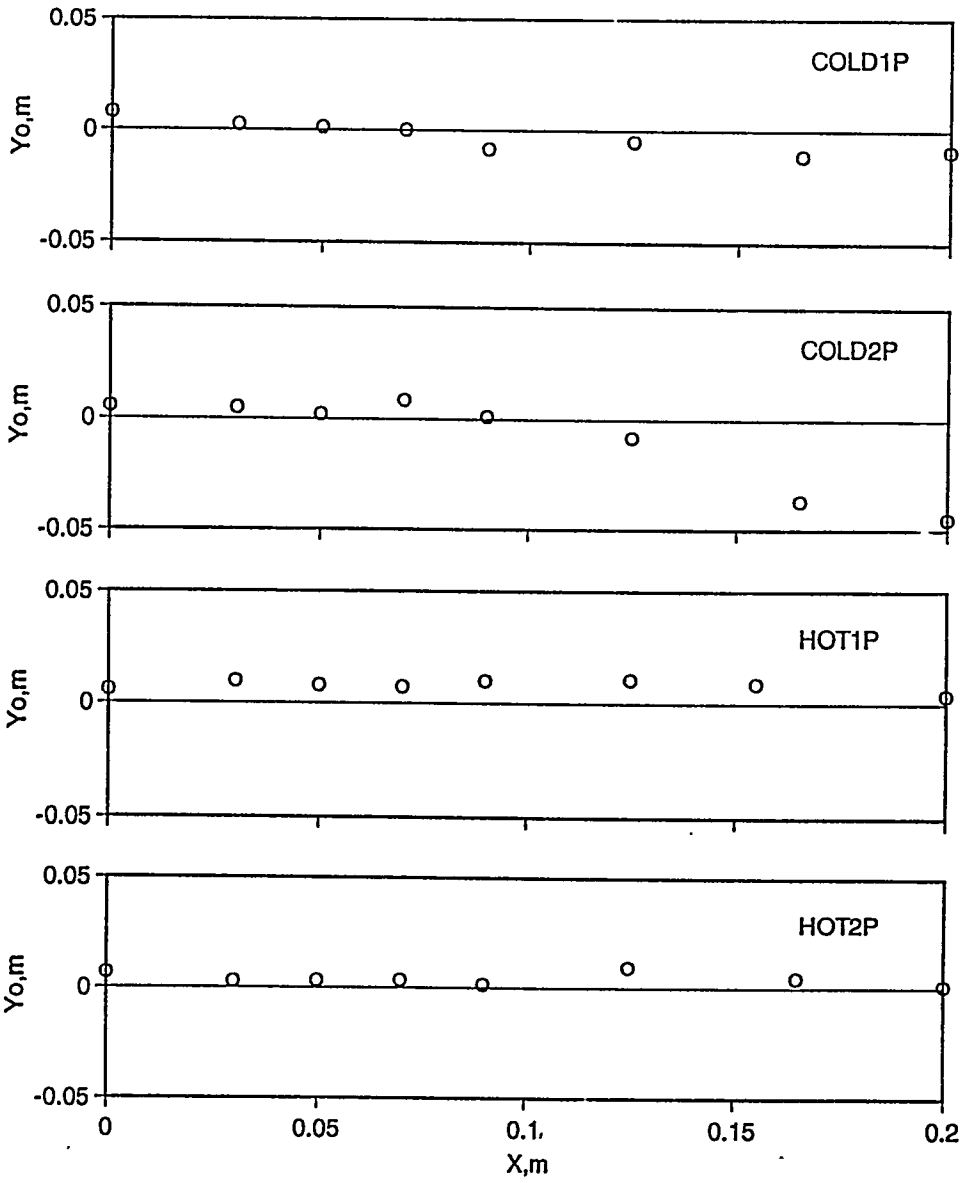

Fig. G.47 Plot of displacement of the central plane (yo) in the streamwise direction in shear layers with particles